EXCHANGE-COUPLED CHROMIUM

ION PAIRS IN RUBY

by

L. F. Mollenauer

M. L. Report No. 1325

May 1965

SPECTROSCOPY AND QUANTUM ELECTRONICS GROUP

VARIAN LABORATORY OF PHYSICS

AND

MICROWAVE LABORATORY

W. W. HANSEN LABORATORIES OF PHYSICS

STANFORD UNIVERSITY

STANFORD, CALIFORNIA

EXCHANGE-COUPLED CHROMIUM

ION PAIRS IN RUBY

by

L. F. Mollenauer

M. L. Report No. 1325

Spectroscopy and Quantum Electronics Group
Varian Laboratory of Physics

and

Microwave Laboratory
W. W. Hansen Laboratories of Physics

Stanford University
Stanford, California

ABSTRACT

This investigation has as its primary objective measurement of the exchange coupling between the various near neighbor types of Cr^{3+} ion pairs in the antiferromagnetic compound Cr_2O_3. The exchange coupling is expressed by the hamiltonian

$$(H_{ex})_i = -J_i \vec{S}_1 \cdot \vec{S}_2 \quad ,$$

where J_i is the exchange integral of the ith nearest neighbors, and $\vec{S}_1$ and $\vec{S}_2$ are the total spin on each of the interacting ions.

Advantage is taken of the fact that the homologous lattice Al_2O_3 will accept Cr_2O_3 in solid solution, and that for solute concentrations on the order of 0.1% to 1.0%, the resultant dark ruby lattice contains a sufficient number of near neighbor Cr ion pairs that the sharp line fluorescence spectrum produced by these can be investigated. At low temperatures, this spectrum consists of a quartet of lines for each pair type whose spacings yield a very accurate measure of J_i . The problem then consists of separating the various and sometimes overlapping exchange multiplets and identifying each with a particular near neighbor type.

When uniaxial stress is applied, differently oriented pairs of a given type are made inequivalent and an apparent splitting of the lines is produced. A constant magnitude of stress is applied to each of approximately eighteen samples whose axes span a full 180° range in the crystal mirror plane; the resultant pattern of splitting versus angle, unique to each pair type, allows the desired identifications to be made.

Only the first four nearest neighbor types were found to have significantly large exchange interaction; the corresponding exchange integrals were found to have the values $J_1 = -183.5$ cm^{-1}, $J_2 = -11.56$ cm^{-1}, $J_3 = -46$ cm^{-1}, and $J_4 = 6.94$ cm^{-1} . The set of four J values can then be inserted into a rather well established expression for θ , the

Curie Weiss constant; the value obtained, $\Theta = 565^\circ K$, is in excellent agreement with the experimental value of $\Theta = 550 \pm 20^\circ K$.

The full set of J values offer a unique opportunity to test certain theories of antiferromagnetic ordering. First, in the special case discovered here, where J_1 and J_3 predominate, it can be shown that at least one other exchange coupling is required to complete long range ordering, and that in fact a change in the sign of J_4 between the corundum compounds Cr_2O_3 and $\alpha\text{-}Fe_2O_3$ is required to explain the observed difference in their respective antiferromagnetic spin arrangements. Attempts to calculate T_N, the temperature below which antiferromagnetic ordering sets in, or the ground state exchange splitting observed in the optical spectrum of pure Cr_2O_3, yield wildly wrong answers when the measured J values are inserted into expressions derived from the molecular field theory; yet more realistic models, such as a clustering theory which calculates effects of the molecular field on the first neighbor pair, are indicated to produce much better agreement between the J values measured in dark ruby and the magnetic and optical properties of Cr_2O_3.

An incidental consequence of these studies is a rather complete empirical knowledge of the large shifts which can be produced in the frequencies of the various pair lines by the application of mechanical stress. This effect suggests the possibility of making a readily and highly tunable laser.

ACKNOWLEDGEMENTS

TABLE OF CONTENTS

I. INTRODUCTION

1.1. HISTORICAL NOTE

Solid state spectroscopy is so strongly associated with the recent invention of the optical maser that it may come as a surprise to learn that the first studies of the spectrum of ruby were made around the middle of the last century, predating not only the quantum theory but Maxwell's classical theory of radiation as well! In a treatise on light published in 1867, Edmond Becquerel[1] devoted nearly a full chapter to "Alumine et ses Combinaisons." Nearly all the observations reported there were made with the aid of his "phosphoroscope," a simple but clever device in which the sample, located between a pair of rotating, segmented disks, would be excited by a shaft of sunlight, then viewed through a prism spectrometer a controllable time after the sunlight had been shuttered off. Becquerel's apparatus is shown in Fig. 1.1. He was thus able to determine that the fluorescent lifetime in ruby was of the order of 4 milliseconds, in excellent agreement with modern observations; he was also able to note the unusual sharpness of the lines and the great similarity of the spectra produced by rubies, sapphires, and samples of alumina powder prepared in various ways. Although he correctly observed that the fluorescence was greatly enhanced by the addition of small amounts of Cr_2O_3 to his alumina preparations, he was misled by the persistence of the red fluorescence in so-called "pure" samples of alumina to theorize that the sharp fluorescence lines were the result of some inherent property of the Al_2O_3 lattice, and that chromium merely played the role of an activator.
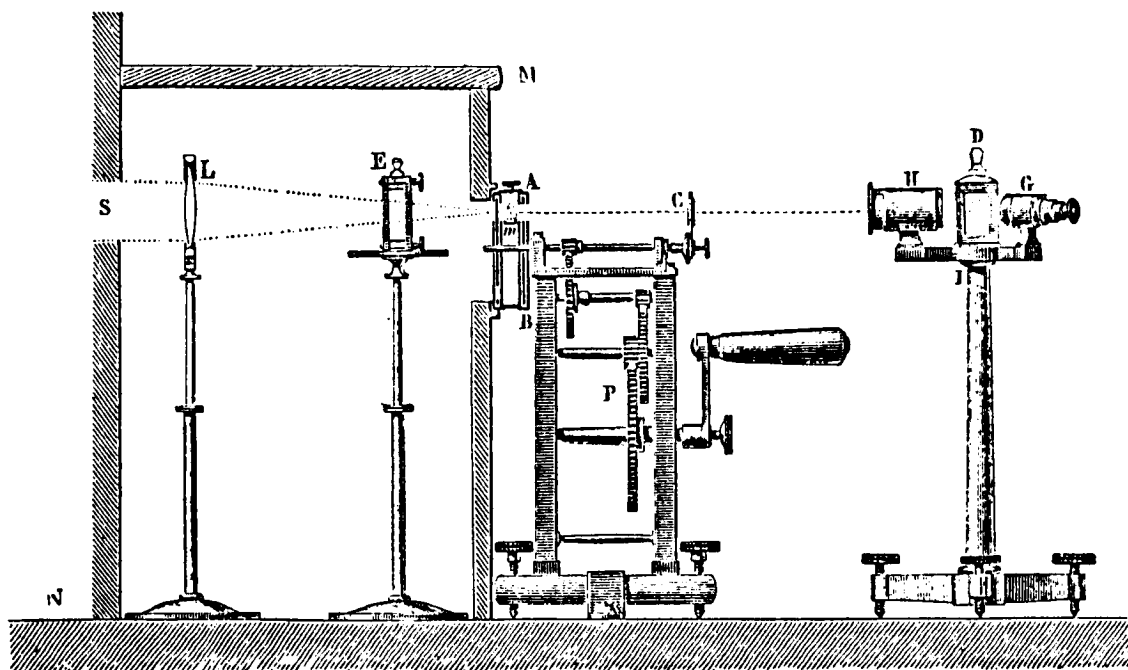
FIG. 1.1--Edmond Becquerel's Phosphoroscope. Sunlight enters at S ,
passes through a water solution filter at E , and excites
fluorescence in the sample located in the upper half of the
enclosure AB. The rotating, segmented disks are contained
in AB and are seen edge on; as the disks rotate, they alter-
nately block off the sunlight and the line of sight to the
spectrometer HDG. (From La Lumiere, ses Causes et ses Effets')

This theory evidently remained unchallenged until 1886, when the following short notice appeared in *Comptes Rendues*:[2]

> "M. Lecoq de Boisbaudran annonce, pour prendre date, que l'alumine calcinée et soumise à l'effluve électrique dans le vide ne lui a pas donné trace de fluorescence rouge. Cette fluorescence [ainsi que son spectre spécial[1]] se montre brillamment quand l'alumine contient 1/100 et même 1/1100 de Cr_2O_3 . Avec 1/100000 de Cr_2O_3 , on obtient encore du rose très visible....
>
> ...D'après ces observations, la présence du chrome paraît être indispensable à la production de la fluorescence rouge de l'alumine..."

The aging Becquerel, revered member of the Académie, made immediate and rather haughty reply[3] to the upstart Boisbaudran, the beginning of a long and sometimes amusing fight, which is well chronicled in *Comptes Rendues*.[4-8] The argument seemed to reach an impasse with Boisbaudran going to ever greater lengths to produce "pure" alumina and Becquerel attacking what we now know to be irrelevant side issues. From a modern viewpoint, both sides of the controversy are unsupportable; in the first place, the chromium fluorescence has such a high quantum efficiency, the lines produced are so sharp, and modern light detectors are so sensitive, that even the most highly purified sapphires produced to date show the R lines of ruby with good signal to noise ratio. Even more important is the consideration that a statement such as "chromium is indispensable in the production of the red fluorescence in alumina" or "chromium is only an activator in ruby" is meaningless outside the context of a complete theory based on the statement in question, such that esentially all predictions of the theory can be checked quantitatively against the results of experiment. On the other hand, it would not be fair to judge Becquerel and Boisbaudran by this modern standard, but rather, in view of the nearly complete theoretical vacuum in which they were forced to work, we should be amazed by their willingness to tackle a seemingly insoluble mystery, and should credit them with bringing one of the most beautiful and useful phenomena of nature to the world's attention.

---

[1] Spectre si bein décrit dans l'Ouvrage classique de M. Becquerel: *La Lumiere*, t. I, p. 340.

Old controversies die hard. Thus it is not too surprising to find, as late as 1904, an article in _Annalen der Physik_[9] by G. C. Schmidt with the subtitle "Antwort an Hrn. J. Tafel," which turns out to be nothing more than a re-run of the Becquerel-Boisbaudran argument. It is surprising, however, that just a few years later, when the Boisbaudran-Schmidt hypothesis seems to have acquired general acceptance among solid-state spectroscopists, Schmidt is given credit for having finally established the correctness of Boisbaudran's contention,[10] although the modern reader will find it difficult to see any essential differences between their methods and arguments.

Although brief mention of the ruby spectrum by J. Becquerel[11] and a not very accurate description by A. Miethe[12] appear earlier, the first thorough study of ruby by means of a high-resolution spectrometer was made by H. du Bois and G. J. Elias in 1908.[10] Du Bois and Elias were able to observe the absorption spectrum as well as the fluorescent emission, since large single crystals of synthetic ruby had become available by that time, and they gave the principal absorption lines their presently used designations, the R (rot) and B (blau) lines. They were able to produce a resolved Zeeman splitting of the R lines for the first time by immersing their samples in liquid air and by using magnetic fields as high as 42 kilogauss.

In reading the du Bois and Elias paper, J. Becquerel realized that some of the observations of the Zeeman effect reported there, such as supposed polarization differences for the same line in absorption as opposed to fluorescence, would lead to strange theoretical consequences, and he soon published a series of corrections backed by his own experimental observations.[13,14] Du Bois and Elias were then prompted to publish a revised and extended version[15] of their original paper. Here they were able to explain their former errors in terms of a badly wandering optic axis in their long absorption sample, along with visible strains and fractures in their crystals—possibly the earliest recognition of the important role played by crystalline defects. They also recognized the rather rare opportunity presented by the R lines to allow an accurate study of the temperature shift of absorption lines in

crystals, and carried out such measurements over a temperature range beginning with liquid air and extending to $845^{\circ}C$. Finally, they report the first measurements of the weak lines and bands seen in fluorescence to the red of the R lines, which they call the "Nebenlinien." Spectroscopists were somewhat handicapped in those days by the lack of red-sensitive plates, and du Bois and Elias were forced to make their measurements directly through a magnifing glass, for the observations would otherwise have used up "too much time and liquid air." Hence, to see the weak neighbor lines, nothing but concentrated sunlight would do as exciter of the fluorescence, and it is amusing to read their apology that "...these observations, which would otherwise have been completed by the end of 1910, had to be delayed until the present spring."

The above work was extended somewhat by Mendenhall and Wood in 1915.[16] They observed resonance radiation with the R lines, and also, by using photographic plates, were able to observe the "most curious" Zeeman effects in the neighbor lines. An attempt to induce Stark effect in the R lines failed, either because of improper alignment of the crystal axis with the field direction or because of the rather large residual line width due to microscopic strain in the rather poor quality crystals available at that time, or perhaps both at once. The failure is unfortunate, since a positive result may have given just a hint of the crystal field effects so important in solid-state spectra.

So far there had been little or no attempt at theoretical interpretation of the relatively well observed spectrum, and the few pronouncements made sound highly cryptic to the modern reader. Then the new quantum theory of the late 20's began to explain the spectra of excited gases in an avalanche of ever-mounting detail, and it was only a question of time until someone would attempt to apply this new theory to the more complex problem of solids. The foundation was laid by Hans Bethe in what is now a classic paper, published in 1929.[17] Here was outlined the modern crystal field theory, which views the electrostatic field imposed by the host lattice as the fundamental perturbation to be applied to the known spectral terms of the free atom or ion, and classifies the new levels thus determined by the representations of the symmetry group

of the crystal field to which the new levels belong. It is therefore disappointing to find no mention of Bethe's theory in a series of papers[18-22] by Otto Deutchbein published in the early thirties, in which account is given of his extensive experimental investigations of chromium phosphorescence in a series of host lattices. In observing the relative invariance of the sharp-line spectra to the particular host lattice type, he was led to believe a suggestion of Saha[23] that such spectra were the result of an electron spin-flip. Thus he was able to correctly surmise that the R lines, were essentially a ^4F-to-^2G transition by noticing that the energy differences between the various components of these terms in the spectrum of CrIV (measured by White in 1929)[24] clustered about the R line frequencies. From this point on, however, his interpretation goes astray; for example, his assignment of definite term values resulting from spin-orbit splitting in CrIV to the various R line components shows that he was unaware of the quenching, so well described in Bethe's paper, of orbital angular momenta by crystalline fields.

Incidentally, Deutchbein was the first to make a distinction between true "neighbor lines" and the vibrational sidebands of the R lines. That is, he observed that the latter obeyed Stokes' law, while the former did not. (Stokes' law states that the vibrational sidebands of an electronic transition will be mirror-symmetric in energy about the zero phonon, or "principal" line, and that at low temperatures only the long-wave side will appear in emission, while only the short-wave side will appear in absorption at those same low temperatures. In modern terms, Stokes' law is a simple consequence of the population of phonon states according to Bose-Einstein statistics.) With the exception of the relatively minor error that he attributed Maxwell-Boltzman statistics to the population density of phonon states, he understood his observations of the vibrational sidebands in an essentially modern way.

With the dawning of World War II, the attention of most physicists was diverted to nuclear physics, microwaves, and other technical projects related to the war effort, with the consequent near abandonment of the optical spectroscopy that just a few years before had been at the very center of physics, both as source and as testing ground for the new

quantum mechanics. Thus it is not too surprising that the careful working out of the implications of Bethe's theory for the spectrum of ruby was delayed nearly a quarter of a century, until the appearance, between 1954 and 1958, of a series of papers by Satoru Sugano, Yukito Tanabe, and Hiroshi Kamimura.[25-29] Their patient and thorough work has provided the basis for almost all modern studies of ions with d electrons in crystal fields of cubic and lower symmetries. (The rather precise predictions of the Sugano and Tanabe theory, especially those concerning anisotropy and Zeeman effect of the R and B lines, were given immediate experimental check by I. Tsujikawa.[30])

1.2. MODERN THEORY OF THE Cr^{3+} ION IN Al_2O_3

Since the Sugano and Tanabe theory of the "isolated" Cr^{3+} ions in ruby has been recapitulated elsewhere,[31,32] only the briefest description possible will be given here, mainly to introduce notation. Figure 1.2 shows the Al_2O_3 host lattice; the Cr^{3+} ion is substituted directly for an Al^{3+} ion in the formation of ruby. Strictly speaking, the metal ion site symmetry is only trigonal. However, since the surrounding six oxygen ions lie on the corners of a not too badly distorted octahedron, the crystal field seen by the metal ion can be analyzed as the sum of a large cubic field and a small trigonal one. Figure 1.3 shows the effects of the cubic field on the energy levels of the Cr^{3+} ion. The old energy levels of the free ion, for which the total angular momentum 1 had been a good quantum number, are broken up into new levels, whose eigenfunctions are now appropriate basis functions for the various representations of the cubic group. The new levels thus formed are simply named after the representation of the cubic group to which they belong.[33] Thus, for example, the ^4F level of the free ion is broken up into $^4A_2$, $^4T_1$, and $^4T_2$ levels, the A_2 being a one-dimensional representation, the T_1 and T_2 being the two three-dimensional representations. (Here the superscript retains its usual spectroscopic meaning of spin degeneracy, i.e., it equals $2S + 1$.) Similarly, the ^2G level of the free ion is split by the cubic field into $^2T_2$, $^2T_1$, and ^2E levels. In ruby,
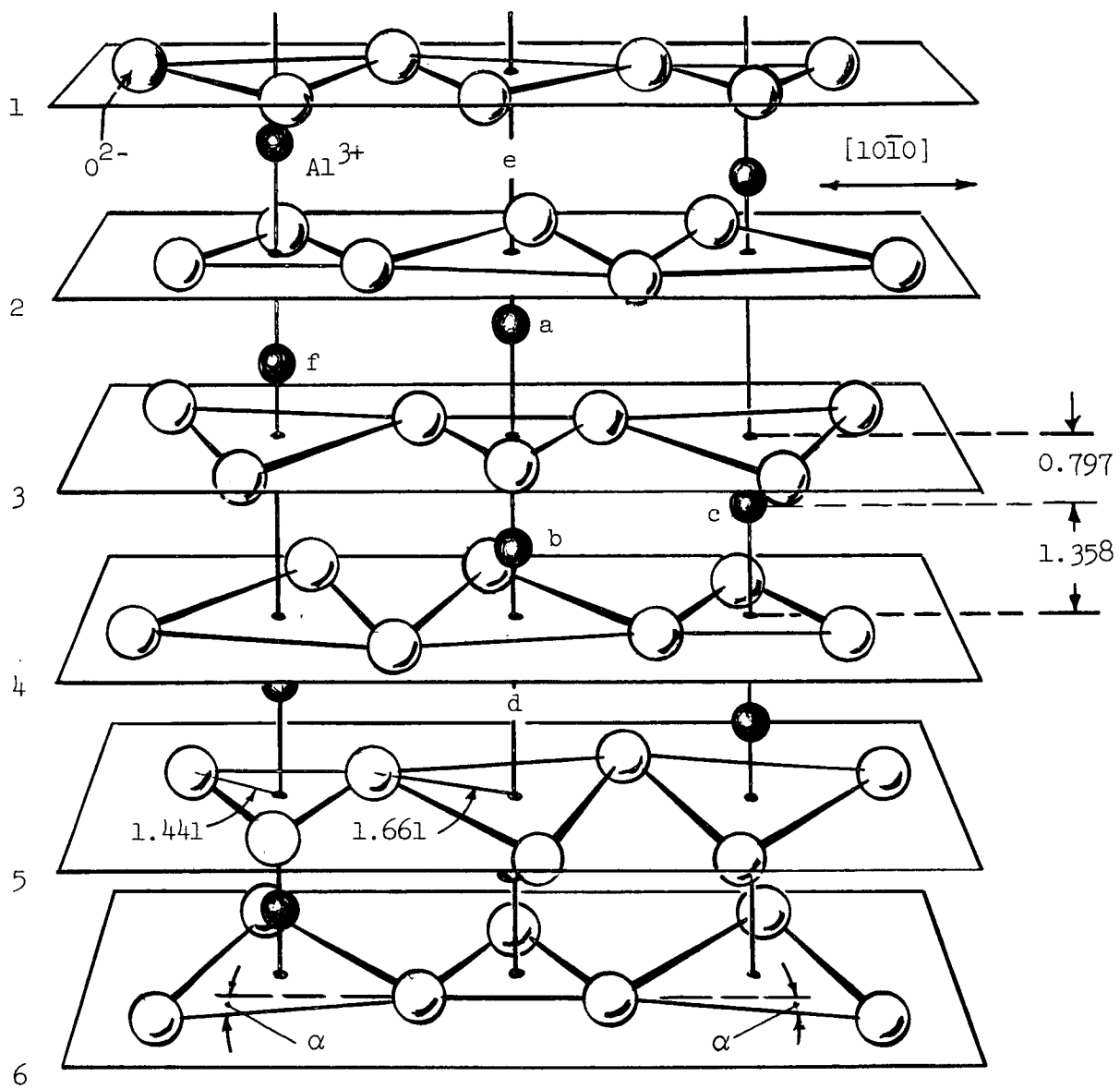
FIG. 1.2--Portion of the Al$_2$O$_3$ lattice. = 4.3° (from Geschwind and Remeika, Phys. Rev. 122, 757).
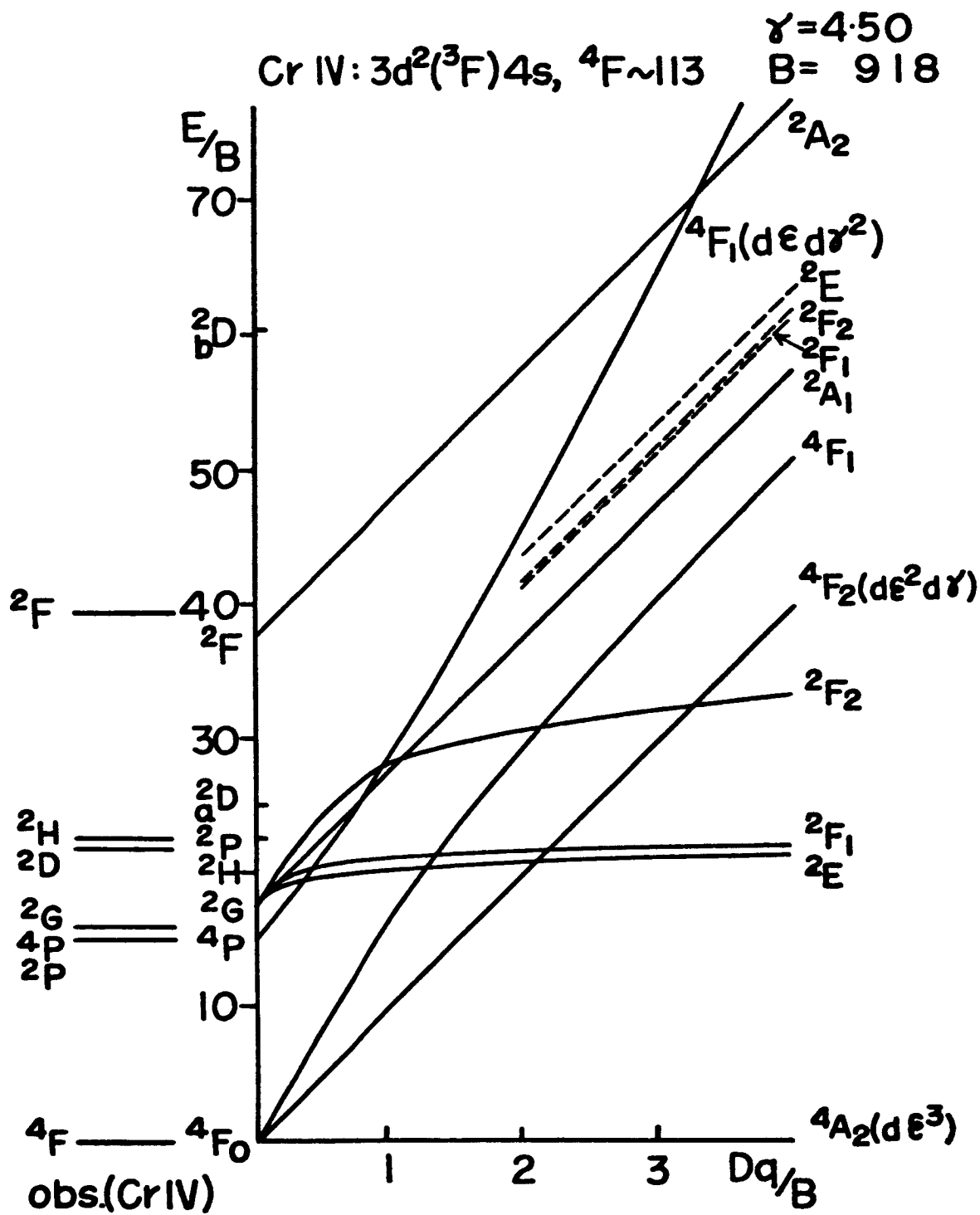
FIG. 1.3--Effects of the cubic field on the energy levels of the Cr^{3+} ion, (from Sugano and Tanabe[27]).

the cubic field parameter Dq is sufficiently strong that the $^4T_1$ and $^4T_2$ levels lie above the ^2E level, and since the splitting between these two T levels and the $^4A_2$ level is directly proportional to the cubic field strength, the transitions $^4A_2 \rightarrow ^2T_1$ and $^4A_2 \rightarrow ^2T_2$ form two bands, each about 2000 cm^{-1} wide. By contrast, the energy separation between ^2E and $^4A_2$ is nearly independent of the cubic field strength, and hence the transition $^4A_2 \rightarrow ^2E$ can be quite sharp at low temperatures, in the best quality ruby less than 0.1 cm^{-1}. In a purely cubic field, the $^4A_2 \rightarrow ^2E$ transition is magnetic dipole, electric dipole transitions being both spin and parity forbidden. The above picture of the behavior of Cr^{3+} ions in a purely cubic field has been well verified experimentally by studies of Cr^{3+} in MgO.[34-36]

In ruby, the small trigonal field (in combination with spin orbit effects) introduces two important perturbations. First, it splits the ^2E level into two levels separated by 28 cm^{-1}. Sugano and Tsujikawa were able to make positive identification of the R_1 and R_2 lines with the two $^4A_2 \rightarrow ^2E$ transitions by comparing observed and predicted Zeeman effect and anisotropy of these lines. Second, it induces an electric dipole oscillator transition (oscillator strength f on the order of 10^{-6}) between the $^4A_2$ and ^2E levels. (The mechanism by which the trigonal field induces the electric dipole oscillator will be discussed in another chapter.) Although the oscillator strength of the R lines is very small compared to the usual allowed transitions encountered in gaseous spectroscopy, it is sufficiently great to allow R line fluorescence to compete favorably with vibrational-sideband emission and with nonradiative processes; i.e., the R line fluorescence in ruby has a very high quantum efficiency.[37,38] It is no wonder, then, that these lines were among the first to be seen by early observers, even with the most insensitive equipment.

1.3. THE PAIR SPECTRUM

Although the R lines and absorption bands were considered rather well understood after Sugano and Tanabe's work, the complex fluorescence and absorption spectrum of the "neighbor lines" remained to be explained.

S. Jacobs, in a thesis written in 1956, demonstrated that this spectrum is very complex indeed, as he had tabulated there accurate wavelength measurements of over 110 lines.[39] Because they usually had only one or two samples of ruby on hand, the earlier workers, including Jacobs, missed the most obvious clue to the origin of the neighbor lines: their increase in intensity, relative to that of the R lines, as the Cr concentration is increased.

This increase in relative fluorescent intensity was first observed and measured by A. L. Schawlow in 1959,[40] and later by Tolstoi and Abramov.[41] Their findings are reproduced in Figs. 1.4 and 1.5, respectively. Both found the same general behavior: the ratio of fluorescent intensity of the various prominent neighbor lines to that of the R lines was directly proportional to the Cr concentration for all but the higher concentrations studied, where the ratio began to increase even faster than linearly. The above result is most readily explainable by the hypothesis that the neighbor lines are due to interacting, near-neighbor Cr ion pairs. Under the assumption that the Cr ions enter specific Al sites in a purely random way, the number of near-neighbor pairs of a given type should increase with the square of the Cr concentration. Hence the first part of the curves of Figs. 1.4 and 1.5 merely represent the increasing proportion of pairs as the Cr concentration increases. The nonlinear part of the curve was explained in terms of nonradiative energy transfer from the "isolated" ions to the pairs, whenever the average distance of the isolated ions from the pairs diminished beyond a certain critical size. Incidentally, a certain tendency for the Cr ions to cluster together would not invalidate the above argument, although no evidence of such clustering has been revealed to date.

The most important clue as to the nature of the interaction between the ions of a Cr pair comes from the fact that pure Cr_2O_3 is known to be antiferromagnetic below $308^{\circ}K$ and to have a Curie-Weiss constant of $550^{\circ}K$;[42,78] this, coupled with the fact that the Cr_2O_3 and Al_2O_3 lattices are homologous with nearly identical unit cell dimensions,[43] leads one to expect sizable exchange coupling for at least one of the near neighbor types.

Concentration of Chromium in WT%
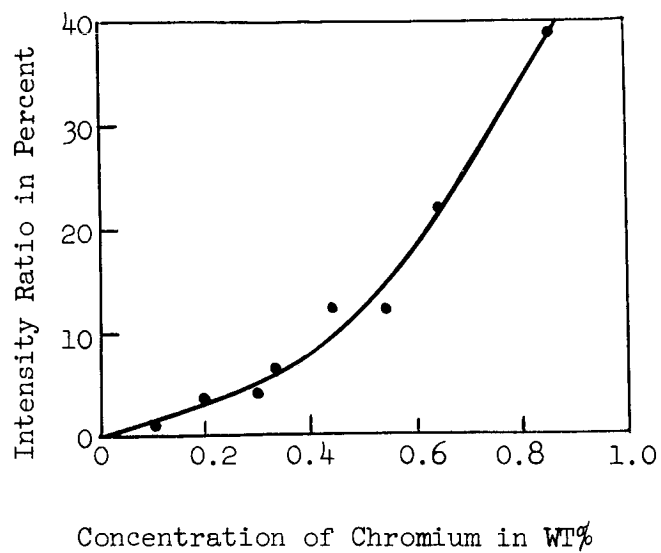
FIG. 1.4--Fluorescence intensity ratio N_2/R_1 as a function of chromium concentration, (from Schawlow et al.,[40]).
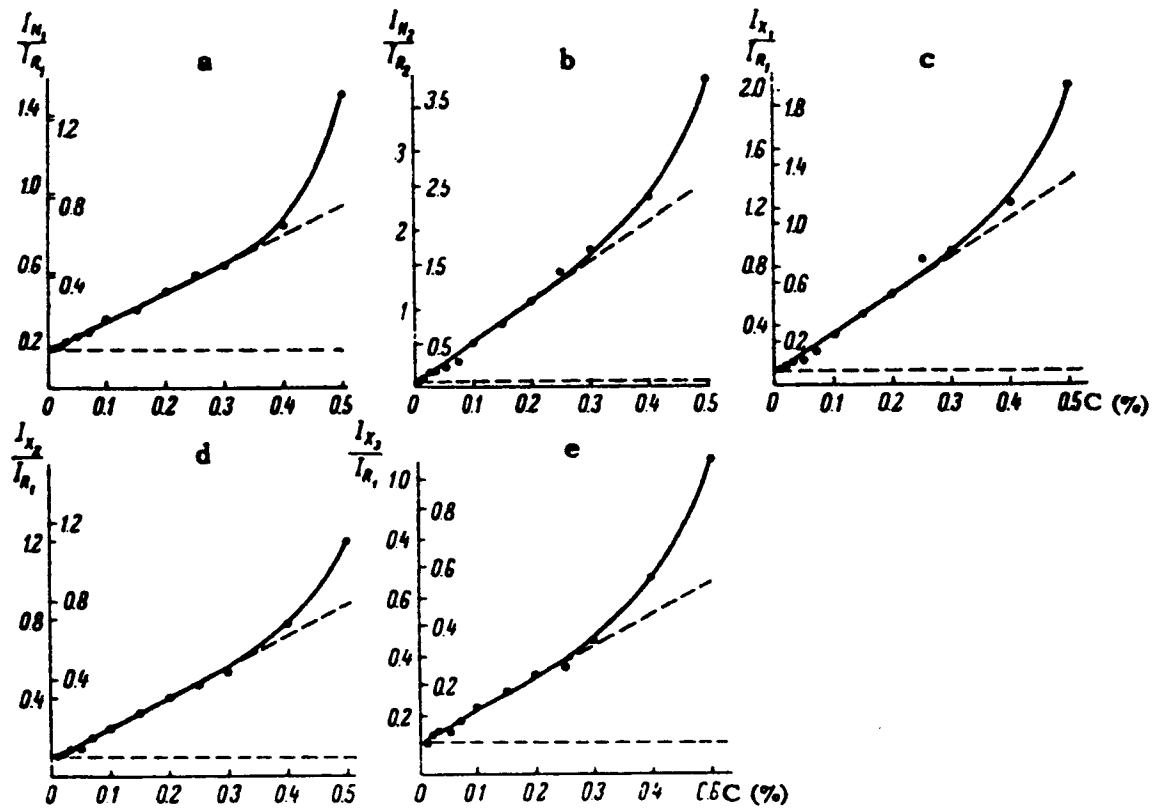
FIG. 1.5--Fluorescence intensity ratio N/R for various satellite
lines, (from Tolstoi and Abramov[41]).

The exchange interaction is a consequence of the Pauli exclusion principle and the overlap of the wave functions of the interacting electrons. For electrons of ion 1 in orbitals ψ_i and electrons of ion 2 in orbitals ψ_j, the exchange interaction can be written[44]

$$H_{ex} = -\sum_{i,j} J_{ij} \vec{s}_i \cdot \vec{s}_j \quad , \qquad (1.1)$$

where J_{ij} is the exchange integral:

$$J_{ij} = \int\int \psi_i^*(\vec{r}_1) \, \psi_j(\vec{r}_1) \left\{ \frac{e^2}{|\vec{r}_1 - \vec{r}_2|} - V(\vec{r}) \right\} \psi_j^*(\vec{r}_2) \, \psi_i(\vec{r}_2) \, dr_1 \, dr_2 \quad ,$$

$$(1.2)$$

where $V(\vec{r})$ means $V(\vec{r}_1) + V(\vec{r}_2)$. The general tensor relation (1.1) can often be simplified to either the isotropic form

$$H_{ex} = -J \, \vec{s}_1 \cdot \vec{s}_2 \quad , \qquad (1.3)$$

or the slightly more general biquadratic form[45,46]

$$H_{ex} = -J \, \vec{s}_1 \cdot \vec{s}_2 + j \, |\vec{s}_1 \cdot \vec{s}_2|^2 \quad , \qquad (1.4)$$

where s_1 and s_2 are the total electron spins for each ion. The use of either (1.3) or (1.4) in the interpretation of the ruby spectrum will be justified by the observed spectrum itself; hence (1.3) or (1.4) will be understood in all future reference to exchange coupling.

The question of the sign of J is rather complex, and the following is offered merely to suggest some of the considerations involved. If only the first term in expression (1.2) is of importance, then J_{ij} is positive, since it then merely represents the self-energy of the complex charge distribution $\psi_i^* \psi_j$. The coupling (1.3) is then called ferromagnetic, since the lowest energy occurs when the spins s_1 and s_2 are parallel. On the other hand, when the attractive potential of the positive ion cores involved is stronger than the electron-electron repulsions, the second term in (1.2) can predominate, making J negative, and the coupling is then antiferromagnetic. As pointed out by Anderson in reference 44, the antiferromagnetic coupling is by far more common in insulators, and the ferromagnetic coupling described above an essentially hypothetical case. The explanation of exchange coupling in real ferromagnetic materials is much more involved.

We are now in a position to calculate the effects of exchange coupling upon the spectrum of a Cr ion pair in ruby. Consider first the ground state. Since, for our purposes, the crystal field splitting of the ground state is essentially negligible compared to the optical linewidths of the pair lines, the total spin $\vec{S} = \vec{s}_1 + \vec{s}_2$ will be a good quantum number for the pair. Hence, we can insert the identity

$$\vec{s}_1 \cdot \vec{s}_2 = \frac{1}{2} [|\vec{S}|^2 - |\vec{s}_1|^2 - |\vec{s}_2|^2] \qquad (1.5)$$

into (1.3) to obtain

$$H_{ex} = -\frac{J}{2} [|\vec{S}|^2 - |\vec{s}_1|^2 - |\vec{s}_2|^2] \qquad , \qquad (1.6)$$

from which it can be seen that the ground state exchange splitting is determined by S alone, according to the well known Lande interval role. Since $|\vec{s}_1| = |\vec{s}_2| = 3/2$ for the ground state, yielding $S = 0,1,2,$ or 3 , the resulting exchange multiplet is a quartet. The splittings are illustrated in Fig. 1.6.

- 15 -

$$\frac{15}{4}\,J \underline{\quad\quad\quad} \quad S = 0$$

$$\frac{11}{4}\,J \underline{\quad\quad\quad} \quad S = 1$$

J

2J

$$\frac{3}{4}\,J \underline{\quad\quad\quad} \quad S = 2$$

0 ------

3J

$$-\frac{9}{4}\,J \underline{\quad\quad\quad} \quad S = 3$$

Ferromagnetic Coupling

$J > 0$

$$\frac{9}{4}\,|J| \underline{\quad\quad\quad} \quad S = 3$$

$3|J|$

0 ------

$$-\frac{3}{4}\,|J| \underline{\quad\quad\quad} \quad S = 2$$

$2|J|$

$$-\frac{11}{4}\,|J| \underline{\quad\quad\quad} \quad S = 1$$

$|J|$
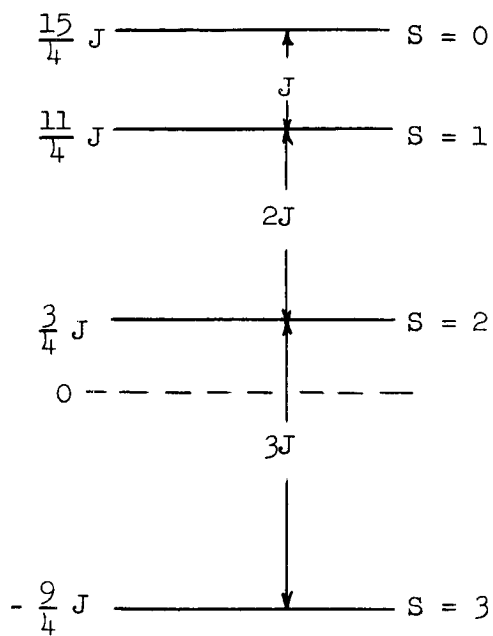
$$-\frac{15}{4}\,|J| \underline{\quad\quad\quad} \quad S = 0$$
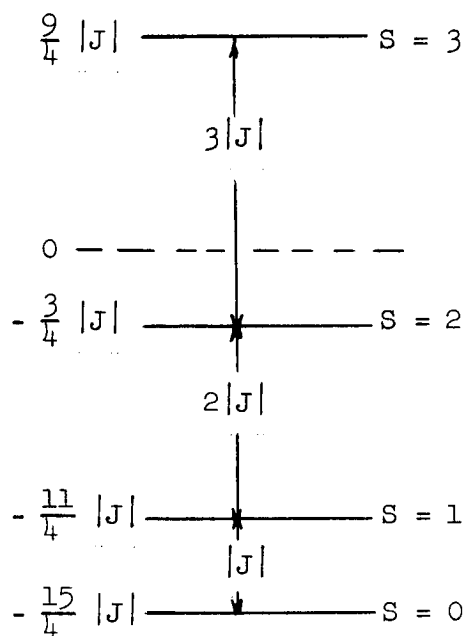
Antiferromagnetic Coupling

$J < 0$

$$H_{ex} = -J\,\vec{s}_1 \cdot \vec{s}_2$$

$$|\vec{s}_1| = |\vec{s}_2| = 3/2$$

$$\vec{S} = \vec{s}_1 + \vec{s}_2$$

FIG. 1.6--Exchange splitting of a Cr^{3+} ion pair ground state.

The optically excited state of a Cr pair presents a more complex problem. The basic theory has been worked out by A. M. Clogston[47] and can be summarized as follows: The excited state of a pair will be formed from the excited state of one ion and the ground state of its neighbor. Energy transfer between the two ions would split the excited state of the pair into an odd and an even state. But it can be argued that the two possibilities for such energy transfer, the exchange coupling itself and direct dipole interaction, would have negligible effect. Thus the excited state in which the excitation resides on one ion will be considered degenerate with the state in which the excitation resides on the other ion. As for the energy level splittings induced by the exchange term, the situation is simple when the excited state exchange integral K is much larger than the crystal field splitting: the two spins $s_1 = 1/2$ and $s_2 = 3/2$ combine to make just two levels of total spin $S = 1$ and $S = 2$, separated in energy by $2K$. (The letter K has been substituted for J to indicate that the exchange couplings may not be exactly the same in the excited and ground states.) That K is much larger than the crystal field splitting seems to be true for the nearest neighbors, as the experiments of this study will show. But for the other near-neighbor pairs, the exchange and crystal field splittings are of the same order of magnitude. In this latter case, since the energy levels cannot be simultaneous eigenfunctions of the exchange and crystal field operators, we no longer have to deal with pure S states, and the level splitting becomes rather complex. Figure 1.7 shows the level splitting E as a function of K, in units of the crystal field splitting parameter Δ, as reproduced from Clogston's paper.

With essentially the above theoretical picture in mind, Schawlow began to search the pair line spectrum for evidence of exchange multiplets in the ground state.[48] His method was simply to compare fluorescence and absorption spectra of a dark ruby sample, both taken at a sufficiently low temperature. (The temperature actually used was that of liquid He_4, $4.2^{\circ}K$.) If the exchange energies involved could be assumed large compared to kT at $4.2^{\circ}K$, the two spectra should have revealed (for each pair type)
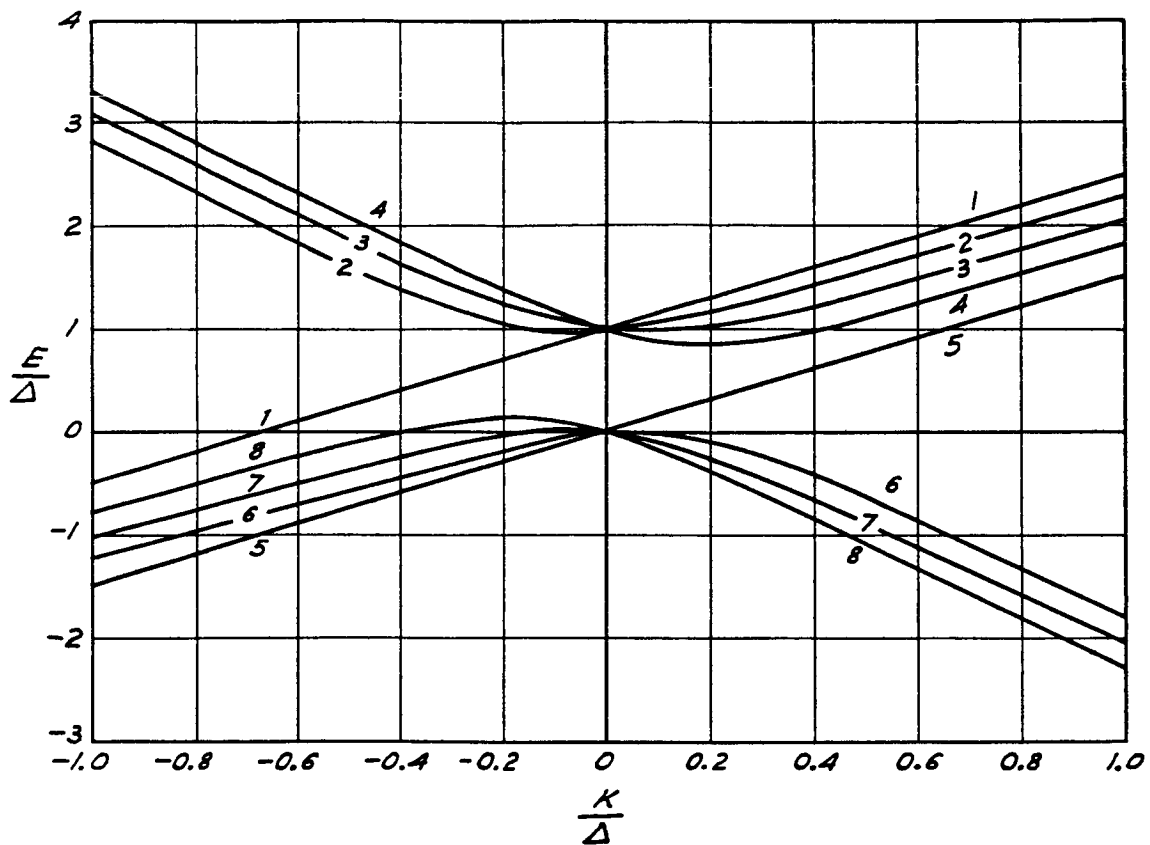
FIG. 1.7--Exchange splitting of Cr^{3+} ion pair excited state. K is the upper state exchange integral, and Δ the crystal field splitting, (from Clogston[47]).

one line as a common turning point, the transition from the lowest-lying of the excited states to the lowest-lying ground state. The fluorescence photograph would reveal only three other lines, and these would be found to the long-wavelength side of the common line; in this manner the full ground state exchange multiplet would be displayed. On the other hand, the absorption photograph would reveal lines only to the short-wavelength side of the common line, representing transitions from the lowest of the ground state levels to the excited state complex. Figure 1.8 reproduces what Schawlow actually found. A moment's study of the photograph will reveal some of the difficulties encountered in attempting to see the above-mentioned pattern in it: First, there is almost certainly more than one turning point, indicating that one must separate the overlapping spectra of at least two different pair types. Second, the selection rules are so strange, with vast intensity differences among the various members of a multiplet, that one can never be sure what lines are lost on that account. Finally, some of the pair lines may lie buried in the vibrational sidebands, making it difficult to distinguish true pair lines from the numerous sharp features of the vibrational sidebands.

Although the above-mentioned difficulties prevented Schawlow from making immediate positive identification of the various ground state exchange multiplets, he was able to determine that two of the more prominent pair lines, at 7009 and 7041 $\mathring{A}$ (respectively, the N_2 and N_1 lines of du Bois and Elias), terminated on levels which would be empty at low temperatures. He was thus led to suggest,[49] shortly before the existence of the first working laser, that if ruby were usable as a laser material, laser action might be more readily obtainable in the N lines than in the R lines on account of the greater ease in attaining population inversion in the former. Although the vastly better optical quality obtainable in pink ruby dictated that the first laser would use the R_1 line, Schawlow was able to prove his point late in 1960 by observing simultaneous laser action in the N lines of a cooled, dark ruby laser rod (Cr_2O_3 concentration approximately 0.5%).[50] As the energy supplied to the flash lamp was raised, first the N_2 line alone, then both N_2 and N_1 lines simultaneously displayed laser action, and
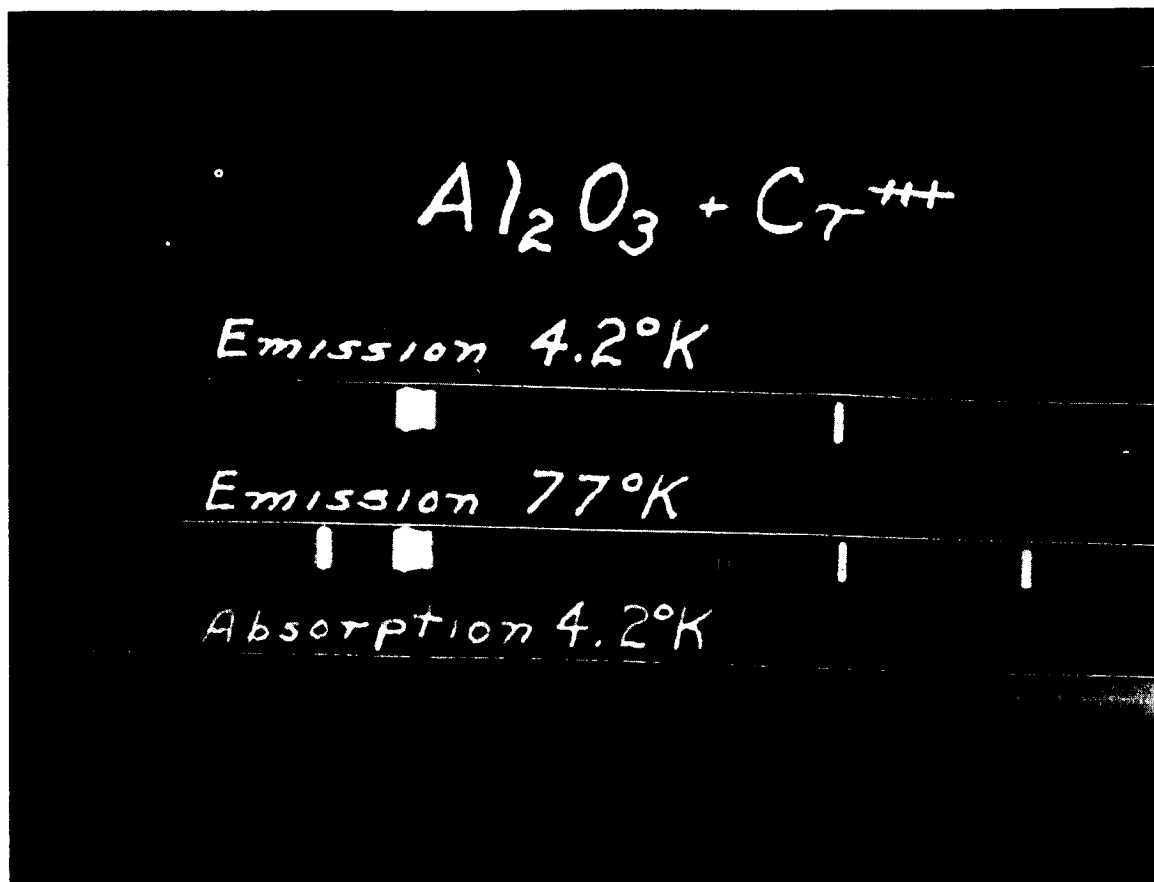
FIG. 1.8--Emission and absorption in dark ruby at 4.2°K, (from Schawlow[48]).

finally, at the very highest pump powers, these two were joined by the R_1 line. (In some instances the order of appearance of N_1 and R_1 was reversed.) Figure 1.9 shows the spectra obtained from the first N-line lasers.[51] The experiment offered dramatic proof that the two N lines stemmed from distinctly different pair types, as laser action from one excited level of a given physical system almost invariably pre-empts the build-up of excess population in the other excited states of the same system.

Final determination of the energy level schemes associated with the two N lines represents culmination of the effort of several workers. From the selective excitation data of Daly[52] and measurements of the absorption strengths of the two N lines as a function of temperature made by Kisliuk, Schawlow, and Sturge, the ground state exchange multiplet and two excited levels of the N_2-line pair were worked out.[53] Tentative assignment of the ground state exchange multiplet associated with the N_1 line was also made in reference 53, but subsequent measurements by Kisliuk proved this assignment wrong.[54] Kisliuk's temperature data is reproduced in Fig. 1.10, and the complete energy level schemes worked out by him are illustrated in Figs. 1.11 and 1.12. (The piezospectroscopic measurements of this thesis have provided strong confirmation of Kisliuk's work, as will be seen later.)

Kisliuk was able to fit the two ground state exchange multiplets found in the above-mentioned study to a biquadratic expression of the form (1.4); for the multiplet associated with the N_2 (7009 Å) line he found $J = 6.94$ cm^{-1} and $j = 0.14$ cm^{-1} ; for the N_1 (7040 Å) multiplet he found $J = -11.56$ cm^{-1} and $j = 0.19$ cm^{-1} . (The signs of both J and j have been altered from those listed in Kisliuk's original paper to make them conform to the opposite sign convention used here.) Thus two exchange couplings of moderate strength had been found so far, one ferromagnetic, the other antiferromagnetic. But since the antiferromagnetic coupling was too small, by more than an order of magnitude, to explain the Curie-Weiss constant of Cr_2O_3 , at least one more antiferromagnetic coupling remained to be discovered from the dark ruby spectrum.

6,919 A. 6,934 A.   7,009 A. 7,041 A.

WAVELENGTH ANGSTROM UNITS

6,900   7,000   7,100
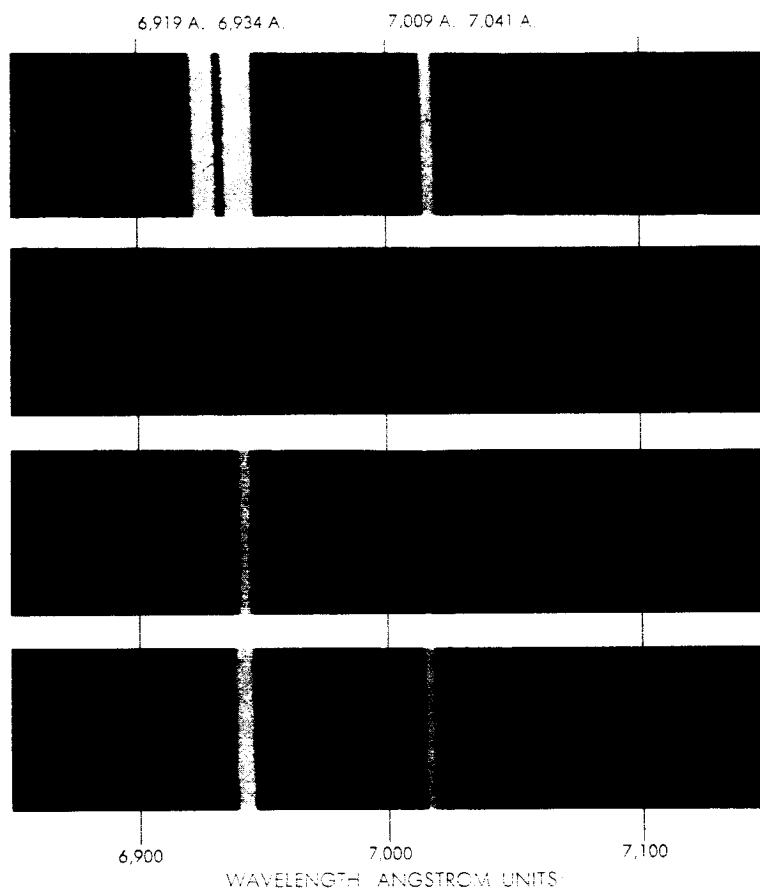
FIG. 1.9--N Line laser action in dark ruby. Top spectrum is ordinary
        fluorescence. Lower three spectra show laser action at
        increasing pump levels, (from Schawlow[51]).
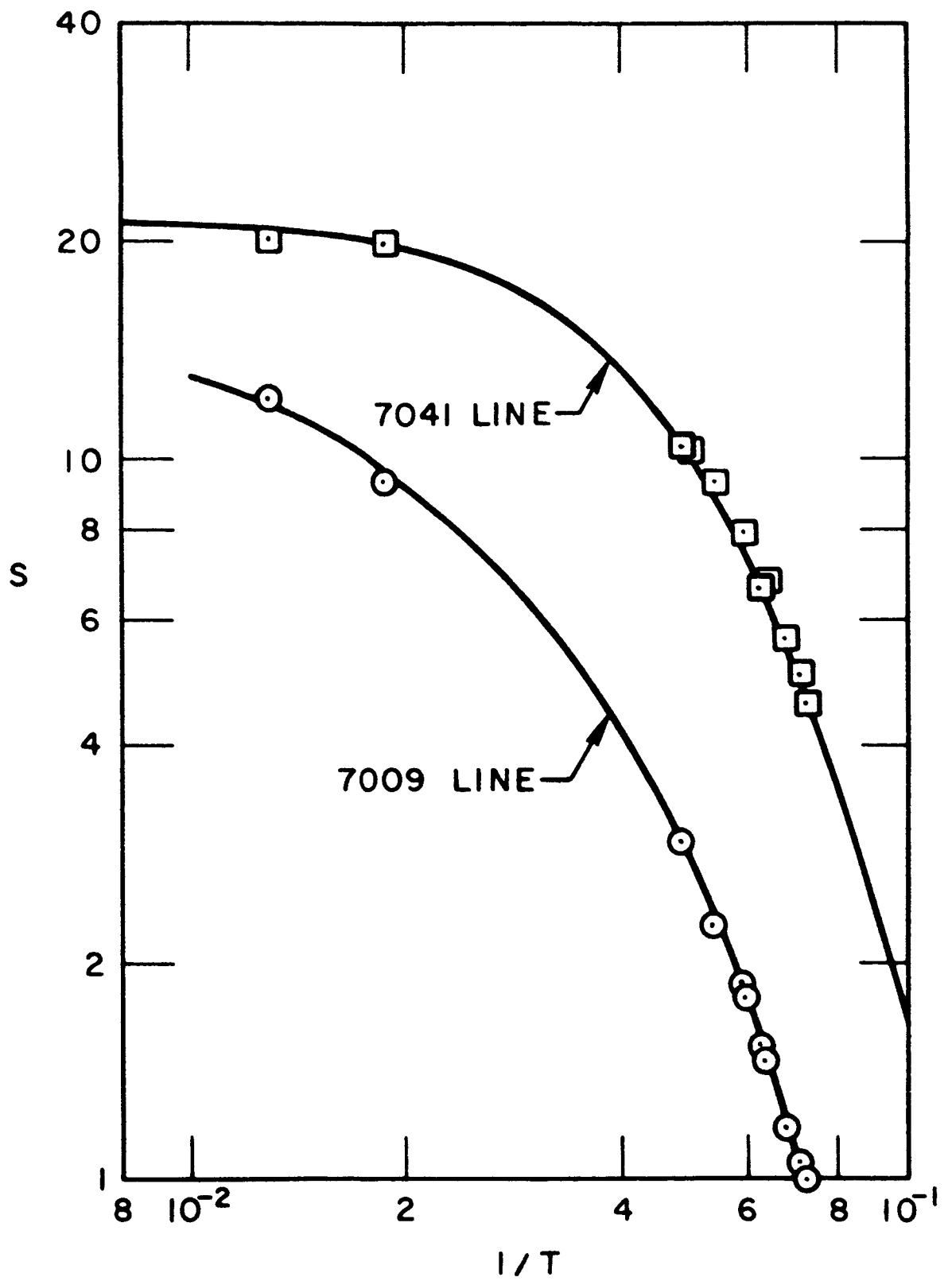
FIG. 1.10--Temperature dependence of N line absorption intensities,
(from Kisliuk[54]).
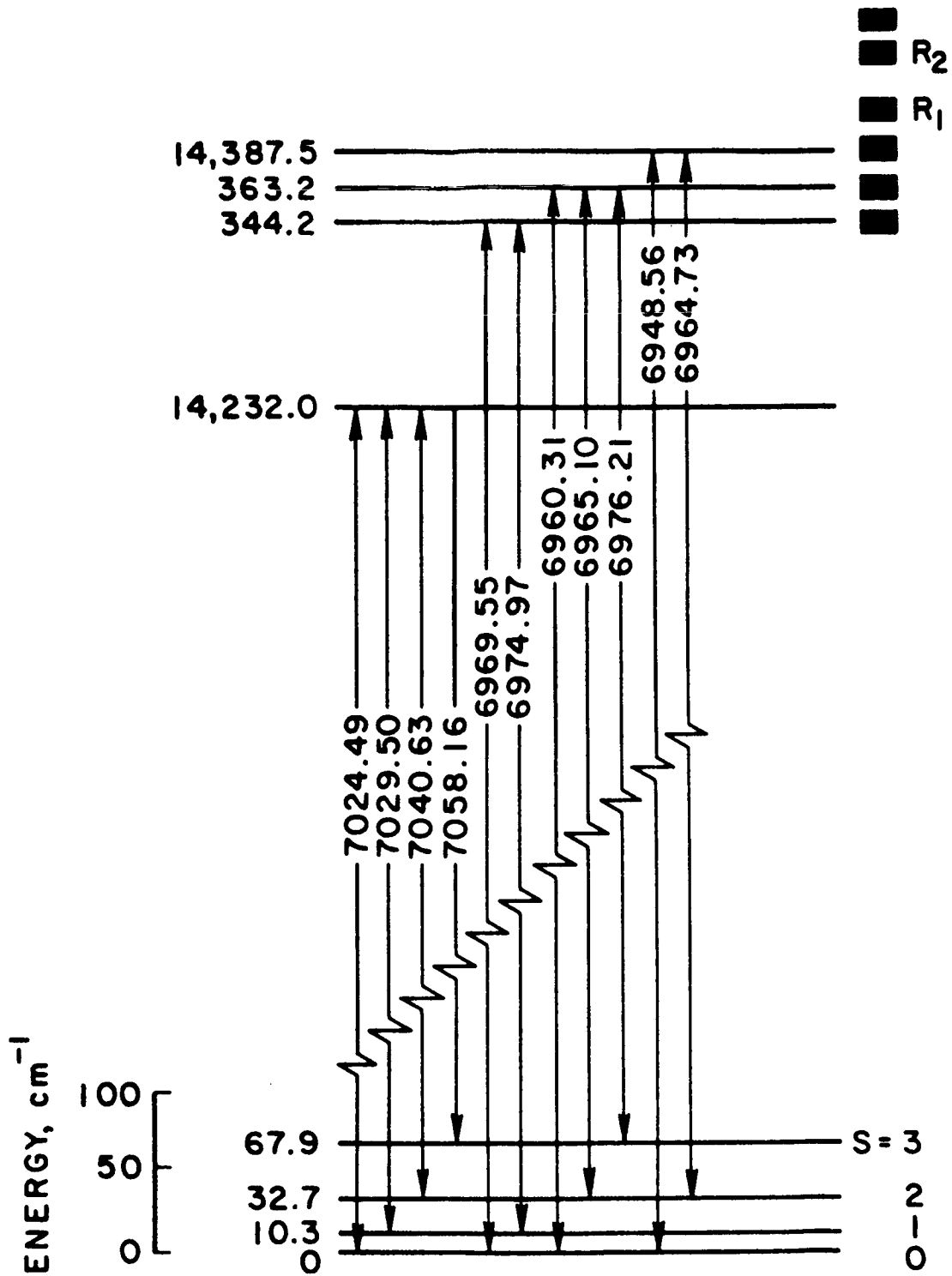
FIG. 1.11--Energy level scheme of pair type associated with N_1 , (from Kisliuk[54]).

R₂ → R_2

R_2

R_1

14,328.1
327.2
324.3
323.8
299.3
14,298.6

6977.37
6987.25
6994.07
6998.22

6977.81
6987.74
6995.01
6998.72

6979.44
6989.38
6996.80
6979.22

6991.43
7001.46
7012.48

6991.75
7001.81
7008.84
7012.88

ENERGY, cm^{-1}

100

50

0

42.9
35.0
20.4
0

S = 0
1
2
3
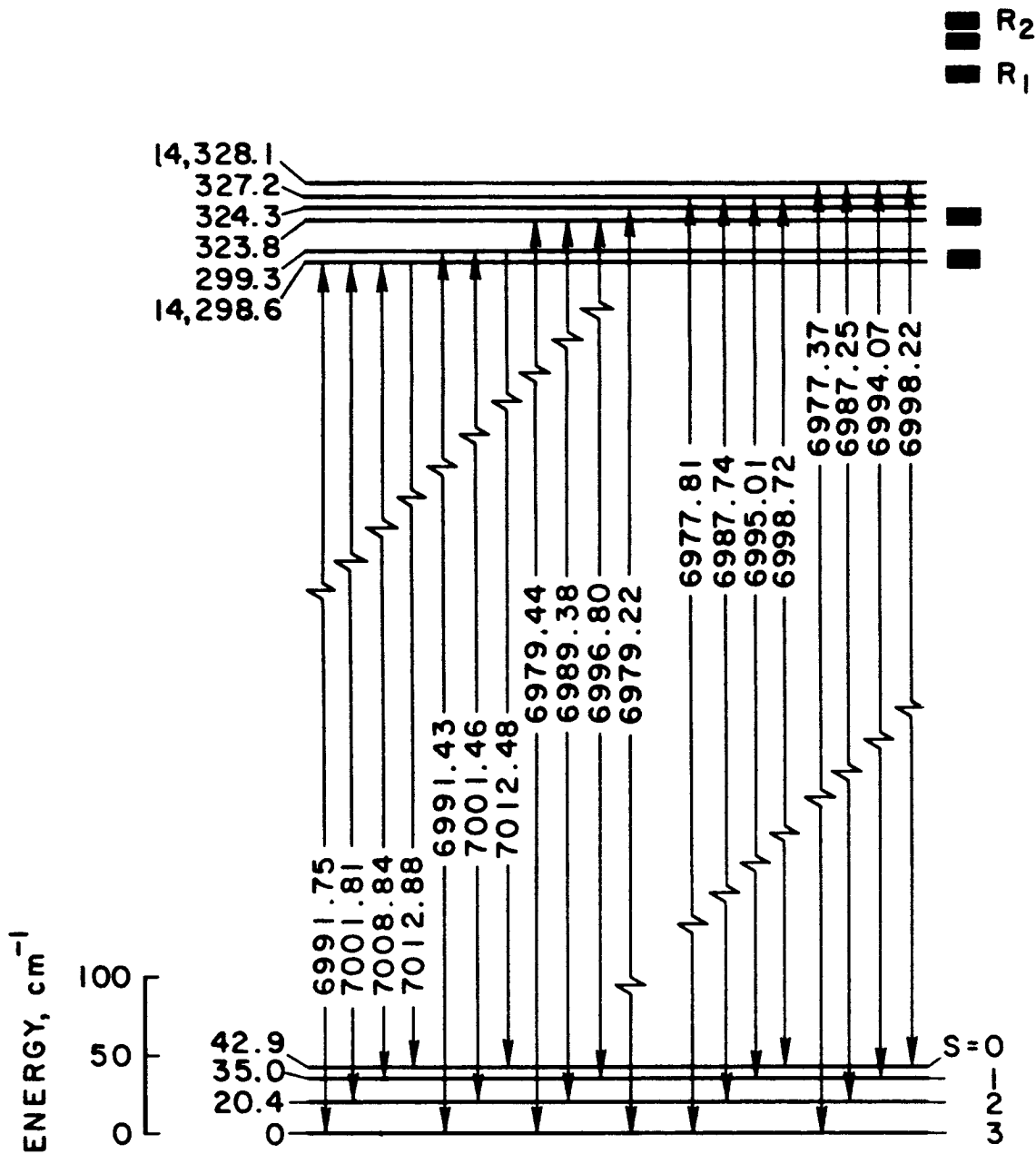
NOTE: UPPER LEVEL IS NOT TO SCALE

FIG. 1.12--Energy level scheme of pair type associated with N_2 , (from Kisliuk[54]).

In addition, the newly determined energy level schemes had yet to be assigned to specific near-neighbor pair types. The problem is very difficult in ruby, since the separation between ion centers increases slowly for the first through fifth nearest neighbors, as shown in Table 1.1, making it impossible to exclude any of these on the basis of a too large ion separation.[55]

TABLE 1.1

Near neighbor pair type	Separation between ion centers, $\mathring{A}$
1st	2.733
2nd	2.809
3rd	3.185
4th	3.504
5th	3.774
6th	4.766

It was thought that the known spin arrangement in Cr_2O_3 , as determined from neutron diffraction studies,[56,57] might provide a clue. The arrangement is shown in Fig. 1.13, as reproduced from a paper of Tachiki and Nagamiya.[58] From the figure it can be seen that in pure Cr_2O_3 the spin arrangement is antiferromagnetic for the first and second and third nearest neighbors, and ferromagnetic for the fourth. Of course, the complete spin arrangement in Cr_2O_3 may be dictated by the two strongest exchange couplings, say that of the first nearest and one other pair type; then there is no necessary relation between that spin arrangement and the signs of all the smaller exchange couplings.

In the meantime, Statz et al., thought that their paramagnetic resonance studies of Cr ion pairs in ruby[59,60] had provided the following information: (1) J values for all but the first, second, and fourth nearest neighbors could be declared less than or equal to 1 cm^{-1}; (2) J was of the order of 390 cm^{-1} for the nearest neighbors; (3) no
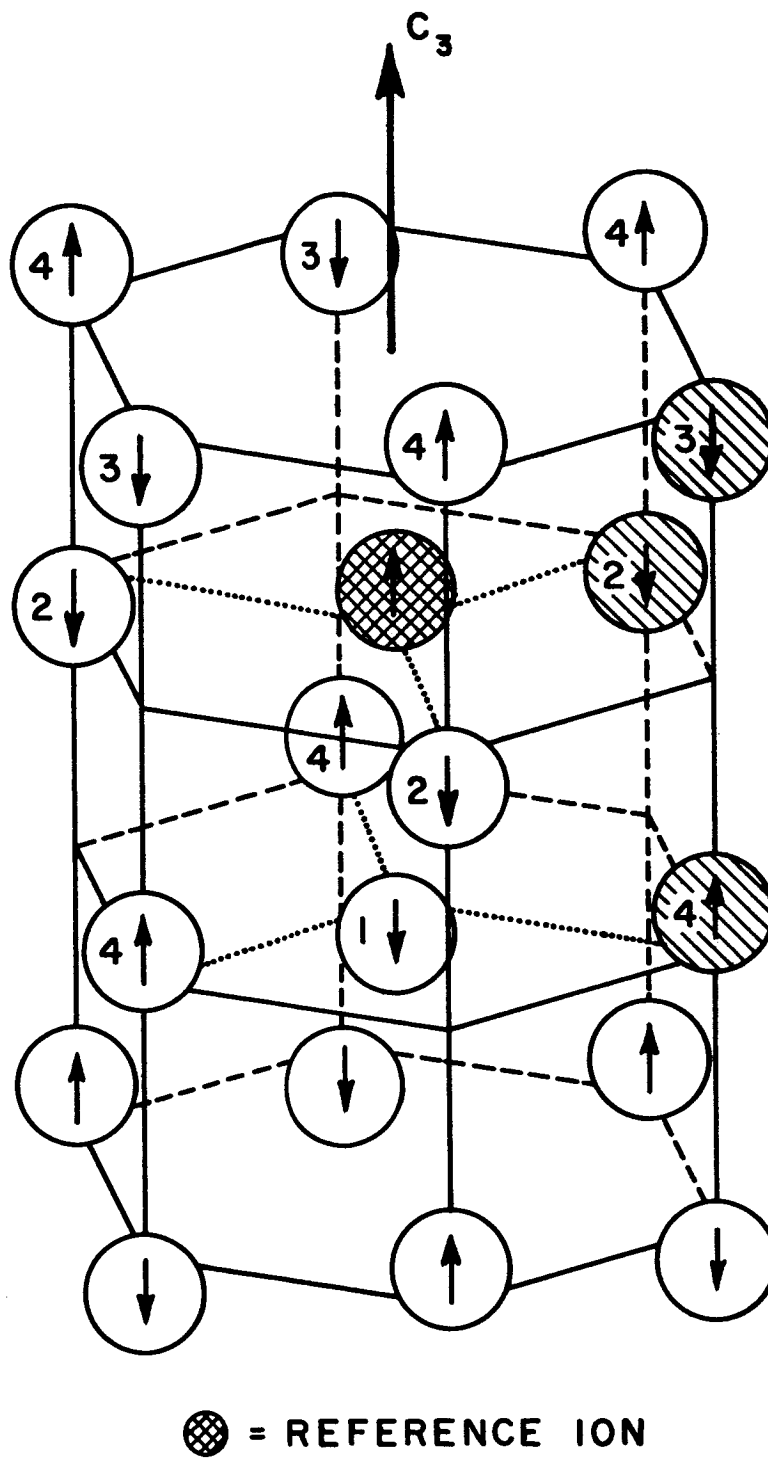
$\bigotimes$ = REFERENCE ION

FIG. 1.13--Antiferromagnetic spin arrangement in Cr_2O_3 as known from neutron diffraction studies. The reference ion is shown cross-hatched; only Cr ions are shown. The figure shows antiferromagnetic spin arrangements for pair types 1, 2 and 3, and a ferromagnetic arrangement for fourth neighbors, (from Nagamiya[58]).

signal could be found corresponding to the second nearest neighbors;
(4) the assignment of a resonance signal to the fourth nearest neighbors
was considered highly tentative. Doubt was first cast upon the validity
of Statz's work by J. Owen,[61] who pointed out the extreme technical dif-
ficulties involved in making unambiguous identification of the first
nearest neighbor pair resonance signal. But the optical studies mentioned
above undermine Statz's most fundamental assumption about the various
near neighbor pairs — that the splitting of the ground state of a pair
will be exactly the same as that observed for the isolated ions, 0.38 cm^{-1}
or 11.5 kMc. On the contrary, the observed splittings for at least the
first through fourth nearest neighbors are often several times that value.
For example, see the beautiful 1 cm^{-1} splitting of the 7041 Å line, or
the complex fine structure of the 7009 Å line reproduced in Fig. 1.14,
from reference 31. Since Statz' method for identifying resonance signals
with pair types depends critically on the value assumed for the ground
state splitting, those identifications would seem rather doubtful, at
least for the first four or five nearest neighbor types. It is no
wonder, then, that the conclusions of this report will often deviate
from those of Statz's paper.

Thus one is led to conclude that any attempt to assign the known
exchange multiplets to specific pair types on consideration of the above
two studies — neutron diffraction and previous paramagnetic resonance
studies — would amount to little more than guesswork. But this negative
conclusion is not without benefit, since it has provided at least part
of the impetus for the piezospectroscopic studies to be described here.
Although the original intent was merely to make positive identification
of the particular near neighbor types associated with the two N lines
possible, the piezospectroscopic studies have paid a rich harvest of
dividends over and above that first object. The accomplishments of this
work can be listed as follows:

(1) Positive identification has been made of the N_2 and N_1
multiplets with the second and fourth nearest neighbors,
respectively.
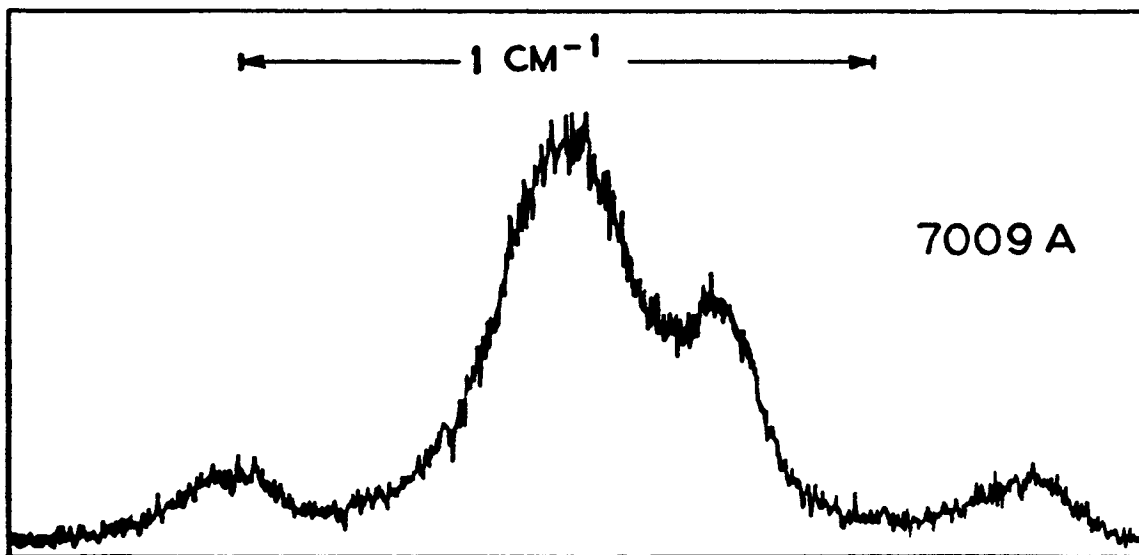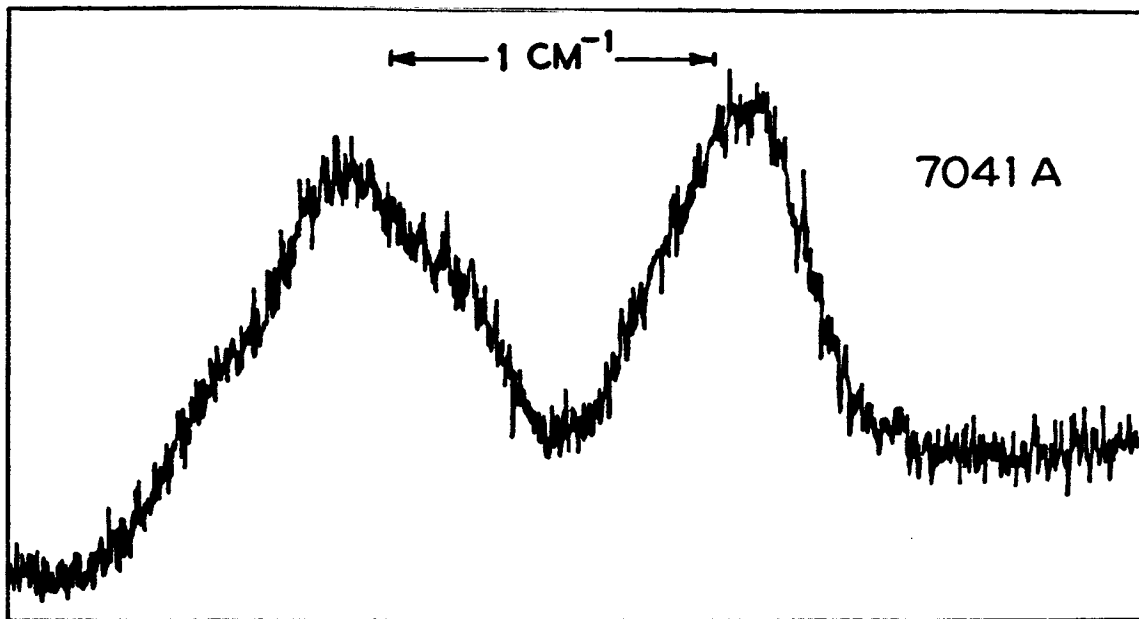
FIG. 1.14--Ground state splitting of N_1 and N_2 lines at $4.2°K$. Exactly the same relative intensities of the various components is seen at $1.4°K$. (from Schawlow[31]).

(2) The previously missing first and third nearest neighbor spectra have been found and the corresponding ground state exchange multiplets determined. A relatively large antiferromagnetic coupling ($J \sim -46$ cm^{-1}) was found for the third neighbors, in contrast to previous conclusions that the J value for this neighbor type was less than 1 cm^{-1} in absolute value. An even stronger exchange was found for the first neighbors ($J - - 183.5$ cm^{-1}).

(3) The four J values determined experimentally in dark ruby agree rather well with all that is known about the spectrum and magnetic properties of pure Cr_2O_3 , at least to within the limitations on accuracy imposed by the theories used in making the correspondences; for details, see Chapter V. It is hoped that the J values given by this report will stimulate the generation of better theories of magnetic ordering in Cr_2O_3 and related structures.

(4) Positions and piezospectroscopic sensitivities of the newly dis-covered lines should pave the way for a valid theory of the opti-cally excited state of ion pairs.

(5) The rather high sensitivity to mechanical stress of the frequencies of the lines investigated, especially that of the strongest line of the third neighbor complex, offer the possibility of making a readily and highly tunable laser.

II. THE PIEZOSPECTROSCOPIC METHOD

2.1. INTRODUCTION

This chapter describes the piezospectroscopic experiments with the object of identifiying the N lines and other pair lines with specific near neighbor Cr ion pair types. Background information relating to the symmetries of the host lattice and the locations of the various pairs relative to the symmetry axes of that lattice are given, leading to development of a scheme for interpreting the piezospectroscopic behavior of the pairs. In addition, a brief description of the techniques used in the orientation and cutting of the ruby samples is given, and, finally, the piezospectroscopic apparatus itself is described, along with techniques related to its use. Results of the piezospectroscopic experiments are given in Chapter III.

2.2. DISCUSSION

Experimental physics can be thought of as consisting of two phases — one passive, the other active. The passive phase was the more common mode of earlier times, as exemplified by the astronomical observations that led to Newtonian mechanics, or the early spectroscopic work that led to the quantum mechanics. More recently, the bulk of our information about the atomic world has come from observations in response to active prodding. Often the desired perturbation is produced by an externally-applied, static, magnetic, or electric field. But in solid state physics the effects of externally applied fields sometimes are masked by the effects of the usually much larger internal crystalline field. For example, Zeeman studies of line spectra in solids are often precluded by too-large residual linewidths due to internal strain. When such a situation arises, it is found that mechanical stress, unsophisticated

as it may be, often provides the only effective "handle" on the atomic system under study. This success can be explained by the fact that mechanical stress almost guarantees a certain percentage modulation of the internal field in question, no matter how large that field may be. And even when other probes can be used, the added information of a stress study may be just that necessary to allow a complete solution.

Thus, for example, in order better to understand the crystal field splittings of the ^2E level of Cr^{3+} in various noncubic host lattices, such as Al_2O_3 or Ga_2O_3 , A. L. Schawlow was led to try to induce such a splitting in the normally degenerate ^2E level of Cr^{3+} in MgO by the application of uniaxial stress along the (100), (110) or (111) axes.[35] A well resolved splitting was in fact produced, and was observed to increase in direct proportion to the applied stress. Stress sensitivity was such as to allow a splitting of approximately 0.6 cm^{-1} for a stress of 10 Kg/mm^2 (approximately 10×10^8 $dynes/cm^2$) applied along the (100) direction. (Although $dynes/cm^2$ are the truly correct units, the more practical laboratory units of Kg weight/mm^2 will be used here to avoid an unnecessary conversion, and by reason of the better "feeling" most physicists seem to have for the latter.) In a theoretical treatment by S. Sugano (also in reference 35), a calculation of the splittings, in which the crystal field was based on a point charge model, produced excellent agreement with experiment. However, the same model predicted a shift to the blue in the average position of the two components of the split line, by reason of the increased cubic field strength with application of pressure; the experimentally measured shift was to the red. The only plausible explanation, according to Sugano, was that the Racah parameter B (describing the coulomb interaction between the t_2 electrons of the Cr ion) was made to decrease faster with pressure than the corresponding increase of the cubic field. Nearly the same red shift was found for each of the two R lines of ruby (approximately -0.3 cm^{-1} for a stress of 10 Kg/mm^2), again roughly independent of the direction of applied stress. In addition to their intrinsic theoretical interest, the above-mentioned studies were valuable, at the time they were made, for suggesting that the limit to line narrowing at low temperatures can

be attributed to a residual microscopic strain field. Now they are valuable for purposes of comparison with the stress induced shifts of the N lines.

Piezospectroscopic studies of the ruby N lines were first made by Kaplyanskii and Przhevuskii, who concentrated their efforts on the N_1 line.[62] They observed an apparent splitting which was highly dependent upon the direction, relative to the crystallographic axes, of the applied stress. Now in ruby, some of the near neighbor pair types can lie in any one of three possible spatial orientations. In an unstressed crystal, these three orientations are energetically equivalent, by virtue of the three-fold rotation symmetry operator (C_3) of the host lattice, and only one line is produced. But C_3 will be destroyed by application of stress to the crystal along any direction, save that of the C_3 axis itself, with the result that the different pair orientations are no longer equivalent. Again here, as in the study of the R_1 and R_2 lines, there is no longer a question of splitting the energy levels of one particular pair, since all orbital degeneracies already have been lifted. By observations on the splitting patterns produced for a few different sample orientations $(P \parallel C_2 , \dot{P} \parallel C_3 , P \perp C_2$ and $C_3 , \angle PC_2 = \pi/4)$, and on the rather complete polarizations of some of the individual stress-produced components, Kaplyanskii was led to assign the N_1 line to the sixth nearest neighbors, although he admitted that his data could be fit almost equally as well by the second neighbors.

Since the crystals available to us were of much higher quality than those used by Kaplyanskii, and since we intended to extend his observations anyway, especially to the other prominent pair lines, we have considered it worthwhile to repeat Kaplyanskii's experiments. Hence his results will not be reproduced here, but instead we merely note that those results (as far as they went) are in good agreement with our own. But we strongly prefer the second of the two assignments suggested by Kaplyanskii for the N_1 line, both on grounds of our extended stress data, and for purely theoretical reasons related to the observed strength and sign of the exchange coupling associated with that line.

2.3 SYMMETRIES OF Al_2O_3 AND LOCATION OF THE PAIRS

The Al_2O_3 host lattice belongs to the point symmetry group D_{3d} (Schoenflies notation), alternately known as $\bar{3}m$ (Hermann-Mauguin symbol). A picture of the symmetry elements and the corresponding stereographic projection are shown in Fig. 2.1. The group D_{3d} formally contains five classes in addition to the identity operator: C_3, C_3^2, C_2 (three of these); m(mirror plane — three of these also); and an inversion center. In sapphire (pure Al_2O_3) or ruby, the C_3 axis is also known as the optic axis, since the index of refraction for light polarized parallel to this axis is different from the index for light polarized perpendicular to it; this fact allows the C_3 axis to be located with the aid of a pair of polarizing filters. The other axes can be located only with the aid of x-ray techniques; more about orientation later.

The location of a Cr ion pair will be described in terms of the line joining the centers of the two ions, or the "pair-axis." Among the pair types under consideration here, only two — the first and fifth nearest neighbors, have axes parallel to the C_3 axis. Hence these two are only one of a kind, and their lines should never split under application of stress. But the axes of all the others — second, third, fourth, and sixth — lie at some angle to ; in this latter situation the C_3 operator produces two additional equivalent pairs from any given one. Thus, as mentioned previously, the lines produced by any member of this second group should undergo a two- or three-fold splitting for all but a few special directions of the applied stress. Figures 2.2 and 2.3 show the locations of the various pair-axes.

It should be noticed from Fig. 2.2 that the second, third and fourth nearest neighbor pairs all lie in a common mirror plane. To specify completely the locations of these three, it is necessary to establish a convention for measuring angles in the mirror plane, relative to the C_3 axis. In the one chosen, the zero angle is perpendicular to C_3, and the quadrant containing the second and third neighbor axes arbitrarily made positive. Thus the second and third neighbors lie at $+11.7^\circ$ and $+30.4^\circ$, respectively, while the fourth lies at -38.3°.
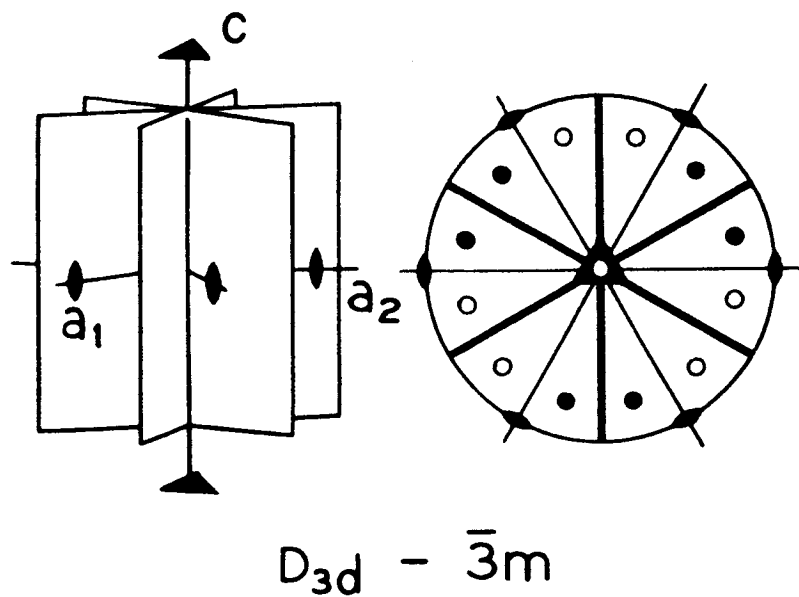
FIG. 2.1--Symmetry elements of the point group D_{3d} and their stereographic projection. (from Wood[64])

Second nearest neighbors

Mirror plane

$\theta = 11.7^\circ$

C_3

C_2
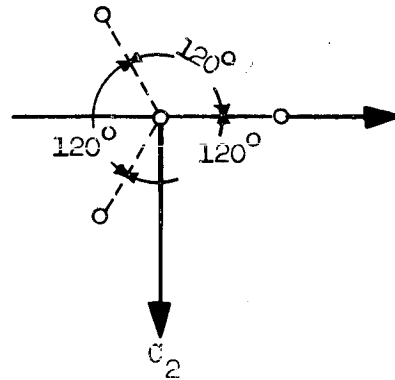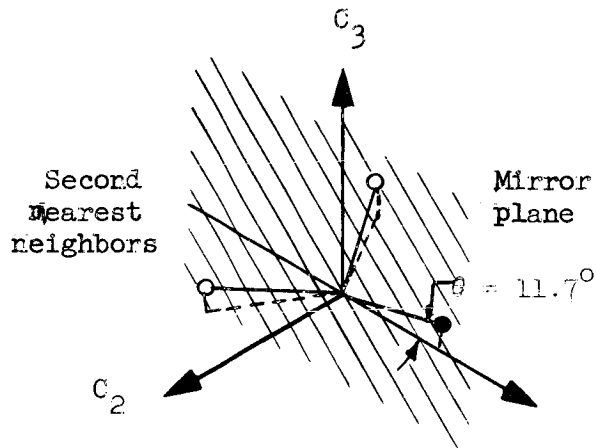
b) Looking down the C_3 axis

Third nearest neighbors

$\theta = 30.4^\circ$

C_3

C_2

Fourth nearest neighbors

$\theta = -38.3^\circ$

C_3 ± 90°

-38.3°
Fourth N.N.

+ 30.4°
Third N.N.

+30.4°

-38.3°

± 90°
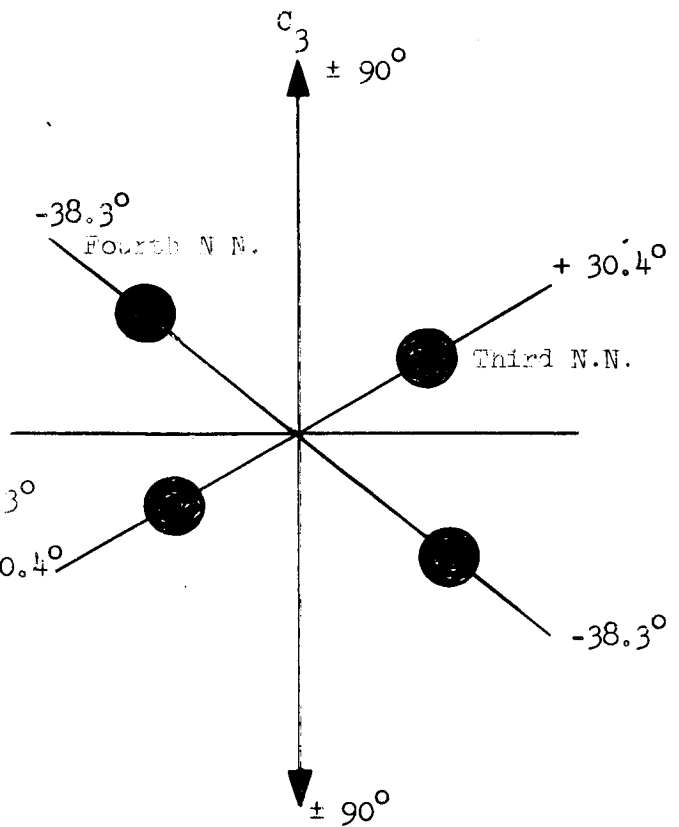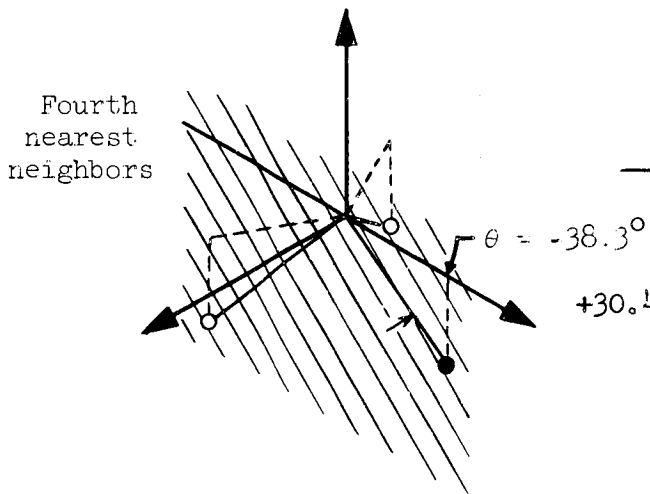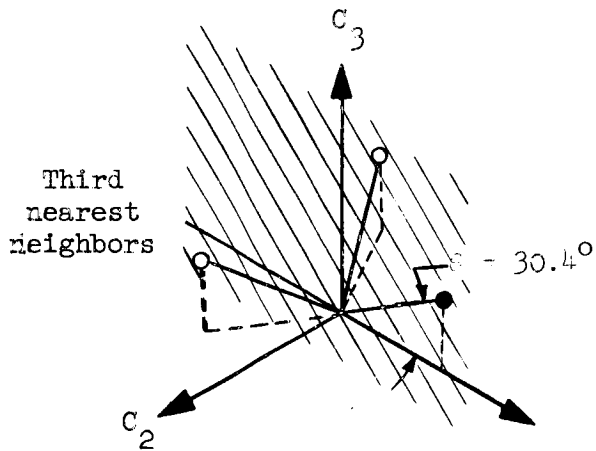
a) Location of pairs

c) convention defining angle θ.

FIG. 2.2--Locations of the second, third and fourth neighbor pair axes.

- 36 -
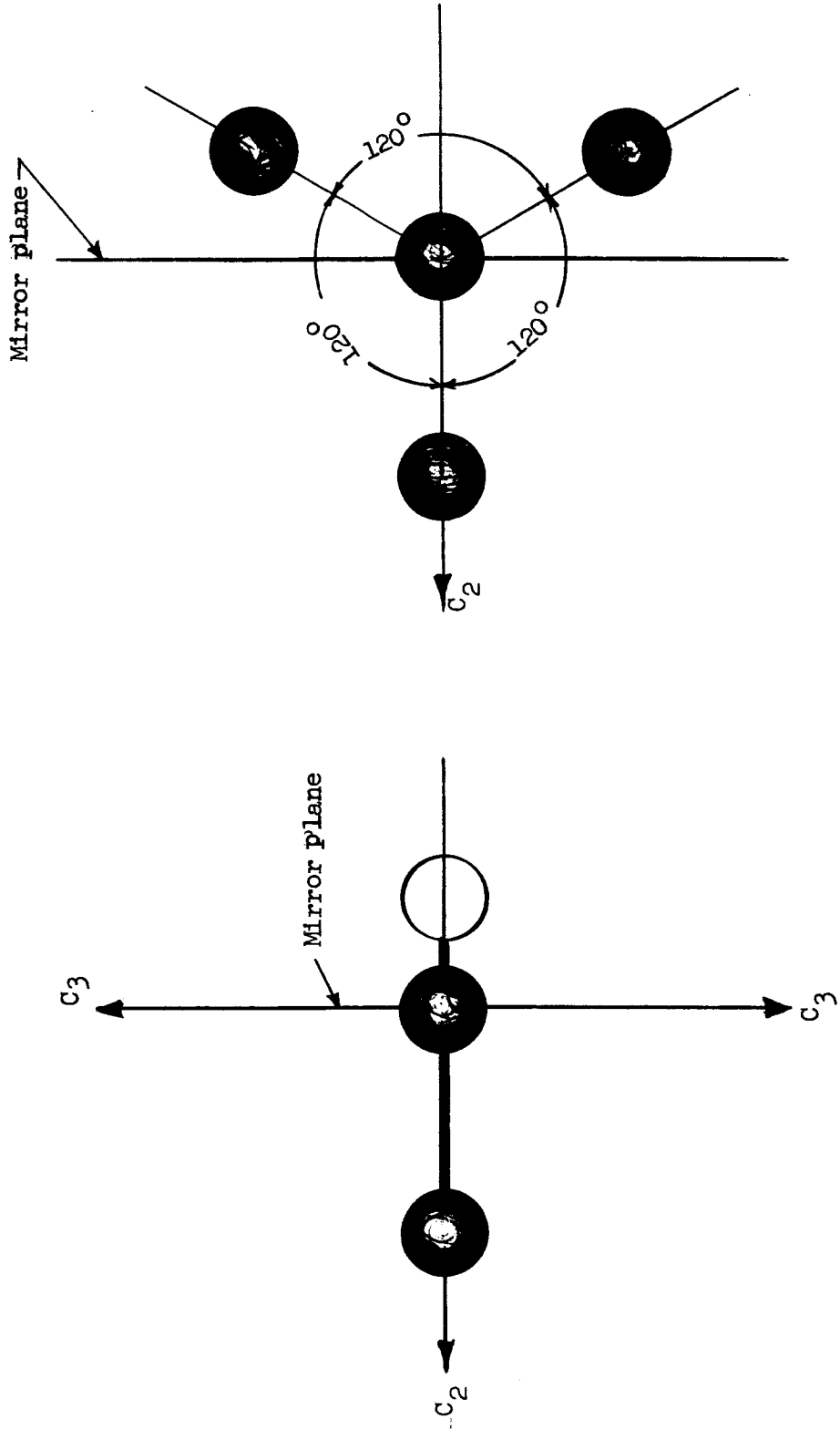
FIG. 2.3--Location of sixth nearest neighbor pair axes.

Use of the pairs themselves in the definition of the angular convention allows the most direct relation possible between the actual pair location in the mirror-plane slab from which the samples are cut and certain features of the back-reflection Laue photograph used in its orientation. The above should not be constructed to imply that plus and minus ends can be defined for the C_3 axis; on the contrary, the $+90^\circ$ and -90° directions are identical, or to put it another way, all possible directions are encompassed in traversing from -90° through 0° to $+90^\circ$ (see Fig. 2.2c).

Finally, it should be pointed out that the sixth nearest neighbors are in a class by themselves, since their axes lie parallel to the C_2 axes (see Fig. 2.3). Thus they lie at right angles to the other pairs, and this fact will be useful in developing a scheme to differentiate between lines due to them and lines due to the second nearest neighbors.

2.4. IDENTIFICATION OF THE PAIR LINES

From the above it is obvious that lines due to the first and fifth nearest neighbors can be readily identified by their refusal to split under stress. Furthermore, since the exchange coupling is certainly known a priori to be much larger for the first than for the fifth nearest neighbors, knowledge of the exchange multiplet should allow the identification to be complete. It is not nearly as easy to make positive identification of the others; one must somehow take advantage of the relatively large angular separations between their various axes. The idea used here is that the energy levels of a pair should be more sensitive to stress applied along the pair axis than to stress applied at right angles to it. Although the above idea may seem a bit arbitrary, originally it was not without a rather clear rationale. That is, it was thought that the observed shifts would be due in the main to induced changes in the exchange coupling. Pushing the ions together would increase the overlap of their electronic wavefunctions, thereby increasing the exchange coupling; whereas stress applied at right angles, in tending to push the ions apart, would have an opposite effect. On the other hand, experiment has shown that modulations of the exchange coupling can account

for only a small fraction of the observed shifts. But those same experiments have shown also that the more general notion that the energy levels of a pair should be most sensitive to stress applied along the pair axis is indeed correct.

The above can be made less vague by postulating that the induced shift should be directly proportional to the component of strain in the direction of the apir axis. Figure 2.4 illustrates the basic mechanics involved. The sample is a long rectangular rod of square cross-section, with a uni-axial stress S_0 applied parallel to its long dimension, the "sample-axis." The axis of the ion pair in question lies cocked at an angle ϕ to the sample axis. The stress parallel to the pair axis can be computed from the simple relation[63]

$$S(\phi) = \frac{S_0}{2} \tau (1 + \cos 2\phi) \quad . \qquad (2.1)$$

Assuming an elastically isotropic material with Young's modulus Y and Poisson's ratio ρ , the strain $e(\phi)$ along the pair axis can be written

$$e(\phi) = \frac{S_0}{2Y} \left\{ (1 - \rho) + (1 + \rho) \cos 2\phi \right\} \quad . \qquad (2.2)$$

Now consider a fan of samples cut from a common slab containing the pair axis and spanning a range of 180°. With the exception of a term constant in ϕ which will be of no real interest here, the frequency shift $\Delta\tilde{\nu}$ for a constant magnitude of stress will undergo a very simple variation as the samples are tested in order, that is

$$\Delta\tilde{\nu}(\phi) = \Delta\tilde{\nu}_0 \cos 2\phi \quad . \qquad (2.3)$$
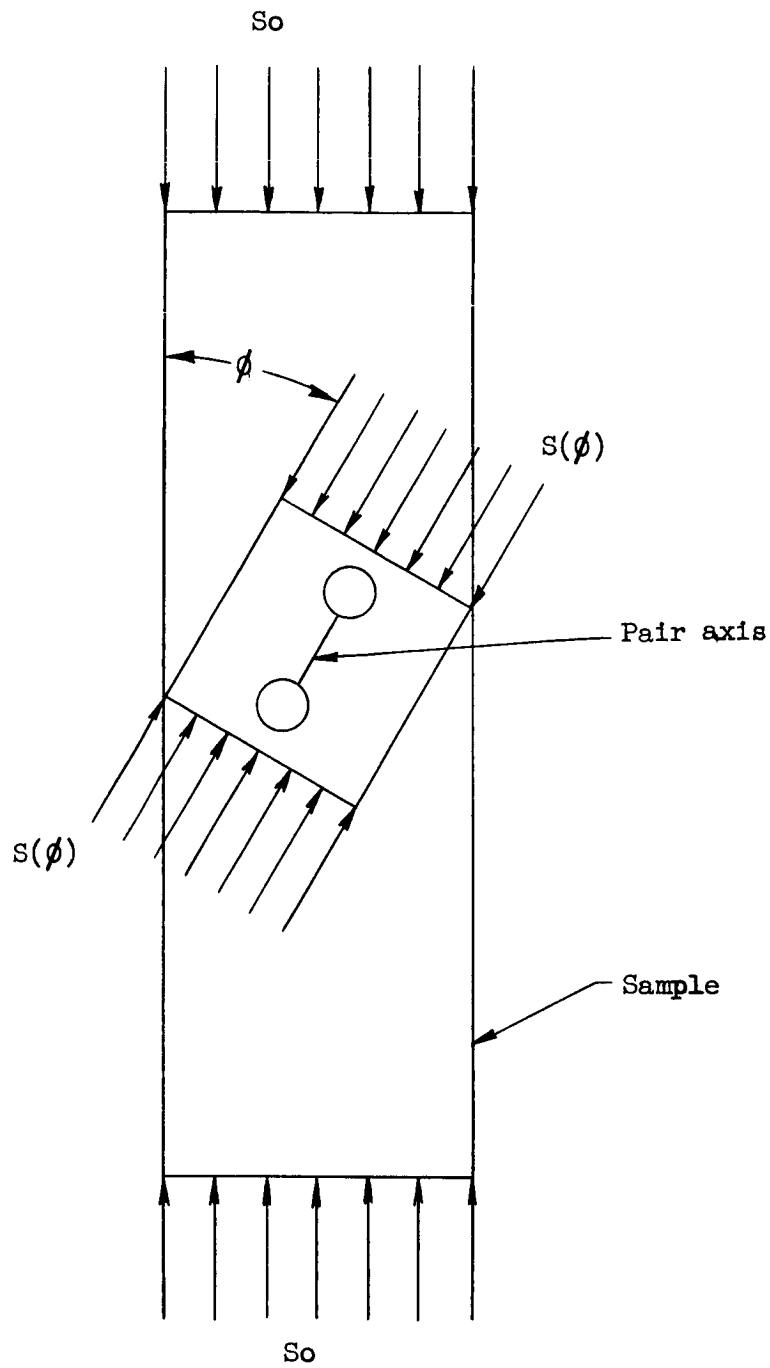
FIG. 2.4--Mechanics of sample under stress.

We are now ready to compute the splitting pattern expected for the pair types that are three of a kind. The situation is illustrated in Fig. 2.5. Here YZ is the mirror plane from which the samples are cut; the Z axis represents the C_3 axis. Inclination of the sample axis is described by the angle Θ . For purposes of illustration, three pairs are shown with axes tilted up 30° from the plane normal to C_3 ; one of the three lies in the YZ plane (hereafter known as I), and the other two out of it (pairs II and III). For pair I, we have $\phi = \Theta - 30^\circ$. For pairs II and III, several intervening steps of trigonometry are required to derive the relation

$$\cos 2\phi = 0.439 \cos 2(\Theta + 49^\circ) - 0.561 \qquad .$$

The result of plugging these two relations into expression (2.3) is illustrated graphically in Fig. 2.6a. The above example corresponds to the third nearest neighbors. Figure 2.6b shows the results of a similar computation for the fourth nearest neighbors.

Several qualitative features of the curves of Fig. 2.5 should be pointed out here. Notice that in each case the curve corresponding to pairs II and III has about half the peak to peak amplitude of the curve corresponding to pair I, and that the smaller amplitude curve is shifted about 90° from the larger one. The latter fact can be readily understood by observing that for the third and fourth neighbors the three pair axes of each type form an approximately mutually orthogonal set of directions. Thus, for these two pair types, when stress is applied along pair I, it is approximately at right angles to II and III. Furthermore, the two sets of curves form a complementary set — the one being very approximately the mirror image of the other across the 0° line.

By way of contrast, Fig. 2.7a shows the splitting curve calculated for the second neighbors — here the amplitude ratio between the curve for pair I and that for pairs II and III is greater, but the angular shift between them is considerably smaller. Figure 2.7b shows the curve calculated for a sixth neighbor pair; now the II and III curve has the larger amplitude, the curve for I being a constant, since the stress is always applied at right angles to it, regardless of the value of Θ .
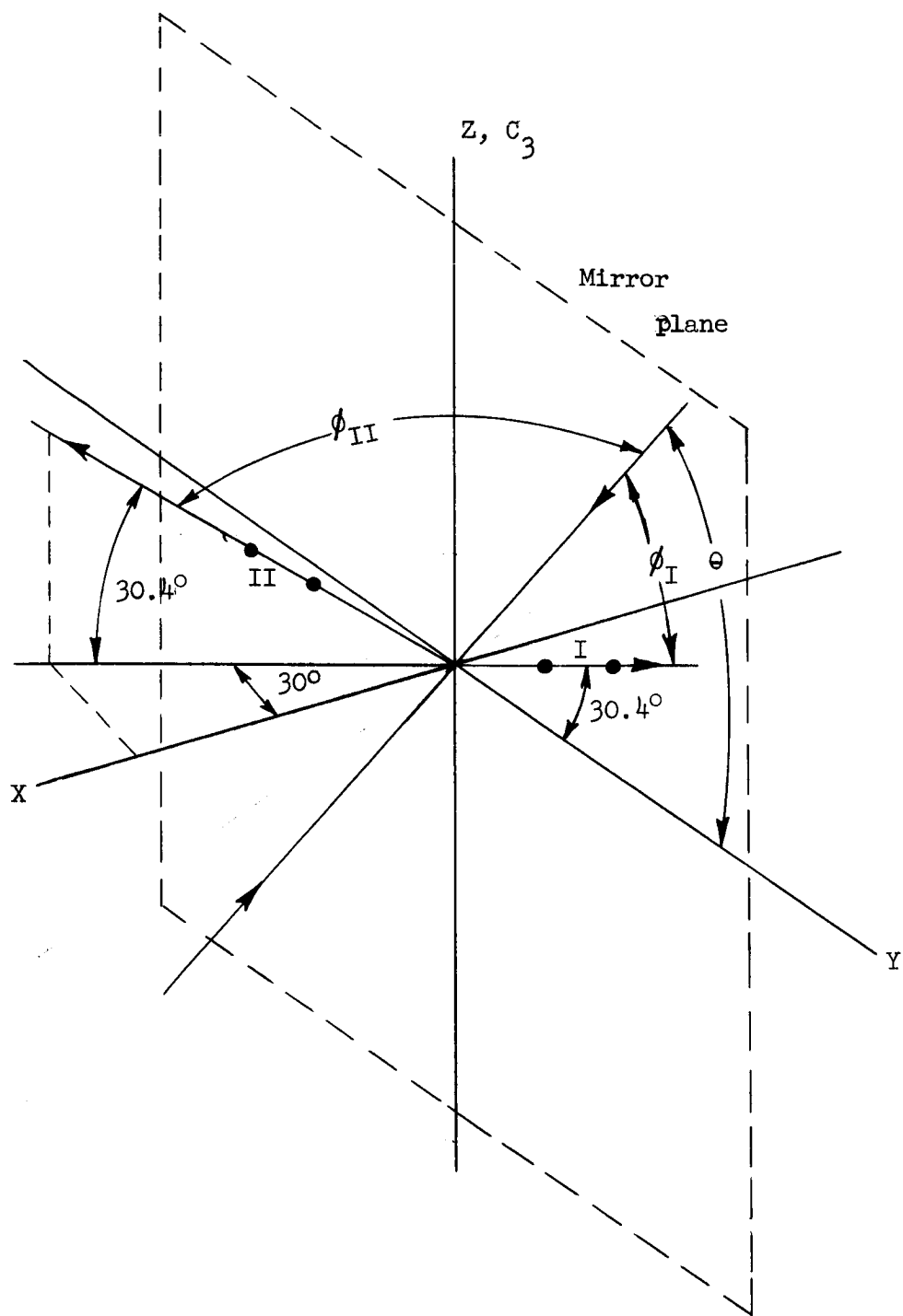
FIG. 2.5--Diagram showing angles used in computing splitting pattern for
for third neighbors.
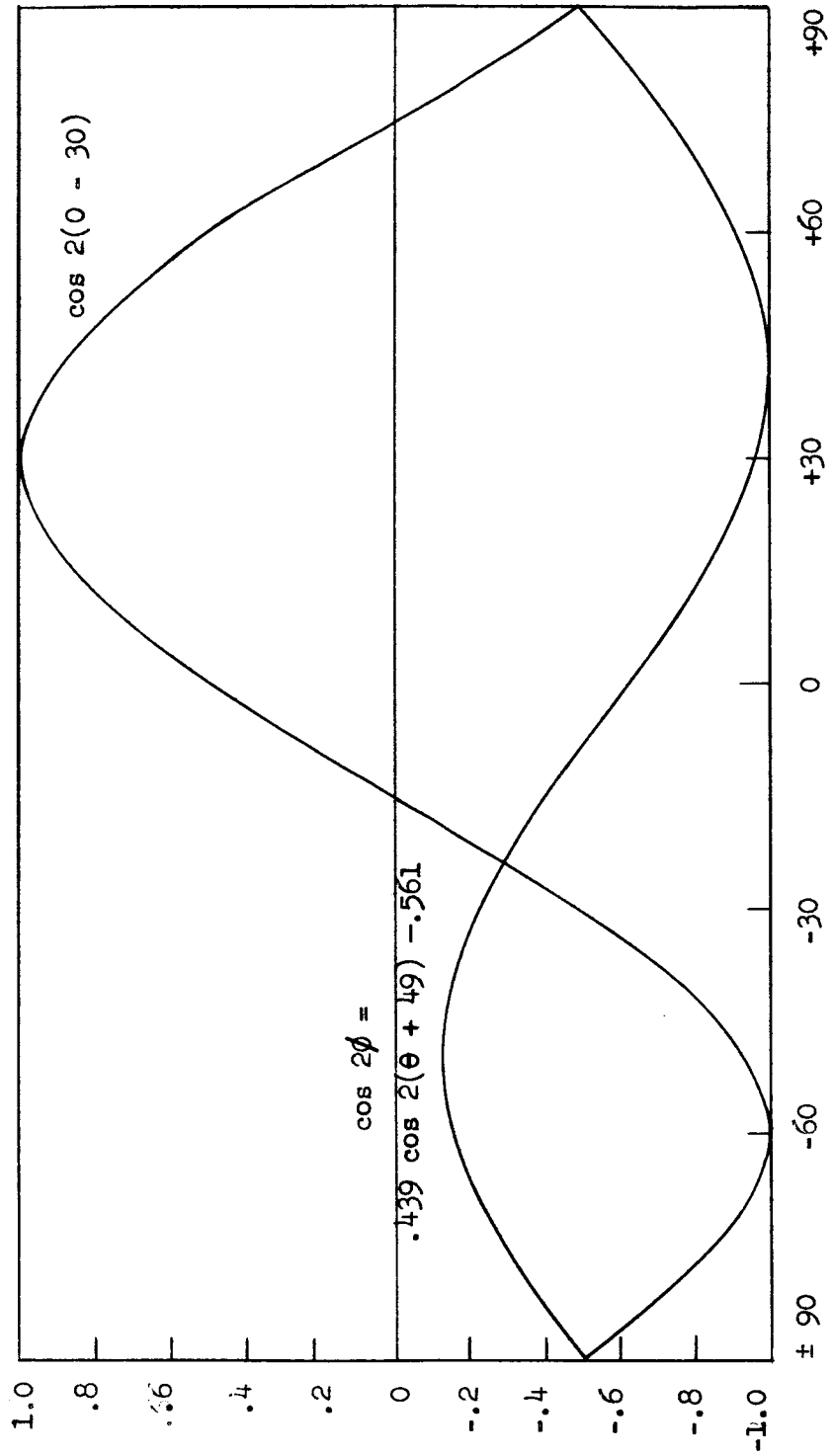
FIG. 2.6a--Predicted third neighbor splitting pattern.

cos 2(θ - 30)

cos 2φ =

.439 cos 2(θ + 49) - .561

cos 2(θ + 38.3°)

.55 cos 2 (θ – 58.1)–.45
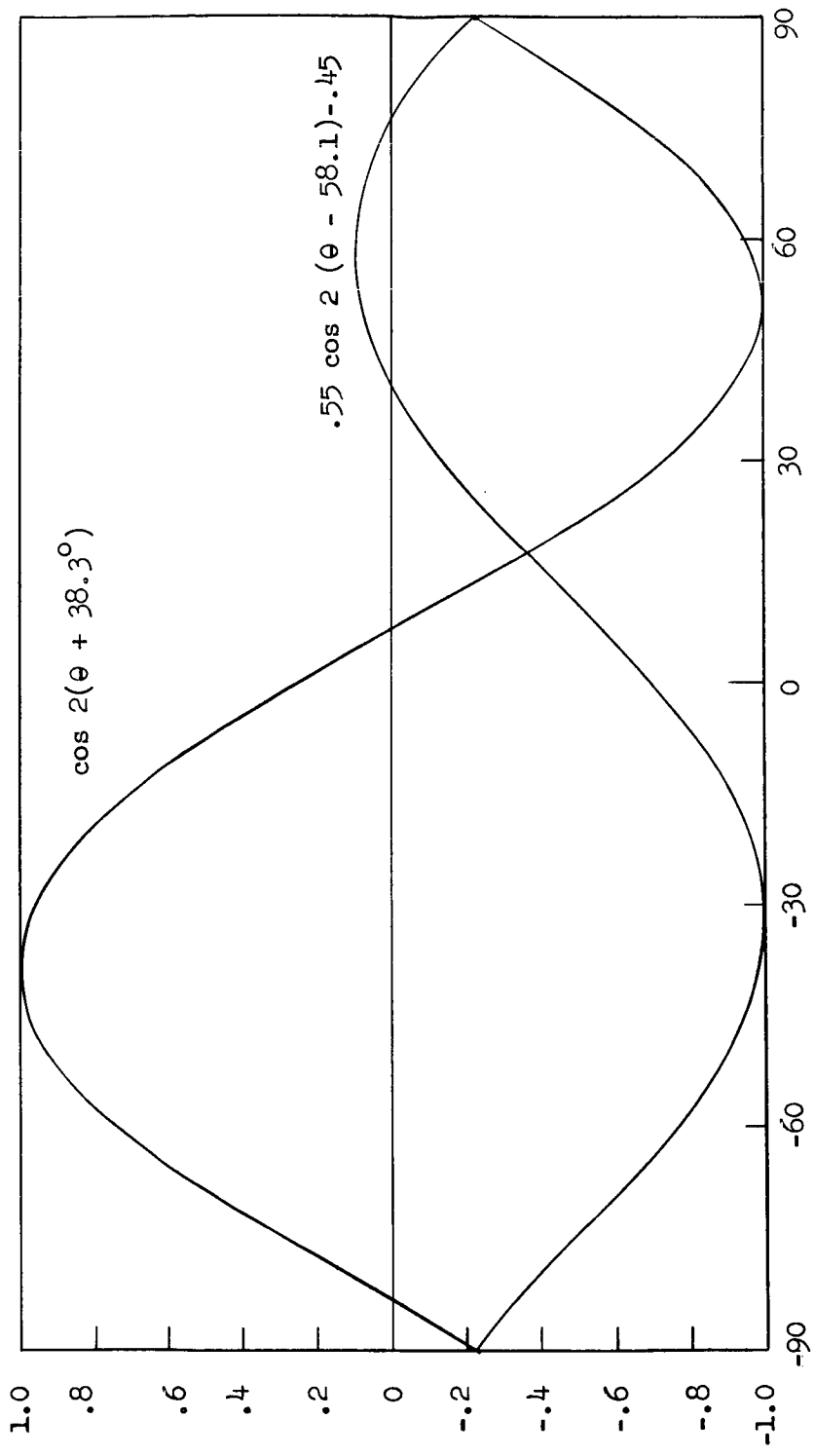
FIG. 2.6b--Predicted fourth neighbor splitting pattern.

$$\cos 2 (\theta - 11.7^{\circ})$$

$$.28 \cos 2(\theta + 22.5^{\circ}) - .72$$

(a)

$$.75 \cos 2\theta - .25$$
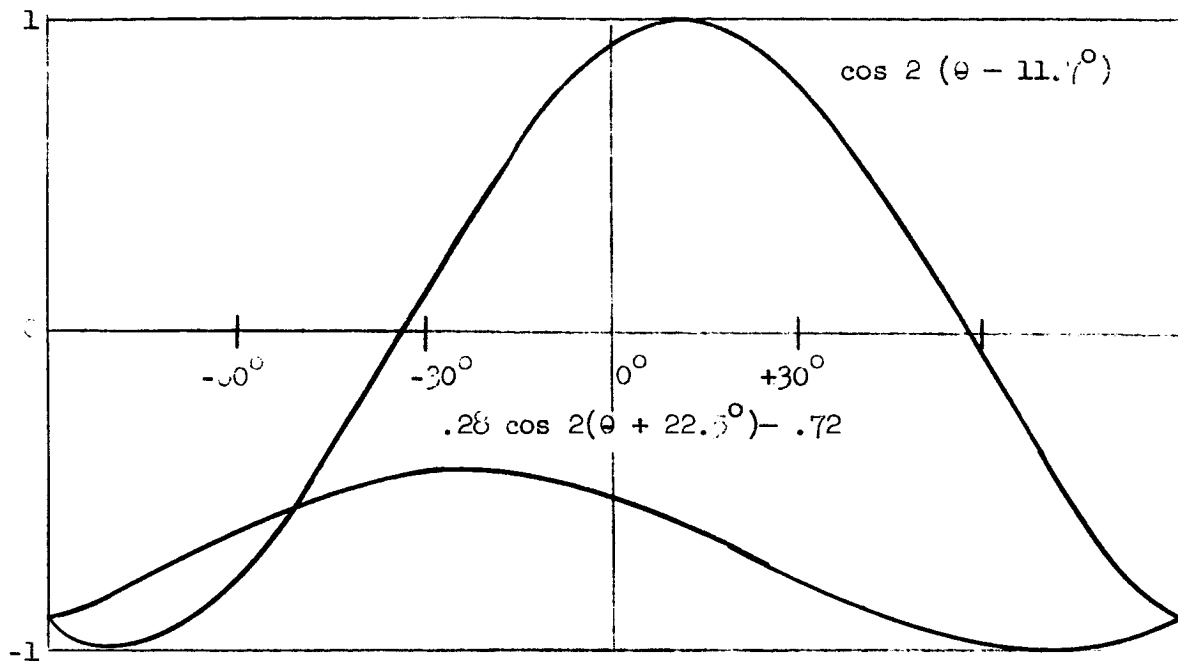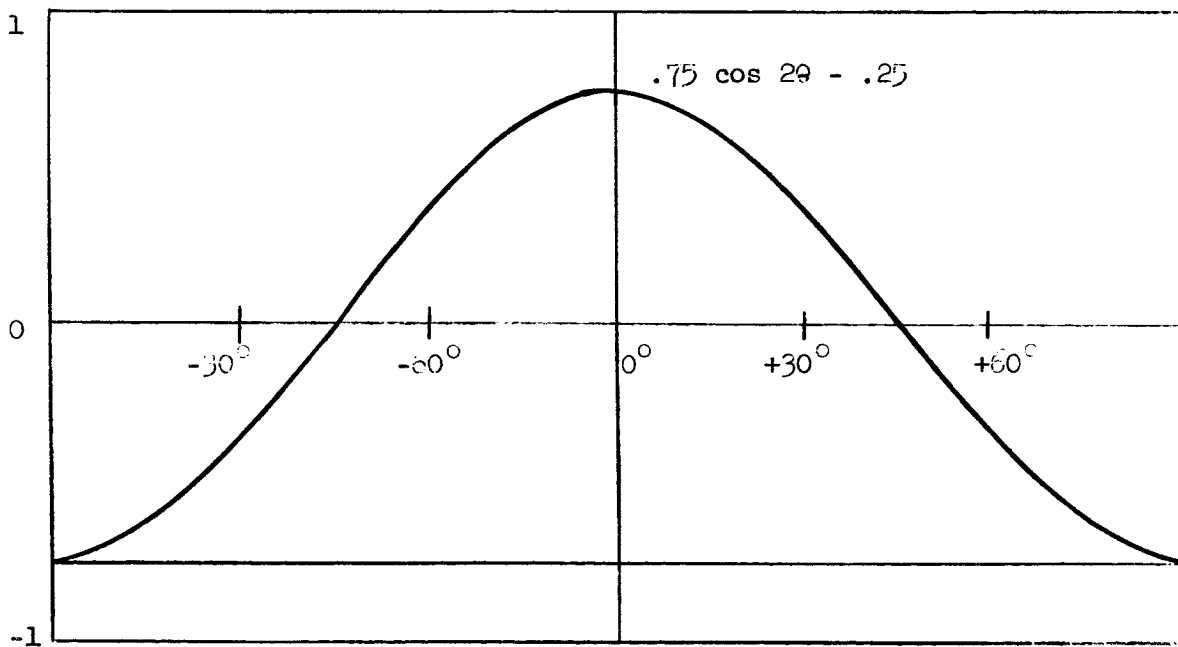
(b)

FIG. 2.7--(a) predicted second neighbor splitting pattern. (b) Predicted sixth neighbor splitting pattern.

Thus, the scheme for identifying pair types consists simply in trying to match up the observed splitting patterns with the patterns computed above. Although the above is obviously an over-simplification, the number of choices possible in the assignment of a given line to a pair type is so limited (only three or possibly four) that no more complicated theory has been found necessary.

2.5. ORIENTATION AND CUTTING OF THE SAMPLES

Except for an initial rough location, by optical means, of the C_3 axis of the boule from which the samples were cut, all orientation was done with the aid of back-reflection Laue photographs. The essential elements of a Laue camera are shown in Fig. 2.8. A beam of white x-rays passes through a hole in the film and strikes the sample. Usually, the minimum wavelength available is sufficiently short to allow satisfaction of the Bragg condition for all atomic plane spacings and angles. Hence the various atomic planes are able to reflect the beam back onto the film, much as a set of plane mirrors would reflect a beam of light.

Since the Al_2O_3 lattice contains a center of inversion, there is a one-to-one correspondence between the symmetry of the Laue spot pattern and the crystal symmetry.[64] This fact makes identification of the various symmetry axes very easy. Figure 2.9a shows the beautiful spot pattern produced when the x-ray beam is parallel to the C_3 axis; three mirror planes can be identified in it in addition to the three-fold rotation symmetry. By contrast, the pattern shown in Fig. 2.9b has but one symmetry — the two-fold rotation of the C_2 axis to which the x-ray beam was parallel.

After a pattern such as Figs. 2.9a or 2.9b had been obtained, small angular corrections could be made on the crystal holder, such that the crystal axis in question would be parallel to the x-ray beam direction to within about 0.2° or better. The holder was so arranged that the information thus obtained could be transferred accurately to the diamond saw used for sample cutting; whenever a crystalline axis was located it was permanently marked by cutting a plane normal to it. Thus, for

Laue spots

Film

X-ray beam

Zone axis

Atomic planes
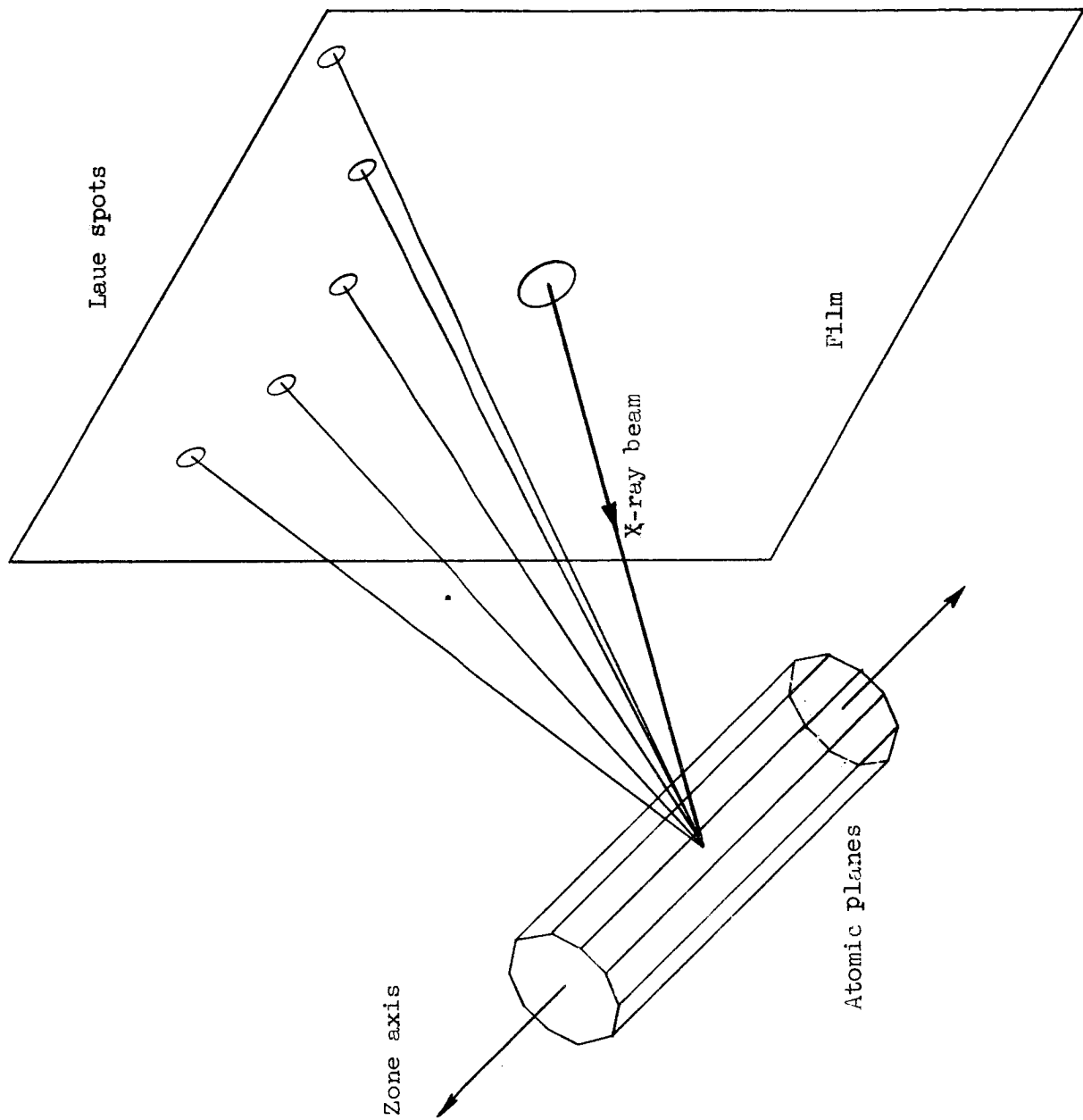
FIG. 2.8.—Elements of Laue Camera.
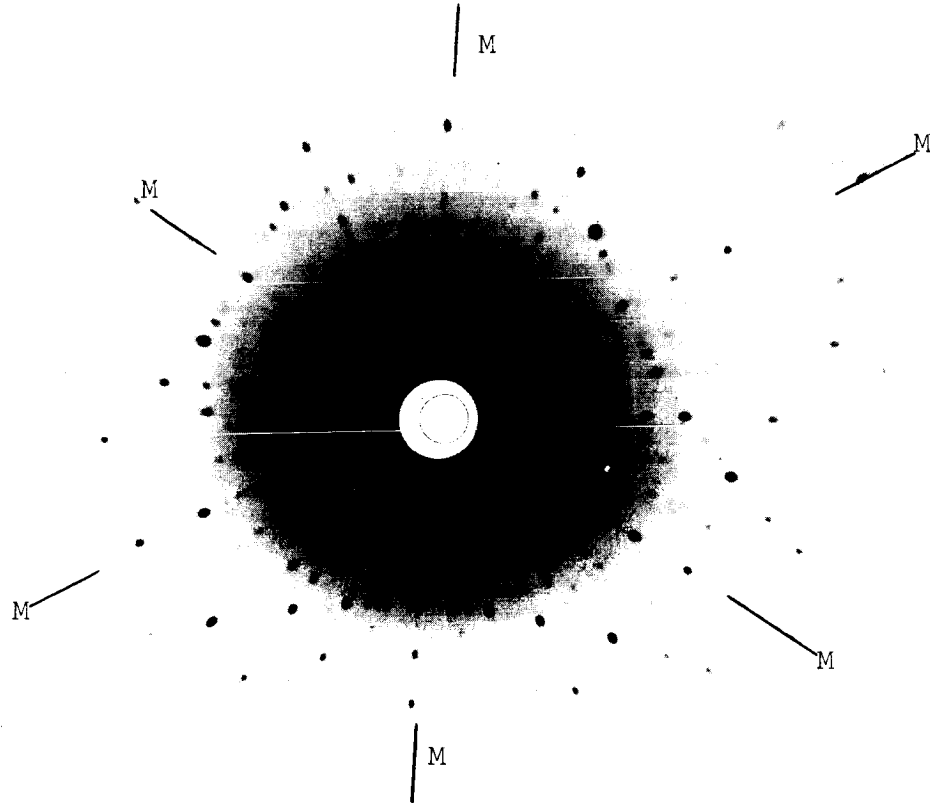
Fig. 2.9a
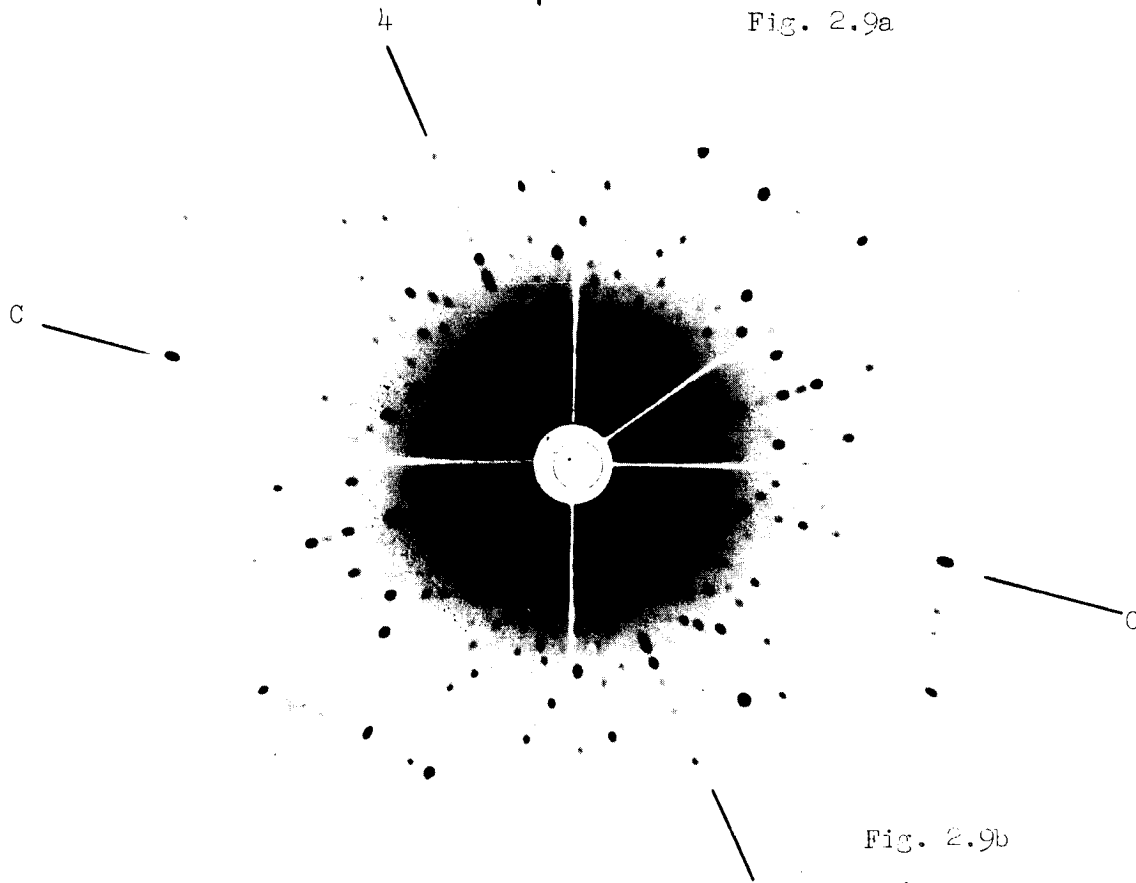
Fig. 2.9b

FIG. 2.9--Back reflection Laue photographs of Al_2O_3: (a) X-ray beam parallel to C_3; M M indicates edge of mirror plane. (b) X-ray beam parallel to C_2; C C' indicates row of Laue spots produced by C_3 zone axis; thus C_3 is at right angles to C C'; 4 4' indicates row of Laue spots produced by zone axis parallel to fourth neighbor axis direction; hence 4 4' is perpendicular to actual fourth neighbor axis direction.

- 48 -

example, a cut made normal to a C_2 axis would be exactly parallel to a mirror plane; a second cut parallel to the first would then produce the desired mirror plane slab.

Location of the pair axes in the mirror plane slab was accomplished on consideration of the following. In a crystal, all the atomic planes parallel to a single direction are known as a zone; that direction itself is the zone axis. All the Laue spots produced by a given zone lie on an hyperbola; in the special case where the zone axis is normal to the x-ray beam, the spots lie on a straight line running through the center of the photograph. Now the fourth nearest neighbor pair corresponds to such a zone axis in a very simple way: it merely represents two successive sites in an infinite row of Al ions whose direction defines that particular zone axis. In a "C_2" photograph, the fourth neighbor zone axis produces a very prominent row of spots. The identity of that row can then be checked by measurement on the photograph of the unique angle between it and the equally prominent row of spots produced by the zone axis parallel to C_3. (There is no question of confusing the two, since the location of C_3 is already known.) Orientation of the crystal is then complete, but as a double check similar measurements can be made on the less prominent rows of spots produced by the zone axes associated with the other near neighbor pairs. Finally, in transferring information from the photograph to the crystal, it must be kept in mind that the row of Laue spots is located at right angles to the zone axis that produced it.

After the mirror plane slab had been oriented in the above manner, the various samples were cut from it and individually boxed and labeled. Final sample dimensions were usually about 1.5 mm square in cross section and about 10 mm long. Before each sample was used in piezospectroscopic measurements, its cross-section was measured with a micrometer, and the exact dimensions recorded.

2.6. THE PRESSURE APPARATUS

The simple mechanical press used in the piezospectroscopic studies described here is shown schematically in Fig. 2.10, and Fig. 2.11 is a photograph of it. The lever arm assembly multiplies by a factor of 60 times the force supplied by a set of adjustable weights; the multiplied force is then transmitted by a stainless steel push rod to the sample itself. Thus a set of weights of convenient size (providing up to 6 Kg) could be used to apply stresses in excess of 100 Kg/mm^2 to samples whose cross-section was of the order of 2 to 3 mm^2. The assembly containing the push rod was made entirely of stainless steel in order to minimize thermal conduction from the top end, at room temperature, to the end containing the sample, which was immersed in liquid N_2. Two sets of windows, cut into the sample holder at right angles to each other, allowed the sample to be exposed to pumping light and permitted the resulting fluorescence to be transmitted to a spectrometer.

In order not to over-constrain the ends of the sample, such that a nonuniform stress might result over the sample cross section, force was transmitted to the samples through two "pillows," consisting of 1/4" dia. copper disks punched from 1/32" thick sheet. The copper was able to undergo plastic flow, even at the working temperature of 77^OK, allowing the sample to form a deep impression in it after pressures of the order of 50 to 100 Kg/mm^2 had been applied. Of course, new copper disks were supplied for each sample tested. That little or no broadening of the line components could be detected, even at the highest values of stress used, attributes to the effectiveness of the above scheme. Figure 2.12 is a photograph of the holder with a sample mounted.

It was discovered, through the rather bitter experience of losing one or two samples that had cost a great deal of labor to produce before any data had been gathered from them, that the samples would not take very much pressure while they were still at room temperature. Evidently the various microscopic crystalline defects are able to propagate and grow much more rapidly and to a greater extent at room temperature than at 77^OK, since most samples were able to withstand pressures up to
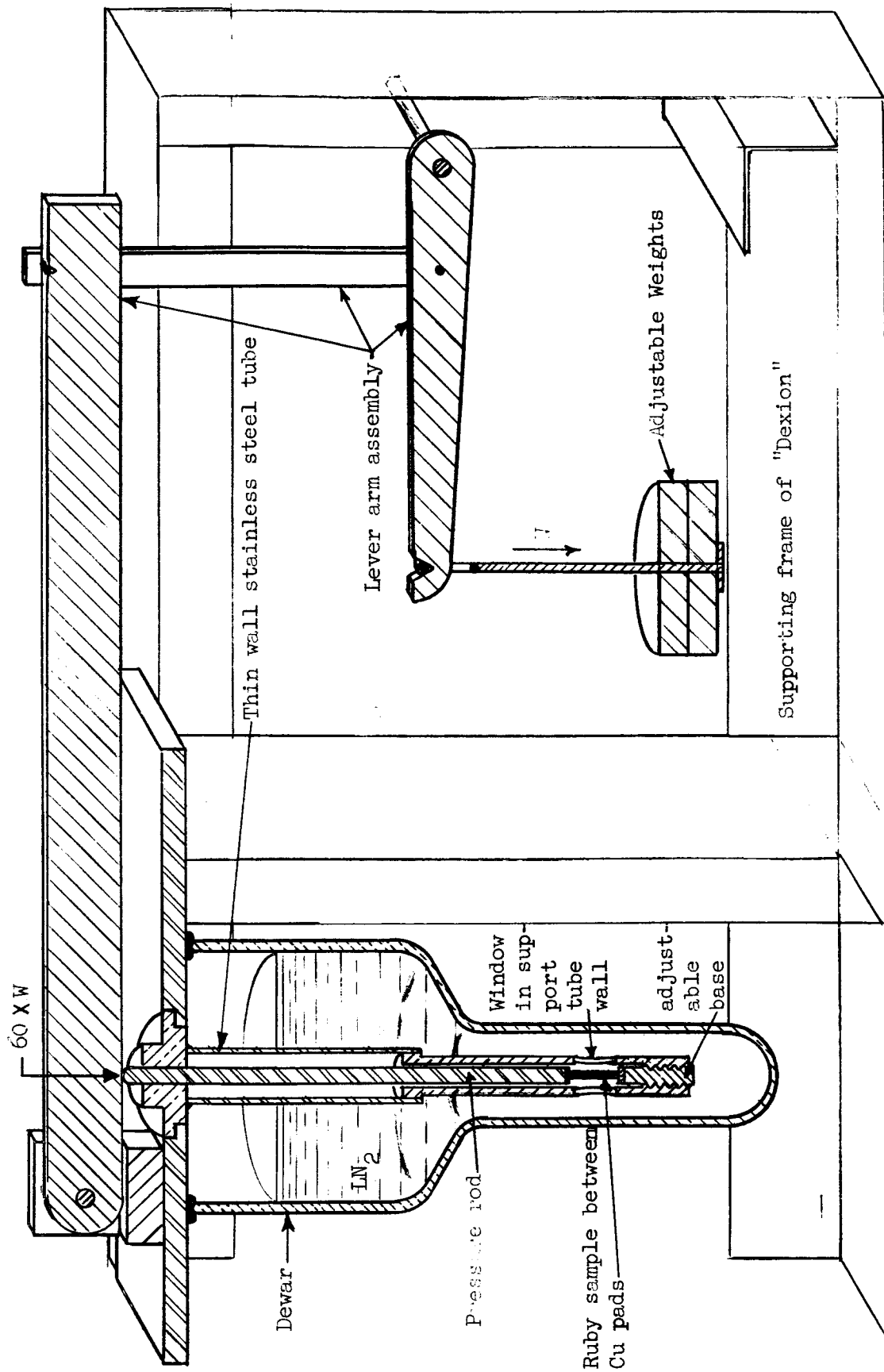
FIG. 2.10--The mechanical press
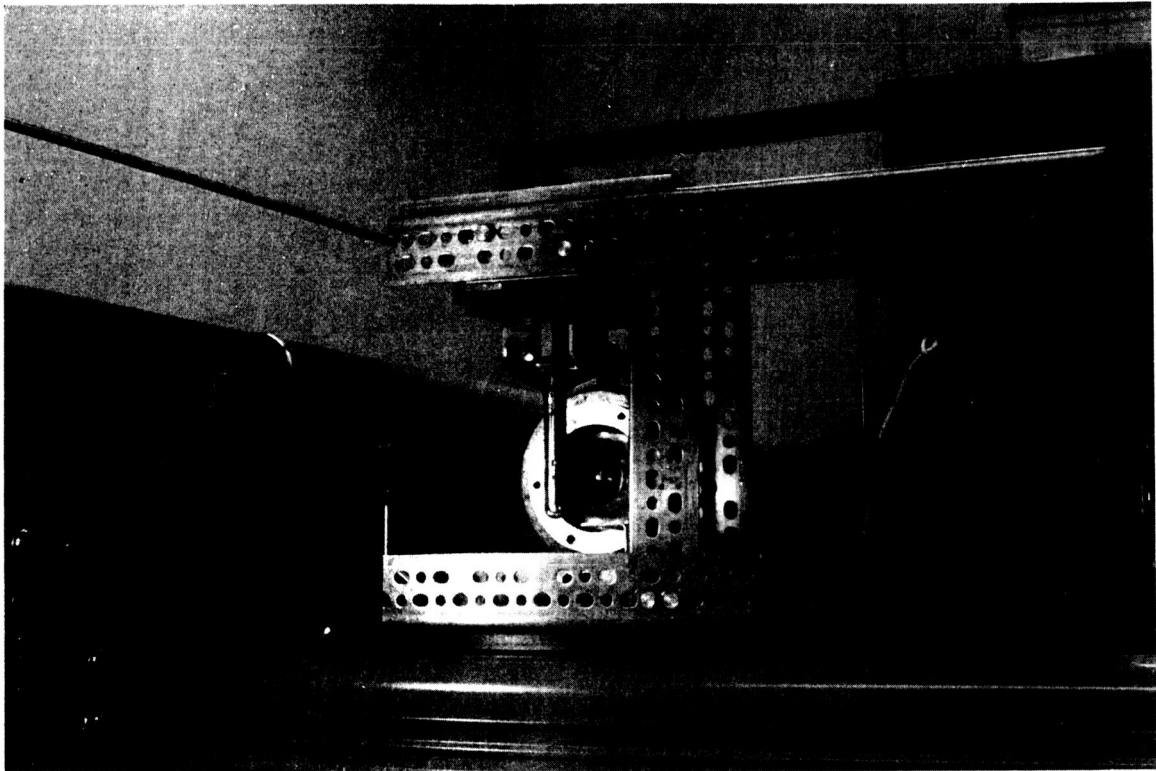
FIG. 2.11--Photograph of the mechanical press. The arc lamp can be seen
behind the dewar tip; part of the photographic spectrometer
can be seen to the left.
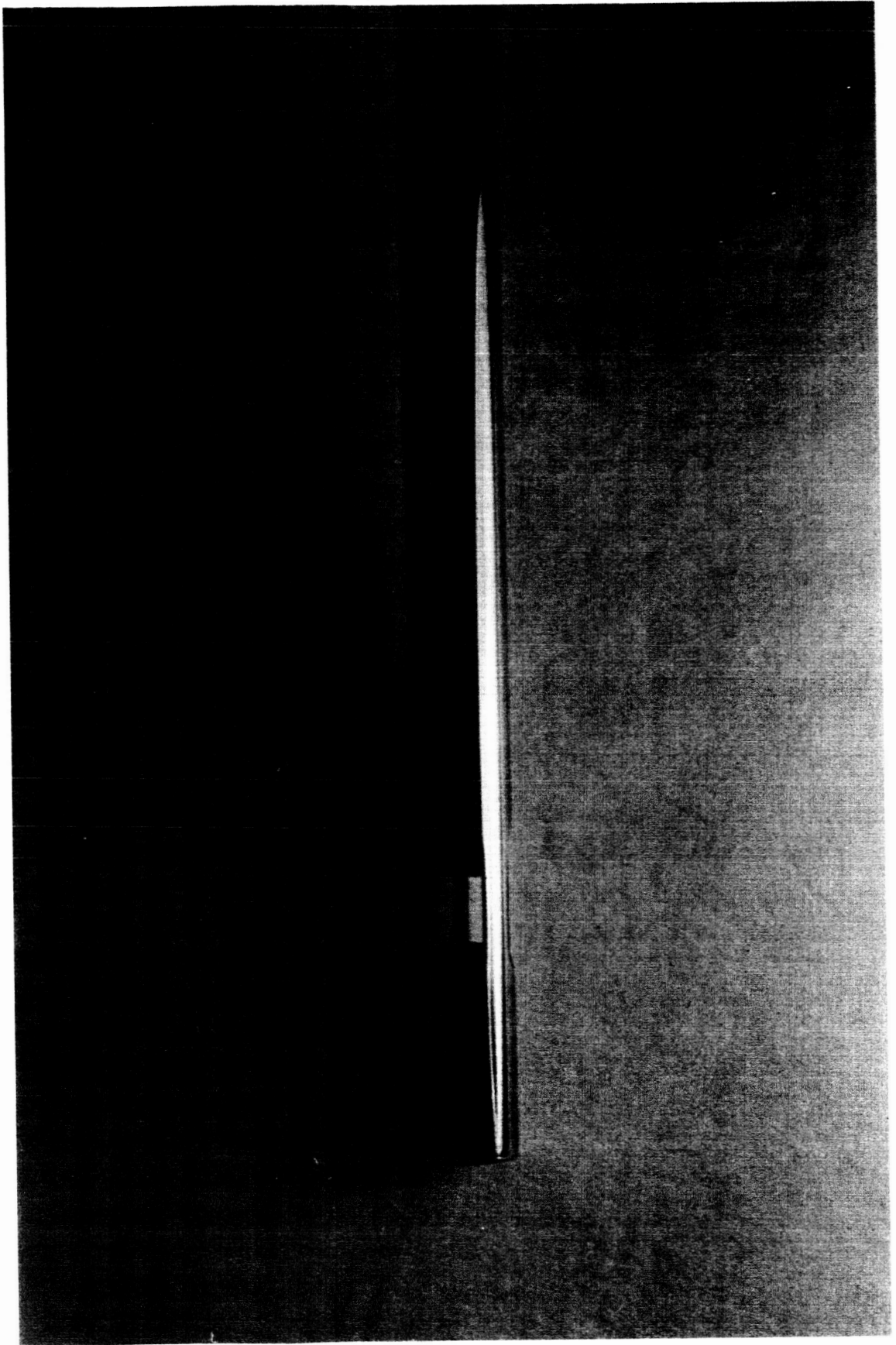
FIG. 2.12--Detail of press, showing sample in holder.

Cooling water for lamp

In → Out

Cooling water tubing wrapped around housing

Standard G.E. water jacket assembly

Cu_2SO_4 Soln. cooled by conduction through heavy Cu ring.

Sample

Plastic fresnel lenses condense arc light onto sample

G.E. type AH-6 lamp arc 25 mm × 1.5 mm DIA. IKW electrical input
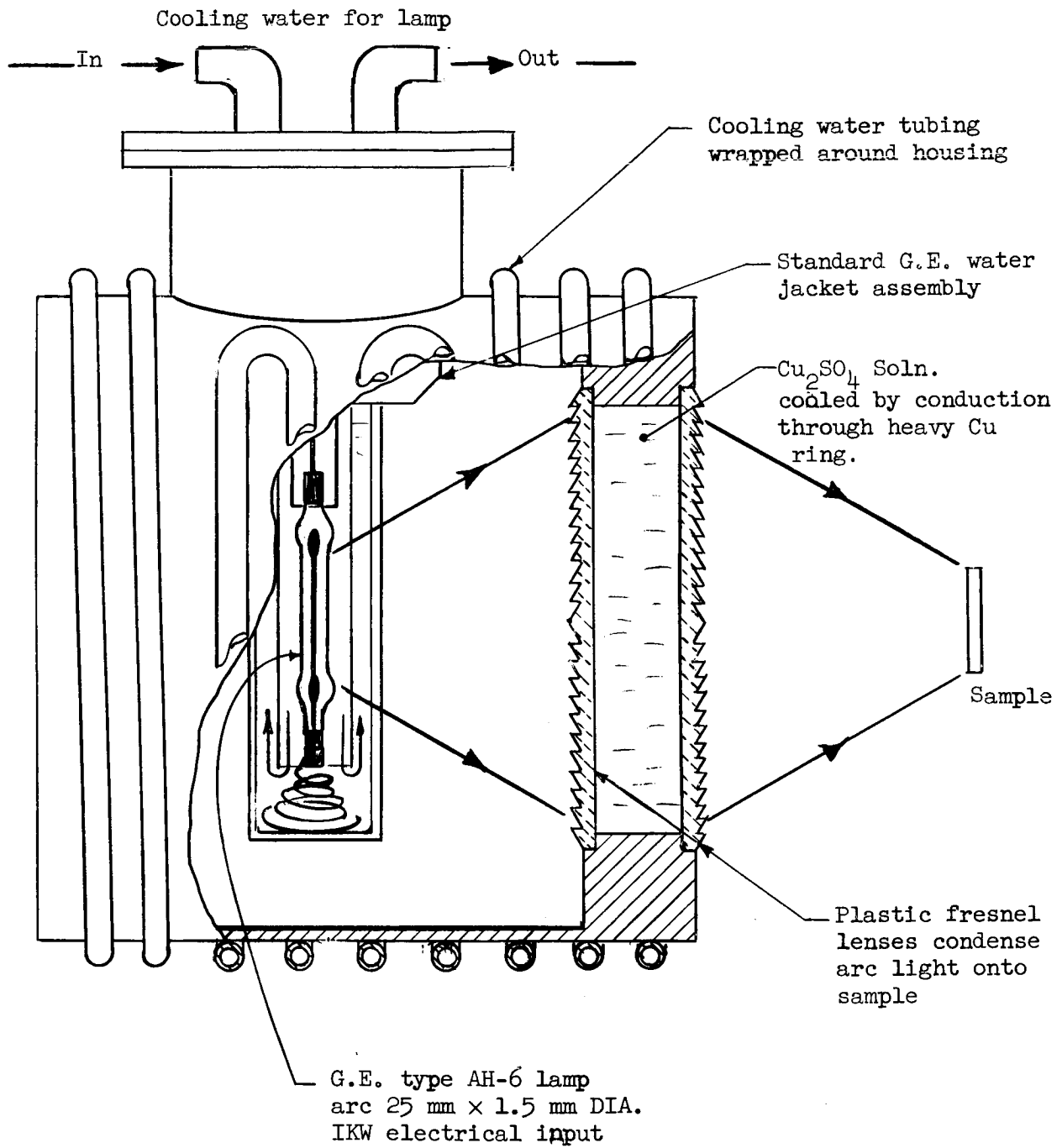
FIG. 2.13--Mercury arc lamp and housing.

100 Kg/mm^2 for an indefinite length of time at the latter temperature, while they would crumble under a pressure only 1/3 or 1/4 as large at the former.

Sample fluorescence was excited by a 1 kW, high pressure, water cooled mercury arc lamp (G. E. type A-H6). The high pressure mercury arc makes a nearly ideal source for pumping ruby, as a very large fraction of its electrical input (nearly 20%) appears as light coincident with the pump bands, and only a small fraction appears in the red and infrared. All trace of the latter was eliminated by filtering the light through a water solution of copper sulfate. Arc light was imaged on to the sample by two plastic Fresnel lenses of low f number, placed with their flat surfaces back to back, thereby creating a space for the copper sulfate solution. Lamp, housing and filter were all cooled by the same stream of tap water. The lamp assembly is shown in Fig. 2.13.

Piezospectroscopic studies of the 7009 Å and 7041 Å lines were performed with a large (1.8 m focal length) scanning spectrometer made by the Jarrell-Ash company. To take best advantage of the grating blaze angle, the instrument was used in eighth order. In that order, instrumental resolution was nearly an order of magnitude greater than the linewidths involved, even when the slits were opened up to 50 μ to allow a large light gathering power. The detector used was an R.C.A. type 7265 photomultiplier with a cathode of S-20 response.

Studies of lines further to the red were made with a dual grating, photographic instrument produced by Bausch and Lomb. The two gratings permit choice of either 4 Å/mm or 8 Å/mm dispersion. Kodak type 1-N plates were used in conjunction with this instrument because of their nearly uniform response from the visible red to 8000 Å.

III. RESULTS OF THE PIEZOSPECTROSCOPIC STUDIES

3.1 INTRODUCTION

This chapter presents detailed information relating to the production of "splitting patterns" - curves of line component shift under a standard stress as a function of sample axis angle θ . The splitting pattern of a newly discovered line of high piezospectroscopic sensitivity, occurring at 7452 $\overset{\text{o}}{\text{A}}$ and here named the N_0 line, is given in addition to the splitting patterns of the well known N_1 and N_2 lines. By matching those patterns to the theoretical patterns predicted in Chapter II, the N_0 is identified with third nearest neighbors, the N_1 with second nearest neighbors, and the N_2 with fourth nearest neighbors. In addition, the principle that all the members of a given exchange multiplet exhibit a common splitting pattern unique to the particular pair type involved is discovered and used to identify part of the first nearest neighbor exchange multiplet. Finally, the various sources of error and probable accuracy of the piezospectroscopic data are discussed.

3.2 SPLITTING OF THE N_1 AND N_2 LINES

The N_1 and N_2 lines were selected for the first studies, since these two were the strongest representatives (in fluorescence at low temperatures) of the only two exchange multiplets known at that time. Since these two are so easily seen in fluorescence, the samples used in their study were cut from a boule of approximately 0.15% Cr_2O_3 by weight, in order to take advantage of the higher crystal quality available at that relatively low concentration.

The raw piezospectroscopic data obtained on the N_1 (7041 $\overset{\text{o}}{\text{A}}$) line were the easiest to reduce, since the splittings obtained with the higher values of stress were usually well resolved for all but a few angles. Figure 3.1 shows several typical recorder traces of the splitting of the N_1 line. For each sample, the shifts of the various line components

SPLITTING OF 7040 Å LINE

$\leftarrow$ 11 cm^{-1} $\rightarrow$

P=100 kg/mm^2 P$\perp$C$_2$

P=0
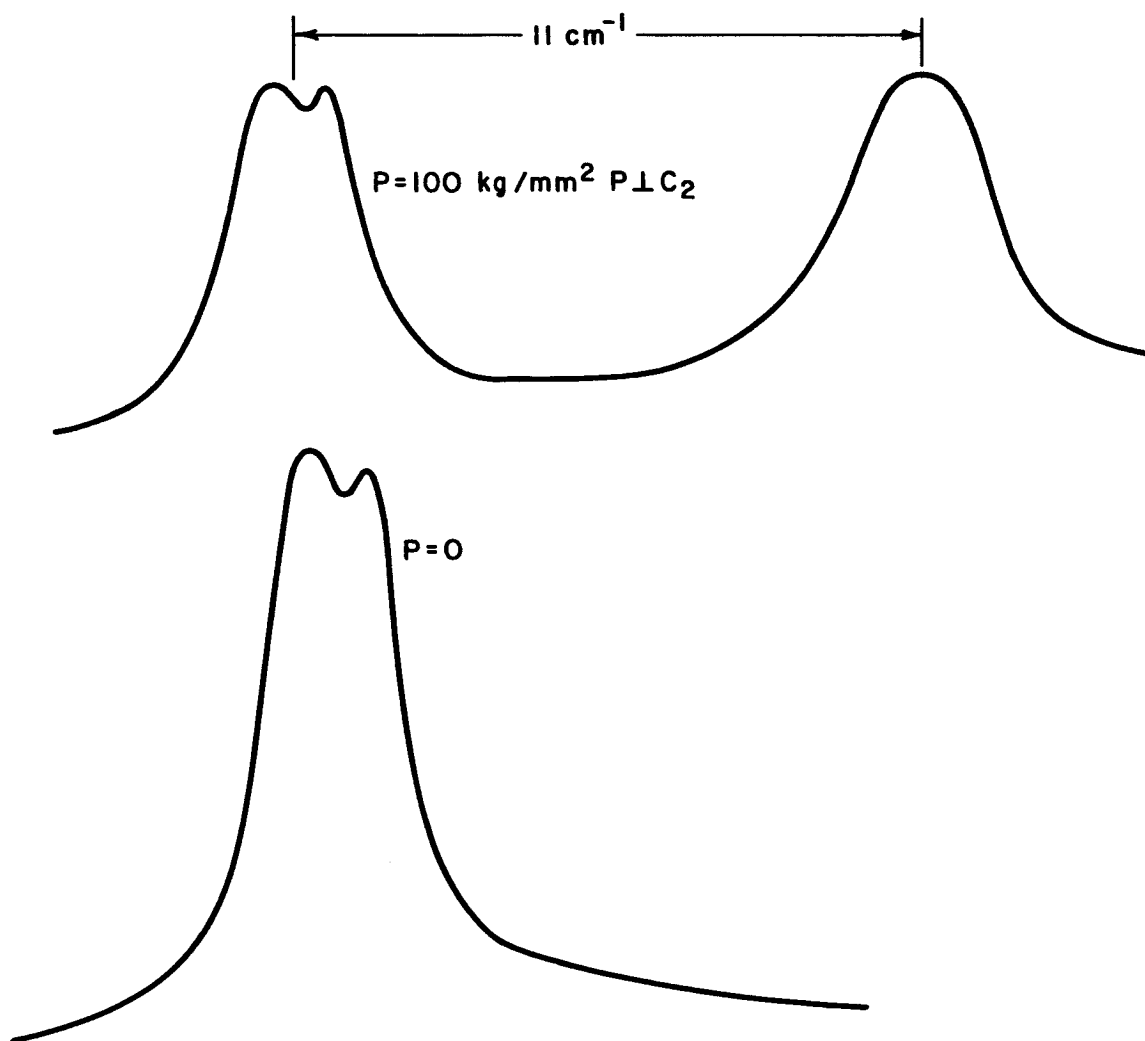
FIG. 3.1--Recorder traces of N$_1$ line splitting.

away from the zero pressure position were measured carefully, and a plot of shift versus pressure was made. In every case, the data points were found to make a close fit to a straight line passing through the origin. Values of shift normalized to a pressure of 100 Kg/mm^2 could then be read from the shift versus pressure plots, and a graph of shift versus angle made. Figure 3.2 shows the resultant splitting pattern for the N$_1$ line, where θ measures angles in the mirror plane according to the convention established in Chapter II.

Splittings of the N$_2$ (7009 $\overset{\circ}{A}$) line were not always as well resolved, and as a consequence the only data points used were those obtained with the highest stress the sample would withstand, on the order of 100 Kg/mm^2 or slightly higher. Even then, in many instances the exact positions of some of the line components had to be determined by fitting a pair of hand drawn curves to the actual recorder trace, such that their sum would reproduce the unresolved trace. The curve fitting is fundamentally an iterative process, and in the more difficult cases several successive approximations were made before a good fit was obtained.

Figure 3.3 shows several recorder traces of some of the better-resolved splittings of the N$_2$ line, and Fig. 3.4 shows the mirror plane splitting pattern produced by that line; here, again, all values of line shift were normalized to a standard pressure of 100 Kg/mm^2. Except for the extra splitting of the lower amplitude curve, Fig. 3.4 strongly suggests the theoretical splitting pattern predicted for the fourth nearest neighbors.

However, the extra splitting has a rather simple and obvious explanation on the basis of a fourth neighbor assignment. Until now, we have talked only in terms of the symmetries of the lattice, thereby giving the impression that the two pairs lying out of the mirror plane slab from which the samples were cut were true mirror images of each other. (From now on, that pair of any given near neighbor type whose axis lies in the particular mirror plane slab from which the samples were cut will be referred to as I , whereas the two lying out of that mirror plane will be referred to as II and III.) That picture is indeed correct when only the metal ions are taken into account. However, when the arrangement of all the ions in a unit cell is considered, the mirror symmetry
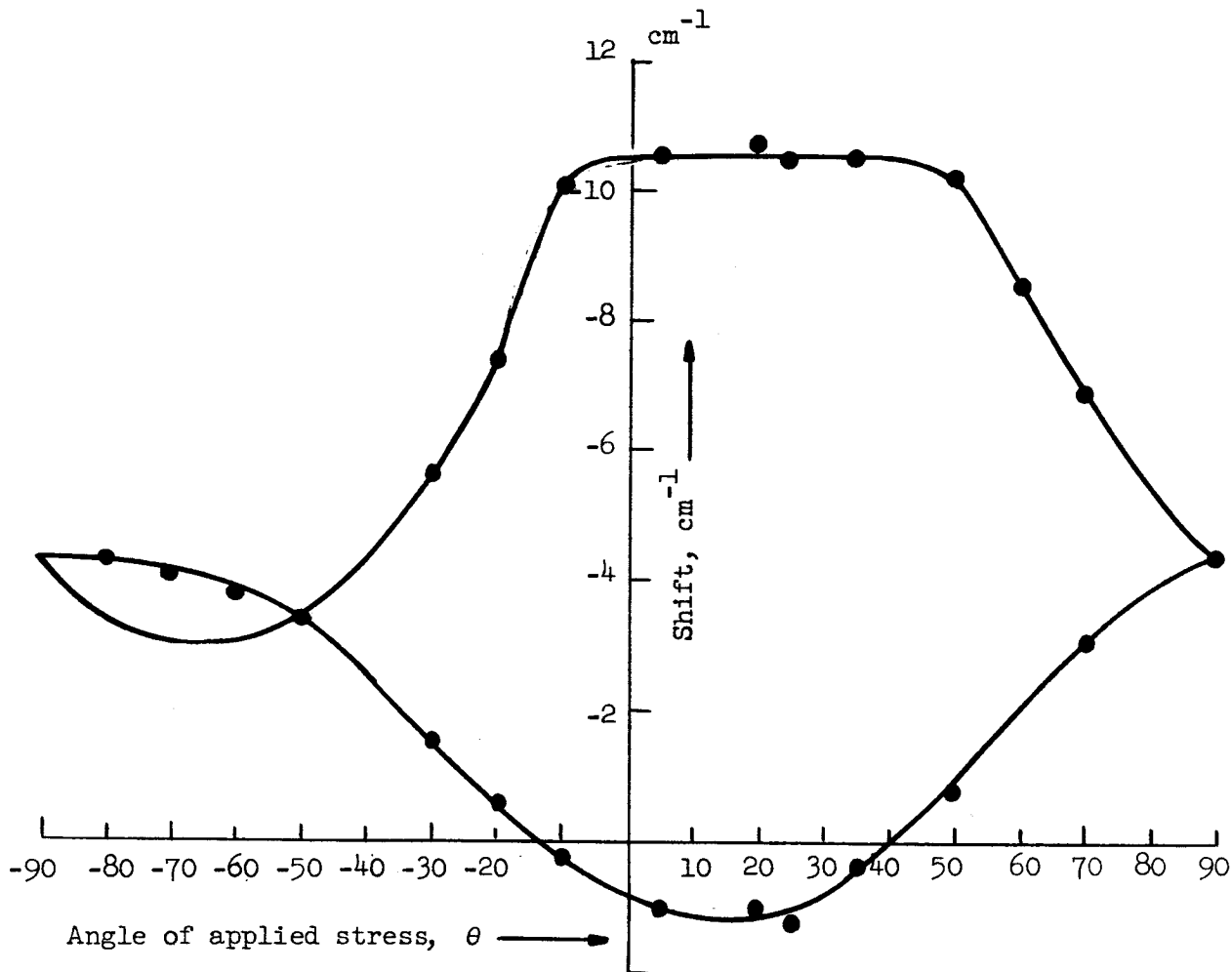
FIG. 3.2--Splitting pattern of N_1 . Magnitude of stress is 100 Kg/mm^2.
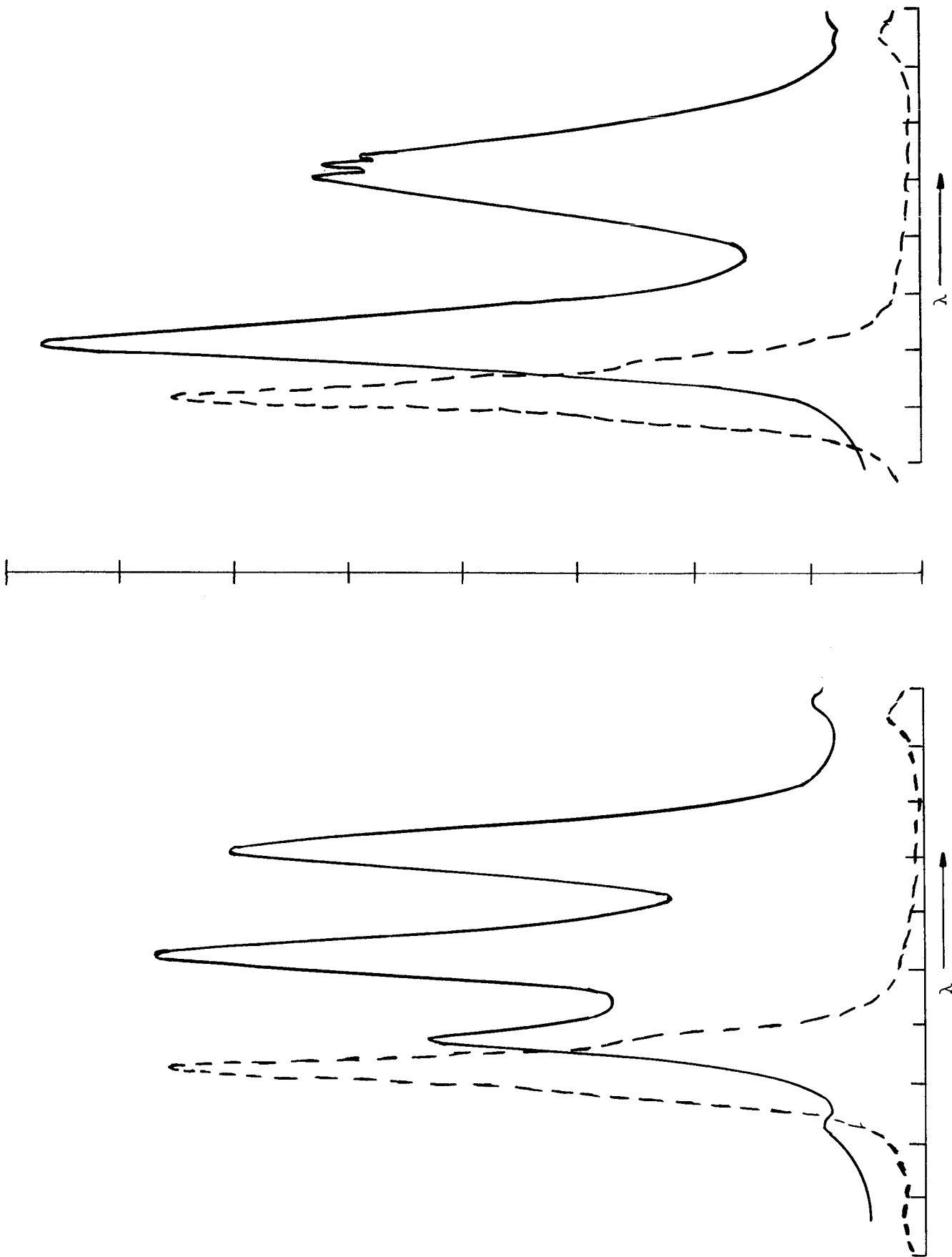
FIG. 3.3--Recorder traces of N splitting for two different sample orientations. Position of line at zero stress shown in dashed outline.
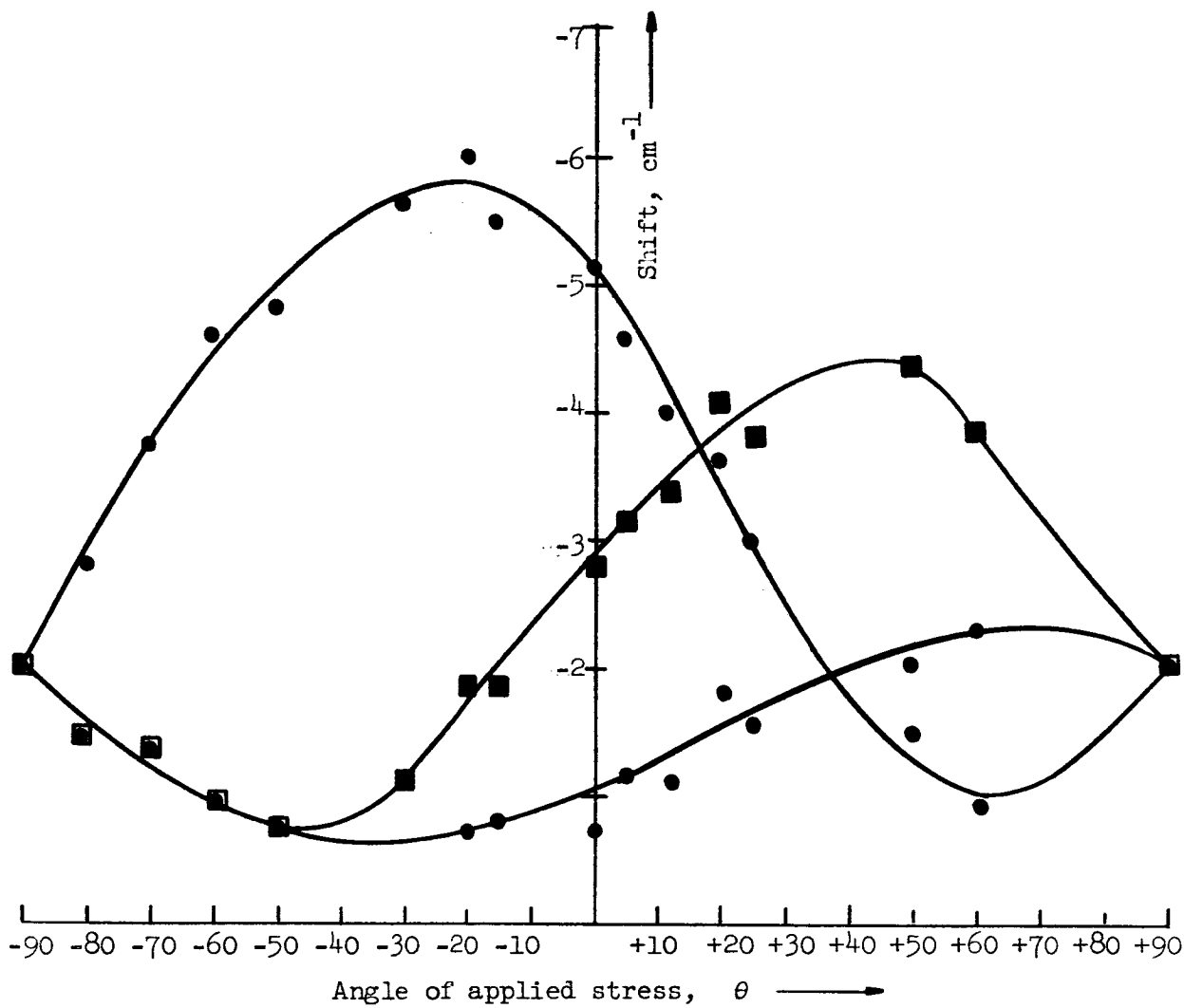
FIG. 3.4--Splitting pattern of N_2 . Magnitude of stress is 100 Kg/mm^2.

degenerates into a glide plane, and pairs II and III are no longer equivalent. Most probably, the single oxygen ion that almost intervenes between the two Cr ions of the fourth nearest neighbor pair is of greater importance than any other. The Cr ion pair might then be more properly thought of in terms of a Cr-O-Cr complex, having a flattened v shape. The Cr-O-Cr complexes and their relation to each other are illustrated in Fig. 3.5.

Perhaps it should be pointed out here, if only parenthetically, that Fig. 3.5 really shows only half the number of possible Cr-O-Cr complexes for a given pair type. However, the other three complexes can be shown to be stress equivalent to the first set. In Fig. 3.6, the two sets are labeled "a" and "b" , hence the individual complexes are labeled Ia, Ib, IIa, etc. The "a" set is related to the "b" set through the inversion center of the Al_2O_3 lattice, and since the inversion operation produces no change in an even perturbation such as stress, the complexes Ia and Ib are stress equivalents; in like manner, IIa is stress equivalent to IIb, and IIIa is stress equivalent to IIIb. Although the above has been stated in terms of the Cr-O-Cr complex, the argument holds equally for the pair taken together with its complete environment.

Tentative assignment of the N_1 and N_2 lines could be made at this point, but that assignment will be delayed until the rather startling piezospectroscopic behavior of a pair line, discovered far to the red of the N lines, has been described.

3.3 SPLITTING OF THE LINE AT 7452 Å

After the above studies of the N lines had been completed, it was thought that the pressure technique could be used in a search for the missing exchange multiplet of the first nearest neighbors. Discovery of that multiplet would provide one of the most significant pieces of information to be obtained from the spectrum of dark ruby, since it was realized that the first nearest neighbor exchange was almost certainly much greater than the two known so far, thereby making the first neighbor exchange the one most significant in the determination of the antiferromagnetic arrangement of Cr_2O_3 . Although the lines of the first neighbors would never split under stress, their piezospectroscopic
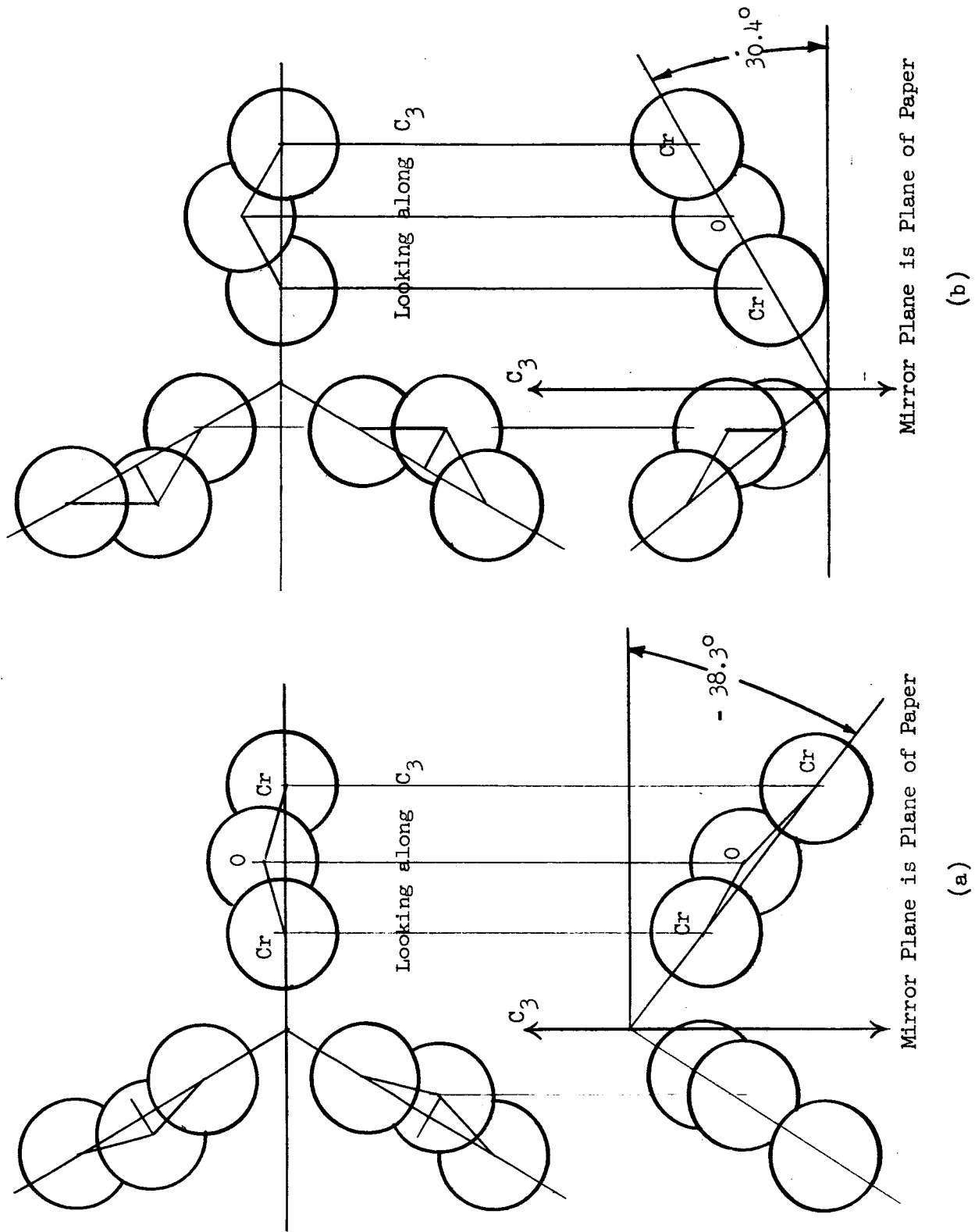
FIG. 3.5(a)--Fourth N.N.   Cr-O-Cr   complex.
     (b)--Third N.N.   Cr-O-Cr   complex.

Looking along C3

Mirror plane is plane of paper
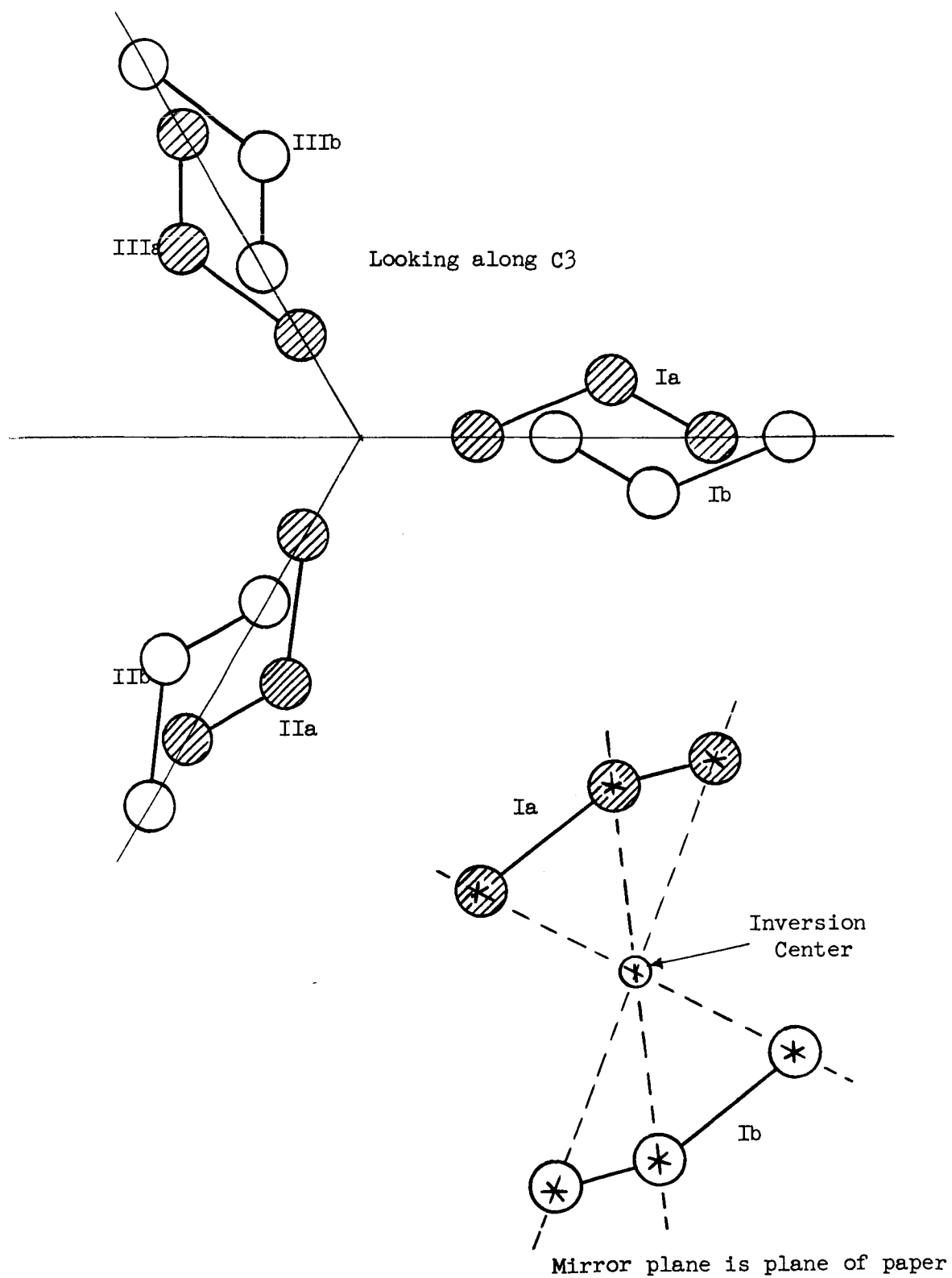
FIG. 3.6--Stress equivalent sets "a" and "b" of Cr-O-Cr complex.

sensitivity would surely be considerably greater than that of the R lines, thereby allowing them to be distinguished from the various sharp features of the vibronics of those lines, through comparison of a survey plate of the ruby spectrum taken at zero stress with one taken with stress applied to the sample. Since the lines in question, if at all detectable, would be much weaker than the N_1 and N_2 lines, two new samples were cut from a boule of 0.29% Cr_2O_3 by weight, with sample axes parallel to C_3 and C_2, respectively. But before the first neighbor lines could be ferreted out with the aid of these two samples, the very first plate taken with pressure applied parallel to C_2 showed a large, three-fold splitting of a line at 7452 $\overset{o}{A}$, and the first neighbor search was temporarily sidetracked.

Intensity of the new line was also known to increase steadily from zero relative to that of the R lines as the Cr concentration was increased. Could the new line possibly be attributed to the previously missing third nearest neighbor pair? To find the answer, a new mirror-plane fan of samples was cut from the 0.29% Cr_2O_3 boule mentioned above, and a piezospectroscopic study of the new line carried out. (To facilitate constant reference to it, the new line at 7452 $\overset{o}{A}$ was named by us as the "N_0" line, consistent with the pattern established by DuBois and Elias. Although their numbering scheme has lost its original meaning, now the decreasing subscripts 2, 1, 0 can be taken to indicate increasing piezospectroscopic sensitivity.) The only difference between the studies on the N_1 and N_2 lines described above and that made on the N_0 line lay in the fact that the latter was carried out on a photographic instrument, rather than on the scanning spectrometer. Although marginal for piezospectroscopic study of the N_2 line, resolution of the photographic instrument was more than sufficient for study of the N_0 line, since the width of that line and its piezospectroscopic sensitivity were, respectively, about four and ten times as great as those of the N_2 line. Choice of the photographic instrument was then a matter of convenience, the most important consideration being that the piezospectroscopic behavior of the whole ruby spectrum would be recorded simultaneously with that of the N_0 line under study at the time. As will be revealed later, important additional information was gleaned from a re-examination of the plates used in the study of N_0.

Positions of the stress produced components of the N_0 line were measured with reference to the line at 7438.90 Å of a superimposed neon spectrum. Figure 3.7 shows a few of the plates. The actual measurements were taken from the trace produced by a recording microphotometer, rather than directly from observations of the plates themselves through a magnifying glass, in order to facilitate accurate location of the line centers. The shifts thus determined were then all normalized to the standard pressure of 100 Kg/mm^2; the mirror-plane splitting pattern plotted from the normalized shifts is shown in Fig. 3.8.

3.4 ASSIGNMENT OF PAIR TYPES TO THE N_0 AND N_2 LINES

Figure 3.9 reproduces the splitting patterns of the N_2 and N_0 lines side by side to facilitate comparison; the striking similarity of the two patterns, when the one is seen as an approximate mirror image of the other across the 0^0 line, leaves little room for doubt that these two represent the complementary set of splitting patterns expected for the fourth and third nearest neighbors, respectively. Note that the similarity in shape exists in spite of a difference in scale (of the shifts) of approximately one order of magnitude; the maximum splitting between components is on the order of 5 cm^{-1} for the N_2 line, while the corresponding splitting is approximately 50 cm^{-1} for the N_0 line.

The extra splitting (between components II and III) should have exactly the same explanation for the N_0 line as was given in Section 3.2 for the splitting pattern of the N_2 line. That is, just as for the fourth nearest neighbors, the third also have one oxygen ion that almost intervenes between the two Cr ions, forming a v-shaped Cr-O-Cr complex. Figure 3.5b shows the Cr-O-Cr complexes of the third nearest neighbor pair.

In addition to the splitting pattern itself, the difference between the shift of component I and the average of components II and III can also be plotted as a function of θ ; that plot will be called the "splitting curve," in order to distinguish it from the splitting pattern. In Fig. 3.9 the splitting curves are shown below the corresponding splitting patterns. Note that the maxima of the splitting curves make much better fit to the actual pair axis directions than do the maxima of the large amplitude curves of the original splitting pattern. The explanation for the
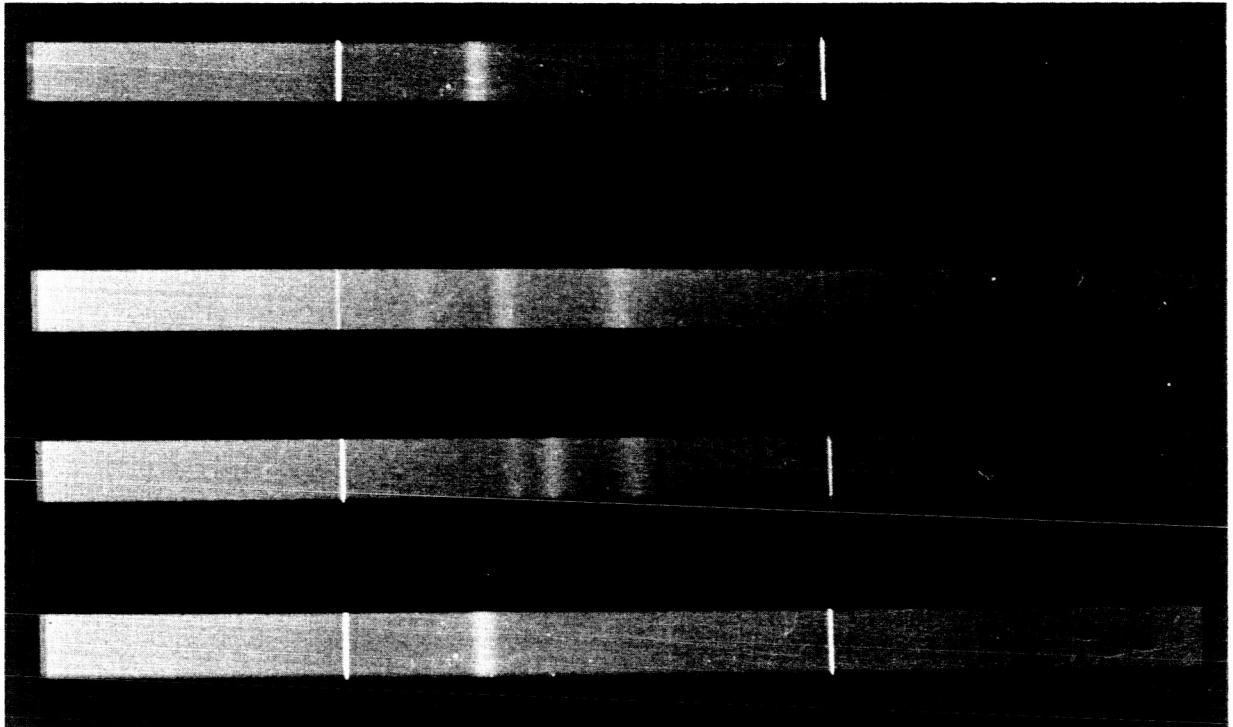
FIG. 3.7-- N_0 splitting as it appeared on the original plates. The two sharp neon lines at 7438.9Å (left) and at 7488.9Å (right) define the wavelength scale. The top spectrum is of the N_0 line at zero pressure; the other three correspond to a stress magnitude of about 80 Kg/mm². From next to the top to the bottom, the angles of applied stress are +30°, 0°, and -15°.
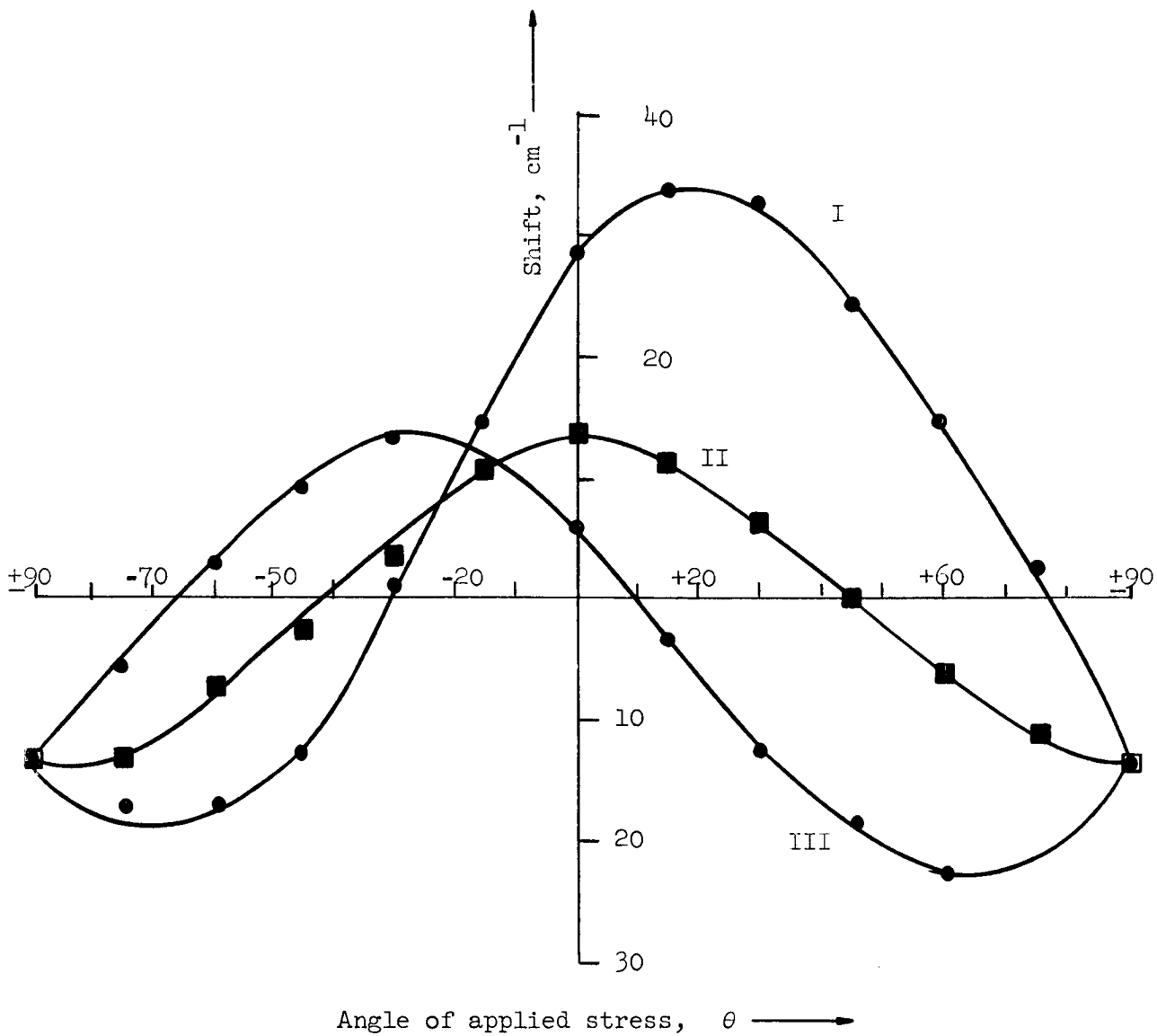
FIG. 3.8--Splitting pattern of N_0 . Magnitude of applied stress is 100 Kg/mm^2.
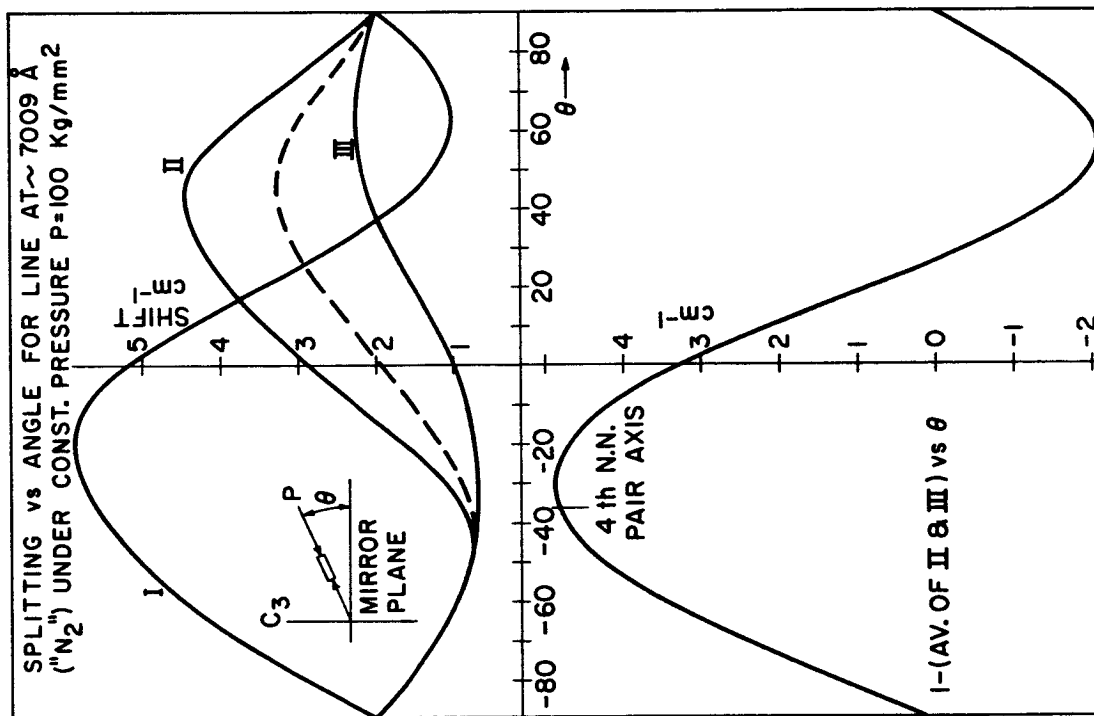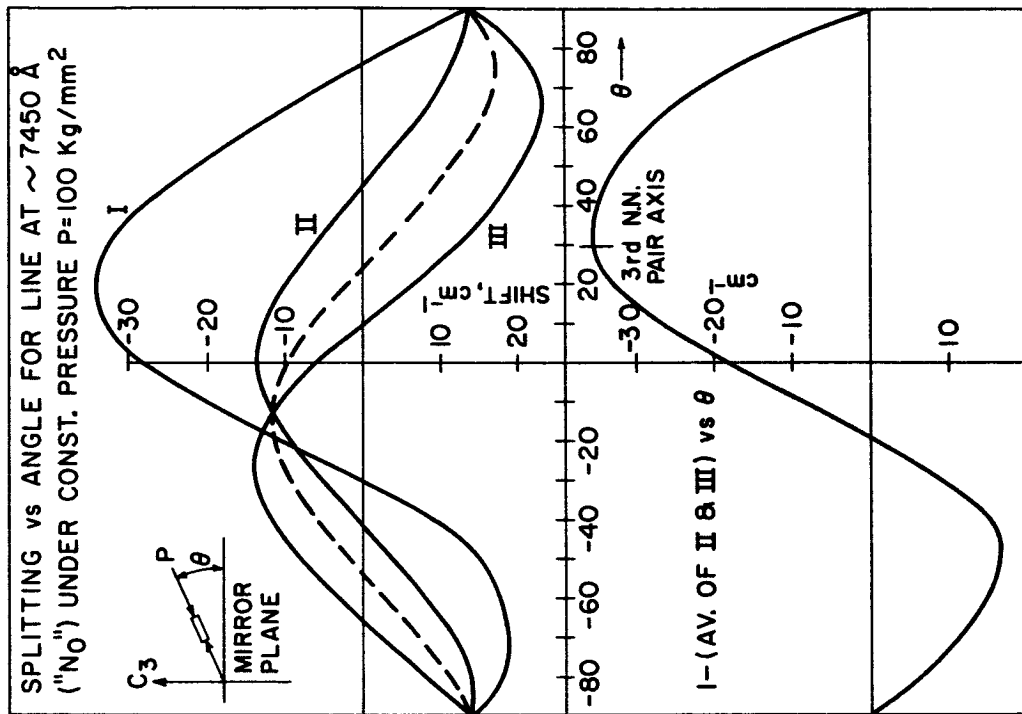
FIG. 3.9.--N_2 and N_0 splitting patterns and splitting curves shown side by side for easy comparison.

improved fit may be that when the difference between curve I and the average of II and III is taken, a term common to all three components, but not accounted for in the simple uniaxial stress theory given in Chapter II, is subtracted out. Such a term may come from response of the Cr-O-Cr complexes to shear strains.

Even if the postulate that the shift should be directly proportional to the strain along the pair axis is entirely correct, there are a number of reasons why the observed splitting patterns would not be expected to fit precisely the theoretical curves calculated in Chapter II. In the first place, the macroscopic strain represents some sort of average of all the atomic displacements within a unit cell, whereas the true relative displacement of the Cr ions of a given pair may deviate somewhat from that average. The proper relation between such microscopic strains and the macroscopic strain is undoubtedly rather complex, and is certainly not known at this time. Secondly, the elastic isotropy assumed previously was only a rough approximation; the correct relation between macroscopic stress and strain in non-isotropic materials is determined by a nine-by-nine tensor of second rank, containing six independent constants.

The six elastic constants for sapphire have been measured accurately by J. B. Wachtman et al., at the National Bureau of Standards.[65] The following table of elastic compliances is taken from their paper.

TABLE 3.1

ELASTIC COMPLIANCES OF SAPPHIRE
(In units of 10^{-13} cm^2/dyne)

S_{11}	2.353	S_{12}	-0.716
S_{33}	2.170	S_{13}	-0.364
S_{44}	6.940	S_{14}	0.489

The tensor in question is written:

$$
\begin{bmatrix}
S_{11} & S_{12} & S_{13} & S_{14} & 0 & 0 \\
S_{12} & S_{11} & S_{13} & -S_{14} & 0 & 0 \\
S_{13} & S_{13} & S_{33} & 0 & 0 & 0 \\
S_{14} & -S_{14} & 0 & S_{44} & 0 & 0 \\
0 & 0 & 0 & 0 & S_{44} & 2S_{14} \\
0 & 0 & 0 & 0 & 2S_{14} & 2(S_{11} - S_{12})
\end{bmatrix}
\quad .
$$

Figure 3.10 shows the relation of the axes 1, 2 and 3 to the crystal axes, and the way in which the subscripts 4, 5 and 6 describe shear strain and stress.

A computer calculation of the predicted splitting patterns might improve the fit to the observed piezospectroscopic behavior, but such a calculation has not yet been attempted. However, the first consideration mentioned above may tend to blur any improvement gained in an exact calculation of macroscopic strain.

The third and final consideration is that the Cr ions, especially those of a pair, may not choose the exact same locations that were occupied by the Al ions they have replaced. There are two pieces of evidence for such a shift in location of the isolated Cr ions, the one unfortunately contradicting the other on the indicated direction of that shift. A crystal-field calculation by D. S. McClure[66] predicted a shift of about 0.1 Å away from the nearest neighbor site; X-ray studies by S. C. Moss and R. E. Newham[67] on ruby of 4% Cr_2O_3 concentration indicated a shift of 0.06 Å in the opposite direction. An improved calculation by J. O. Artman and J. C. Murphy[68] could be said to be in partial agreement with both McClure's calculation and the x-ray studies, since it predicted an absolute shift away from the nearest neighbor, but since their calculation took a more general distortion of the lattice into account, the shift, expressed as a fraction of the separation between oxygen layers, was toward the nearest neighbor site. But no matter which of the above predictions is correct, such shifts in location of the two Cr ions of a pair would rotate the second and third nearest neighbor axes by a few
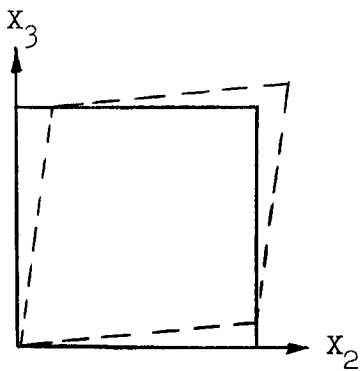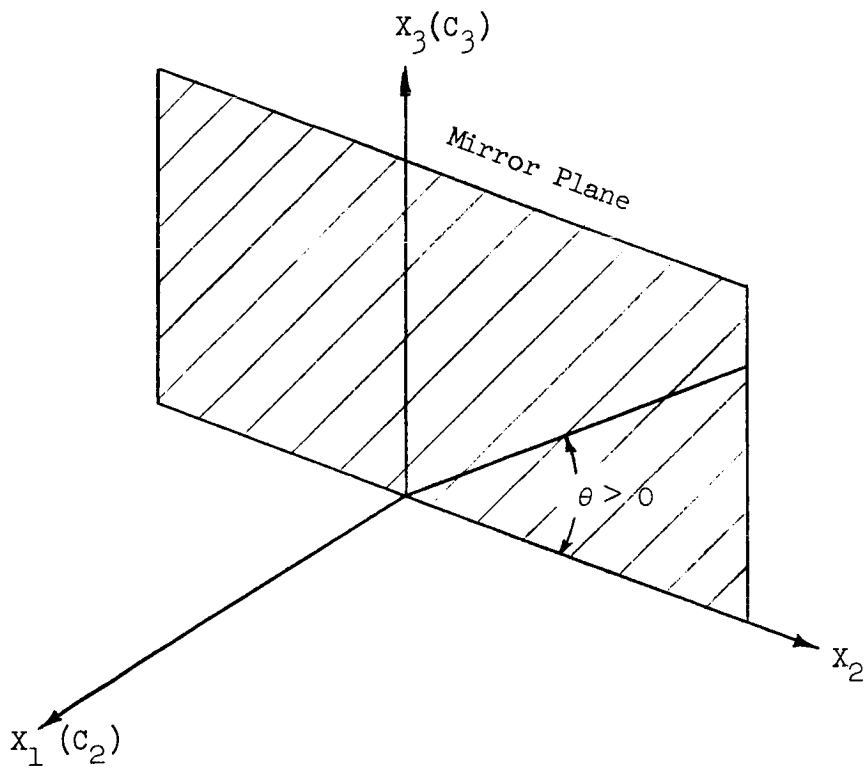
"4" component of shear strain   "4" component of shear stress
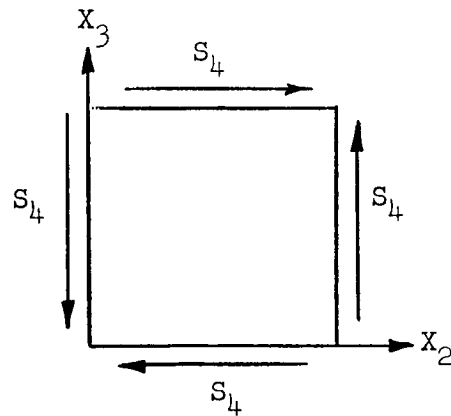
FIG. 3.10--Definition of axes relevant to the stress tensor given in
Section 3.4.

degrees in one or the other direction. (Such a shift in the Cr ion location would not be expected to produce a rotation of the fourth nearest neighbor pair axis, since for that pair both Cr ions are shifted in the same direction.)

3.5 ASSIGNMENT OF A PAIR TYPE TO THE N_1 LINE

Positive identification of the N_0 and N_2 lines with the complementary set of pairs, the third and fourth nearest neighbors, leaves only one or possibly two choices, either the second or sixth nearest neighbors, for assignment to the N_1 line. Discrimination between these two alternatives could probably be left to the simple consideration that the observed exchange — with a J value of -10 cm^{-1} (antiferromagnetic) — would be extremely difficult to explain on the basis of a sixth nearest neighbor assignment. However, the stress data on the N_1 line provide good confirmation of the second neighbor assignment.

The sixth nearest neighbor assignment is ruled out by the fact that both the large amplitude curve of the splitting pattern and the splitting curve for the N_1 line (see Fig. 3.2) are anything but symmetric about the 0° direction, instead, their peaks lie well into the quadrant containing the second neighbor axis. In fact, by any reasonable criterion for establishing a center of symmetry of the splitting curve, that center lies within 3° to 7° of the second nearest neighbor pair axis direction. And despite the rather strange shape of the large amplitude curve of the splitting pattern, if the fundamental sinusoidal variation is extrapolated from it, it will be seen to make fairly good fit to the pattern predicted for second neighbors.

Note that in the splitting pattern of the N_1 line, the curve attributed to pairs II and III (the two lying out of the particular mirror plane slab from which the samples were cut) does not display the extra splitting observed for the third and fourth nearest neighbor patterns. This splitting, exactly two-fold, should be unique to the second nearest neighbors within the set comprised of first through fifth nearest neighbors. Of course, pairs II and III of the second neighbors are not mirror images of each other, when the intervening oxygen ions are taken into account, just as pairs II and III are not mirror images of each

other for the third and fourth nearest neighbors. However, unlike the situation for third and fourth neighbors, pairs II and III of the second neighbors can be shown to be stress equivalents for stress applied anywhere in the I mirror plane.

For the second neighbors, two nearly intervening oxygen ions are equally involved in the formation of a $Cr-O_2-Cr$ complex. The complex is diamond shaped (nearly square, in fact), with the two Cr ions on diagonally opposite corners, and the O ions on the remaining corners. Again, as already indicated in Section 3.2 with respect to the third and fourth nearest neighbors, there are "a" and "b" sets of complexes, which can be related to each other through an inversion center. The six complexes Ia, Ib, IIa, etc. are illustrated in Fig. 3.11. From the figure, it can be seen that the IIa and IIIb (also the IIIa and IIb) complexes are (very nearly, at least) exact images of each other across the I mirror plane; hence these two should be stress equivalent for stress applied anywhere in the I plane. By the same argument given in Section 3.2 with respect to the third and fourth neighbors, IIa and IIb are general stress equivalents, as are IIIa and IIIb. Therefore, all four complexes — IIa, IIb, IIIa, IIIb — are stress equivalents for stress applied in the I mirror plane. Since the two remaining complexes, Ia and Ib, are stress equivalents, the mirror plane splitting pattern for second nearest neighbors will show a precisely two-fold splitting. Incidentally, the above argument cannot be applied to the third or fourth neighbors, since, for example, complexes IIa and IIIb are not images of each other across mirror plane I for either type of pair.

The strange shape of the large amplitude curve of the splitting pattern is itself a kind of evidence for the second neighbor assignment. The deviation from the predicted pattern probably has as its major reason the difference between microscopic and macroscopic strain discussed in Section 3.4 with reference to the third and fourth nearest neighbor patterns. Furthermore, the degree to which the relative displacement of the ions of a pair would conform to macroscopic strain should decrease markedly with the size of the pair separation. Thus the second neighbor pair is expected to produce a more badly distorted pattern than more distantly separated pairs.
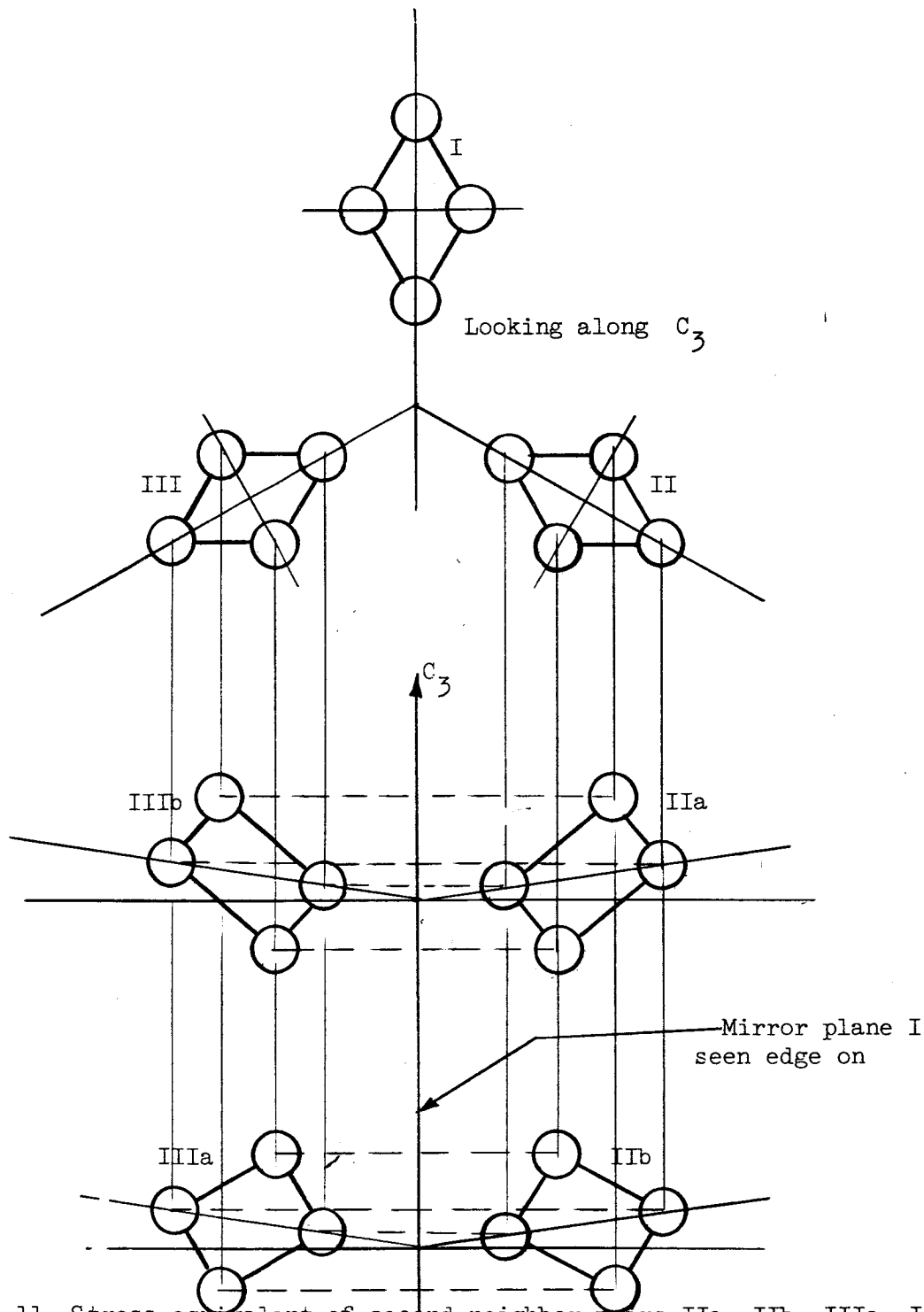
FIG. 3.11--Stress equivalent of second neighbor pairs IIa, IIb, IIIa, IIIb for stress axis lying in mirror plane I. Unlike the situation found for third and fourth neighbors, sets "a" and "b" are not related to each other through an actual inversion center of the lattice, but the $Cr-O_2-Cr$ complexes can nevertheless be related to each other through an inversion center by translation of one of the complexes parallel to itself. Since the stress is unaffected by translation parallel to itself, the stress equivalence of sets "a" and "b" is still maintained.

Finally, the relative intensities of the stress-produced components agree with the second neighbor assignment and contradict a sixth neighbor assignment. That is, when polarization effects are taken into account, the low amplitude curve of the N_1 splitting pattern corresponds to a component having twice the intensity of the component from which the large amplitude curve was obtained, in agreement with assignment of the low amplitude curve to the two pairs II and III, and the high amplitude curve to just one pair. For the sixth nearest neighbors, the high amplitude curve would be produced by pairs II and III, giving just the reverse of the observed intensity ratio.

3.6 VERIFICATION OF THE KNOWN EXCHANGE MULTIPLETS

When the second and fourth nearest neighbor exchange multiplets were examined on the plates originally used in the piezospectroscopic study of the N_0 line, the various members of a given multiplet were found to produce nearly identical splitting patterns. Figure 3.12 shows one example of the common pattern produced for each of the two known multiplets. The most important implication of the above is that stress-induced variation of the ground state exchange coupling can provide at most only a tiny fraction of the observed piezospectroscopic effect. That is, if modulation of the exchange coupling were largely responsible for production of the observed pressure effect, the magnitude of splitting would be expected to vary greatly from one member of the multiplet to another, since the exchange energy itself represents a radically different multiple of J for each member of the multiplet.

The relative insignificance of modulation of the exchange coupling terms by stress can probably be understood in terms of the following simple dimensional argument. Since the exchange energies in question are of the order of a few tens of cm^{-1}, those energies would have to be modulated by nearly 30 to 100 percent in order to produce the observed shifts. In the meantime, the standard stress of 100 Kg/mm^2 produces strains on the order of 2×10^{-3}. It is unreasonable to expect the degree of overlap of the wavefunctions in question to be so sensitive to changes in the Cr ion separation that a change of 0.1% in that separation could modulate the overlap by nearly 100 percent. However, under the assumption that the
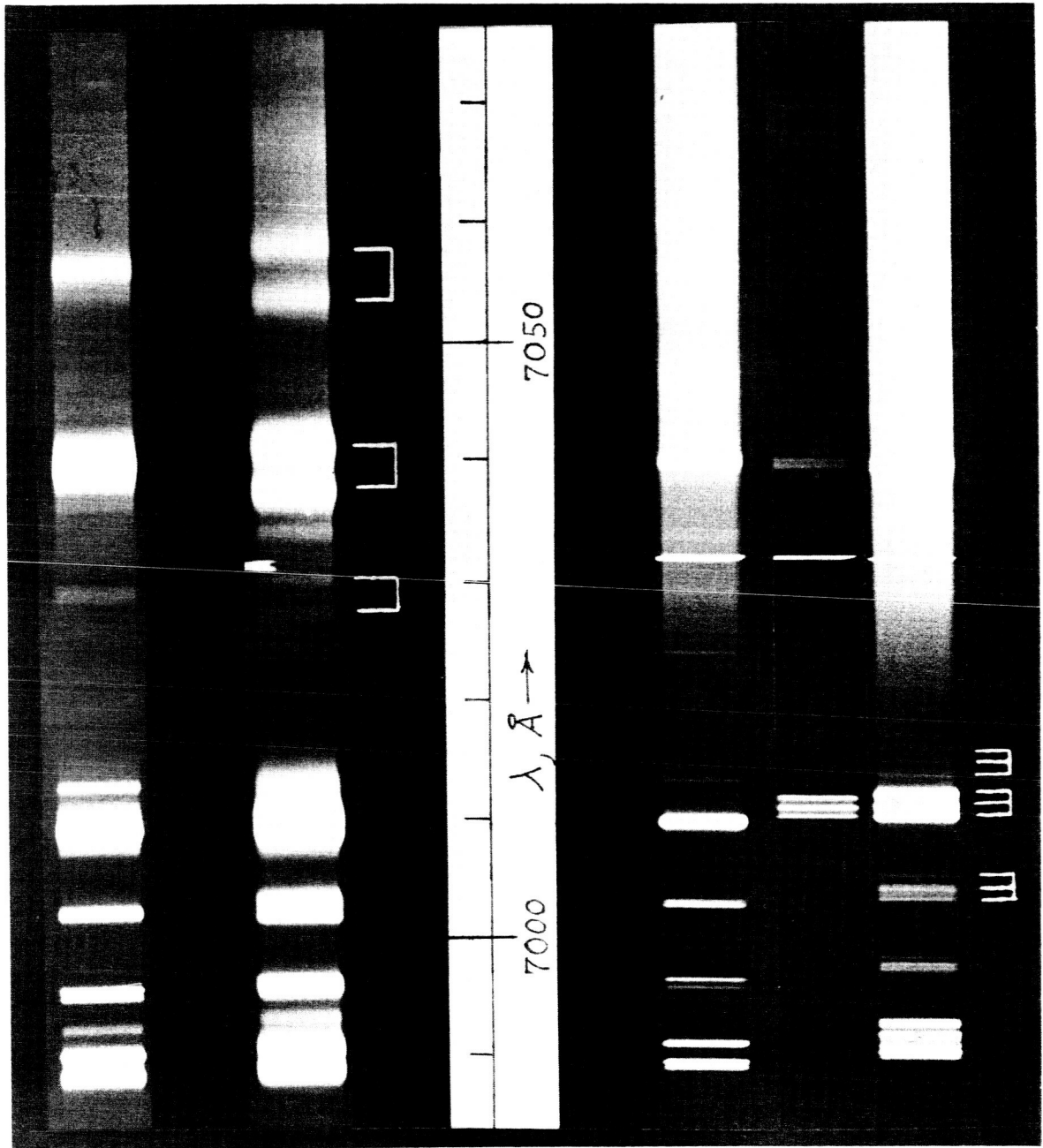
FIG. 3.12--Illustration of the splitting pattern common to all members of a given exchange multiplet. Above, second neighbor splitting; below, fourth neighbor splittings. Each stress split spectrum has a zero stress spectrum above it for comparison.

stress somehow is able to modulate the over-all energy separation between the ^2E and $^4A_2$ states, multiplying that energy of approximately 14,000 cm^{-1} by the strain of 10^{-3} yields shifts more nearly commensurate with those observed.

The above consideration makes the stress effect a powerful tool for the identification of the various members of a given exchange multiplet with each other. That is, one can formulate the principle that all the members of a given exchange multiplet undergo a common splitting under stress, where the common pattern is unique to the particular pair type involved. When that principle is applied to the second and fourth nearest neighbors, it merely provides verification of exchange multiplets previously determined by other means. However, as will be revealed shortly, the same principle has allowed discovery and identification of the first nearest neighbor exchange multiplet.

3.7 DISCOVERY OF TWO FIRST NEAREST NEIGHBOR LINES

While measurements of the N_0 splitting were being taken from the plates intended primarily for that purpose, a not too distant line, centered at 7540 Å (13,259.0 cm^{-1}), was observed to undergo a rather large shift to the red (-22.8 cm^{-1} for the standard pressure of 100 Kg/mm^2) on the plate corresponding to stress applied along the C_3 axis, yet shift of the same line for stress applied at right angles to C_3 was very small by comparison. Furthermore, the line at 7540 Å was never observed to split or broaden at any angle of applied stress. Finally, examination of spectra of rubies of different Cr_2O_3 concentration showed that the intensity of the line at 7540 Å, relative to that of the R lines, increased steadily from zero as the Cr_2O_3 concentration increased. Thus, behavior of the new line was exactly that expected for a line stemming from first nearest neighbors. Without the piezospectroscopic evidence, the new line would have been dismissed as being some sort of vibronic of the R lines or of the N_1 or N_2 lines, on account of its strange flat-topped shape and its rather unusual width, which was about 16 cm^{-1}.

A careful search of the plates finally revealed a second line, at 7302 Å (13,691.1 cm^{-1}), whose piezospectroscopic behavior was identical to that of the line at 7540 Å. The line at 7302 Å was very difficult to spot, since at

zero pressure it lay atop the edge of a broad feature of the long wave-
length tail of the R line vibrational sidebands. But for a pressure
of about 50 Kg/mm^2 applied parallel to C_3 , the line was pushed into
a clear space and was readily identifiable as a rather sharp line. At
a pressure of 80 Kg/mm^2, the line had been pushed out of the clear space
and could be seen intensifying the edge of another vibronic feature
farther to the red. Again, without the piezospectroscopic technique,
the line at 7302 Å would never have been discovered in the fluorescence
spectrum.

As pointed out earlier, at least one of the nearest neighbor types
must have an exchange coupling of several hundred cm^{-1} in order to
explain the Curie-Weiss constant of Cr_2O_3 . Since the other near
neighbor types (second, third, fourth), for which such a strong coupling
might have been plausible a priori, had been shown experimentally to
have exchange couplings an order of magnitude or more too small, the
first nearest neighbor pair was expected to have a J value in the range
of -200 cm^{-1} to -400 cm^{-1}. (Although the third nearest neighbor multiplet
was not yet known, it was thought to have an exchange somewhat like that
of the fourth nearest neighbors, by virtue of the similar atomic arrange-
ment of these two pair types.) Thus the approximately 430 cm^{-1} difference
between the two lines at 7302 Å and 7540 Å appeared to be a likely candi-
date for the exchange splitting of. J or 2J found between the S = 0
and S = 1 , or the S = 1 and S = 2 levels of the first nearest
neighbor pair type. Furthermore, the two new lines were known to rep-
resent transitions from the lowest lying levels of the excited state,
since their strength in fluorescence remained unchanged as the sample
temperature was lowered from 77° K to 20° K.

If the 430 cm^{-1} difference between the lines at 7302 Å and 7540 Å
represented splitting between the S = 1 and S = 2 levels, then the
line representing the transition from the lowest excited state to the
S = 0 level would lie hidden (in a fluorescence photograph) in the most
intense part of the vibrational sidebands of the R lines. Hence the
only way to decide between assignment of the line at 7302 Å to a trans-
ition terminating on the S = 1 level or terminating on the S = 0
level was to study its behavior in absorption. If it were a transition

to $S = 1$, absorption by the line should increase rapidly as the sample temperature was raised from very low temperatures, but if it were a transition to $S = 0$, the absorption should remain strong even at zero temperature. The absorption **studies are** the subject of the next chapter.

Incidentally, two other features were finally discovered to have the same piezospectroscopic behavior as the lines at 7302 Å and at 7540 Å: first, a line of a few cm^{-1} width centered at 7497 Å (13,335.0 cm^{-1}), whose intensity was much less than that of the near by line at 7540 Å, and second, a very diffuse feature centered at 7744 Å (12,909.7 cm^{-1}). The very diffuse nature of the line at 7744 Å, when combined with its approximately 350 cm^{-1} spacing from the line at 7540 Å, would make it appear to be a vibronic of that line. The line at 7497 Å might also be thought of as being a vibronic, in this instance of the line at 7302 Å, but its relative sharpness also makes it seem to be the equally likely result of a splitting of the level upon which the line at 7540 Å terminates.

3.8 ACCURACY OF THE PIEZOSPECTROSCOPIC MEASUREMENTS

Discussion of the various sources of error and the over-all accuracy of the piezospectroscopic measurements has been delayed until now in order not to interrupt the logical sequence in the assignment of pair types. Such a discussion would not have been pertinent to the above, since the accuracy of the measurements generally exceeds the degree to which the experimental curves could be expected to fit the simple theory used in interpreting them. However, for future reference, if it is ever desired to extract more from the piezospectroscopic measurements than has been obtained above, the following should indicate the most important sources of error and their probable effect on the accuracy of the measurements.

The measurements connect three variables — sample orientation, magnitude of applied stress, and displacement in frequency of the components of a line away from the zero pressure position. Orientation of the sample axis can probably be guaranteed to lie within a cone of half angle 2° from the supposed direction. The figure given is simply an estimate of the error involved in the transfer of information from the Laue camera to the cutting operation; a slight tendency for the plane of the saw blade to

wander produces the greatest part of that error. Determination of the orientation of a crystallographic axis relative to the x-ray beam direction was relatively more accurate, since the position of a Laue spot could be read to within 0.2° or better.

Positions of the rotation axes and pressure points of the lever arm assembly were sharply defined and known to within a small fraction of one percent; the weights themselves were guaranteed accurate to better than $\pm$ 0.1% by the manufacturer. The sample cross sections were rather precisely rectangular and the two nearly equal dimensions could be read with a good micrometer to within a small fraction of one percent. Hence the magnitude of the applied stress could certainly be guaranteed to be within $\pm$ 1% of the supposed value.

The grating drive mechanism on the large scanning spectrometer used in the study of the N_1 and N_2 lines was known from past experience to be precise to much better than one $\overset{\circ}{A}$ unit on its digital wavelength indicator, implying a precision of wavelength determination for the order used (eighth) of better than ± 0.05 $\overset{\circ}{A}$ or, equivalently, about $\pm$ 0.1 cm^{-1}. Study of each sample was begun with determination of the line position at zero stress; after the run was completed, the zero pressure line position was measured once more; no drift in that position could be detected. Hence the shift of a well resolved component could be determined to within better than $\pm$ 0.1 cm^{-1}.

By far the most uncertain process was that of determining the centers of lines involved in an unresolved or only partially resolved splitting. It would be rather foolish to try to attach a number to the accuracy of that process, since its value depends so critically on the degree of resolution already present. When the curves of the splitting patterns were drawn, the data points from well resolved components were taken most seriously, and the shape of the curves in the vicinity of badly resolved splittings were based on considerations of simplicity of shape and derivative continuity as well as on consideration of the data points themselves. For example, splitting in the vicinity of $\theta = -70^{\circ}$ for the splitting pattern of Figs. 3.2 and 3.13 is largely the product of imagination, and errors as high as $\pm$ 0.5 cm^{-1} are possible in that region, whereas points taken from the well resolved region can probably be considered correct to within $\pm$ 0.1 cm^{-1} .

- 31 -
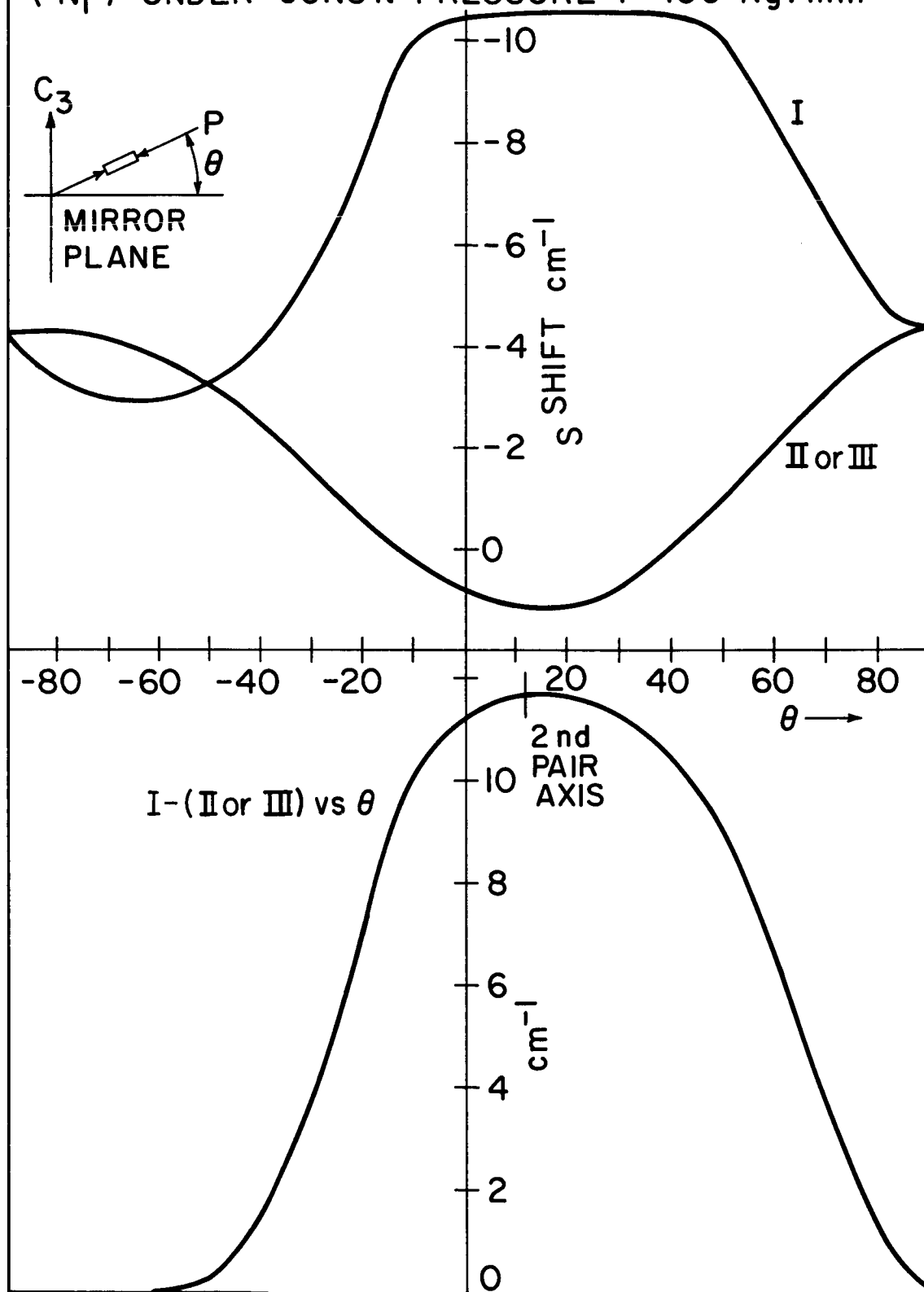
FIG. 3.13--N_1 splitting pattern and splitting curve.

Error inherent in the production of the plates used for study of the N_0 line should have been essentially negligible, since the neon marker from which all line positions were measured was superimposed directly on the ruby spectrum before the plate position was changed for a new exposure, and since emulsion shrinkage was certainly negligible. Here again the chief source of error was the uncertainty involved in the determination of the centers of incompletely resolved lines, with the nonlinear response of the photographic emulsion providing an added difficulty in the fitting of overlapping line profiles to the unresolved microphotometer trace. Fortunately, the various line components were often well resolved, and the resulting points fit very closely on a set of smooth curves. The curves thus determined are probably accurate to at least $\pm$ 0.5 cm^{-1} in most regions.

IV. ABSORPTION MEASUREMENTS

4.1 INTRODUCTION

Measurements of the absorption strength of the first nearest neighbor line at 7302$\overset{o}{A}$ as a function of temperature showed that the transition begins on a level approximately 220 cm^{-1} to 260 cm^{-1} above the ground state. By searching in the region thus indicated for a transition from the true ground state, a line was found at 7175$\overset{o}{A}$ whose strength in absorption remained constant as the temperature was lowered from 77°K to 20°K. Thus the line at 7302$\overset{o}{A}$, and a complex of lines surrounding it, were shown to be transitions from the S = 1 state. When the average position of the full S = 1 complex was taken into account, the exchange splitting between the S = 1 and S = 0 states of the first neighbor exchange multiplet was found to be approximately 227 cm^{-1}. Similar measurements on the absorption strength of the N_0 line showed the absorption to begin on a level 100 cm^{-1} or more above the true ground state of the third neighbor exchange multiplet. A re-examination of old piezospectroscopic plates revealed a number of other features belonging to the third neighbor multiplet, and several energy level schemes were suggested, all requiring a J value such that $|J| \rangle$ 40 cm^{-1}. The scheme most probable at this point is antiferromagnetic, with J = -46 cm^{-1}.

4.2 EQUIPMENT FOR DETECTING WEAK ABSORPTIONS

It was soon realized that the absorptions to be studied were rather weak, since a plate taken on the photographic instrument had revealed no trace of those lines in absorption through a 5 cm thick slab of dark ruby (Cr_2O_3 concentration approximately 0.7%). Since it would have been impractical to increase the absorption path length by more than a factor

of two or three, some way had to be found to improve upon the sensitivity of the photographic process, which seemed to be limited to detecting absorptions whose over-all strength was on the order of 1% or stronger.

Photoelectric detection represents a real gain over the photographic process if the electron current reaching the photocathode is large enough. That is, the generation of photoelectrons by a steady photon flux is a stochastic process. If an average number of electrons NT is generated within the integration time T, then, as is well known, the random fluctuations in that number have themselves an average value of $(NT)^{\frac{1}{2}}$ (shot noise). Let f represent the fractional change in the electron current brought about by the absorption, i.e., fNT is the signal strength. Thus the signal-to-noise ratio is given by the following

$$\frac{\text{Signal}}{\text{Noise}} = \frac{fNT}{(NT)^{1/2}} = f(NT)^{1/2} \quad . \tag{4.1}$$

Since inevitable slow drifts or very low frequency flicker in the various power supplies associated with the absorption experiment limit the maximum practical integration time T to about 1 sec, it is absolutely necessary to make the electron current N as high as possible.

Use of a photoelectric detector provides one other important advantage over the photographic process for measurement of weak absorptions. The photographic process usually requires that the sample be inserted between the white light source and the spectrometer, thereby allowing for the possibility that the desired weak absorption will be masked by fluorescence of the same line, where the fluorescence is brought about by pumping of associated bands by the white light. However, in an arrangement using photoelectric detection, it is possible, and in fact even desirable on still other grounds, to insert the absorption sample between the spectrometer output and the detector, thus subjecting the sample to light whose frequency corresponds to the absorption in question, and to no other.

The apparatus used is shown schematically in Fig. 4.1. The filament of a low voltage, high intensity tungsten lamp (GE Type 93) is carefully

- 85 -
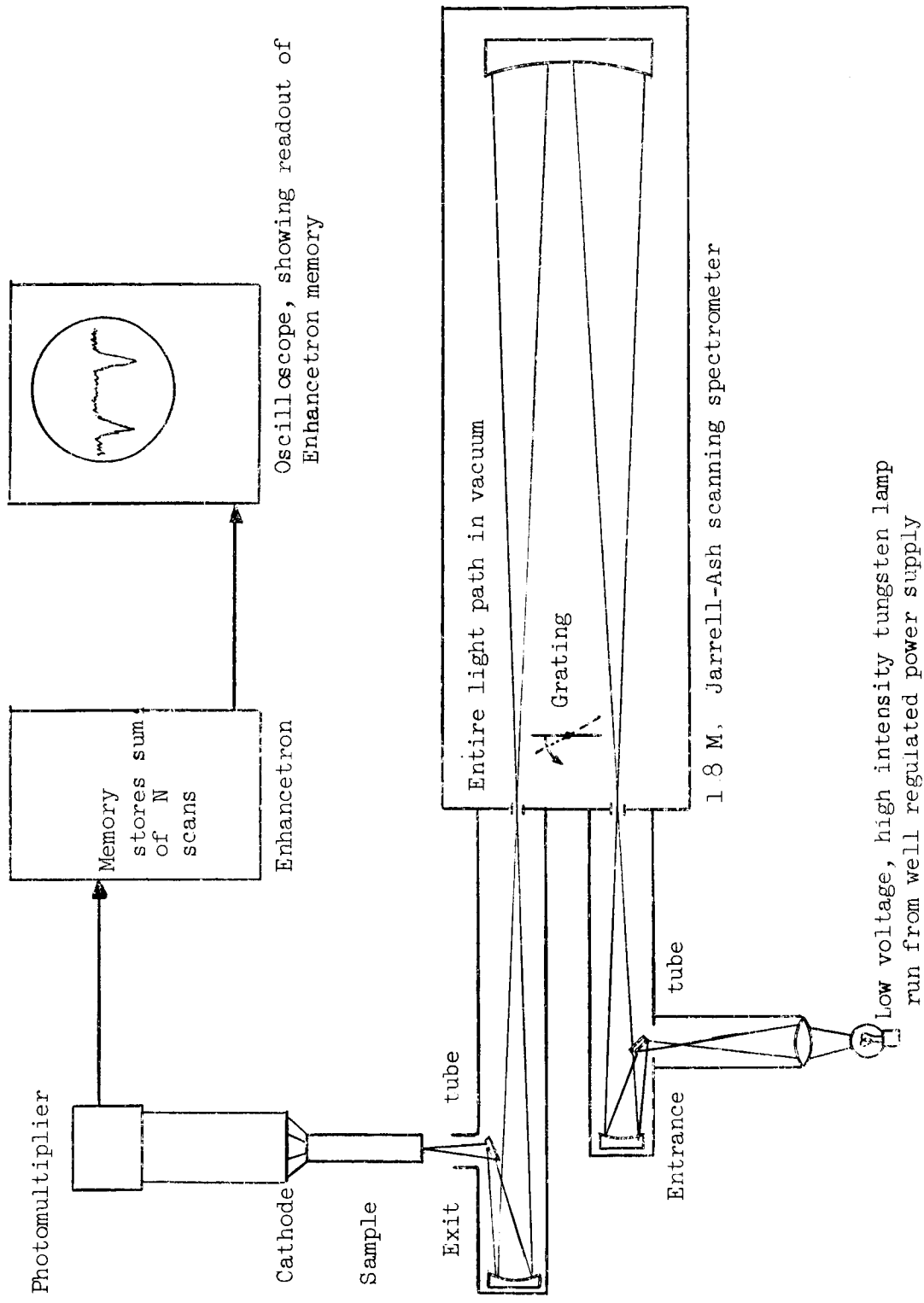
FIG. 4.1--Schematic representation of arrangement used to detect weak absorptions. Entire light path must be in vacuum or through an inert gas to a oid absorptions due to O_2 and H_2O.

focused onto the long entrance slit of the 1.8 M Jarrel Ash instrument and, after being filtered by the spectrometer, is focused onto one end of the absorption sample. The polished side walls of the sample allow it to act as a light pipe, and thereby transmit to the photocathode nearly 100% of the light put into it, exclusive of loss brought about by internal scattering centers. The sample was a cylindrical rod 1.6 cm in diameter and 15.3 cm long, of 1% Cr_2O_3 concentration, and of the best quality available at that concentration, as evidenced by the relative sharpness of the N lines at low temperatures. The phototube was an RCA Type 7265, having an S-20 cathode and a 14 stage electron multiplier. Although the wavelengths studied lay near the long wavelength cut-off of the S-20 response curve, the quantum efficiency of that photocathode type is so high (about 20% in the green) that its absolute quantum efficiency in the region of interest was still higher than that of other cathode types having more uniform response in the near infrared.

It was found possible to produce photomultiplier output currents of three to ten microamperes with the above mentioned apparatus, the exact value depending on the wavelength involved; that output current implies a cathode current on the order of 3×10^6 electrons per second. Since the integration time was about 1/3 sec, according to (4.1), a signal-to-noise ratio of one is implied for an over-all absorption of 0.1%. That signal-to-noise ratio can then be improved by scanning over the same wavelength region many times and taking the average of all the signal traces produced; if the number of scans is S , the signal-to-noise ratio will be improved by the factor $(S)^{1/2}$. The averaging was made feasible through use of a small electronic computer called the "Enhancetron" (Type ND800) made by Nuclear Data, Inc.

The Enhancetron itself works in the following way. The parameter to be varied (wavelength in this instance) is scanned uniformly in time over a given total interval; the corresponding time interval is broken into 1024 separate channels by the Enhancetron; and the signal voltage occurring in each channel is digitally analyzed and stored in a magnetic core memory. Each successive scan adds its signal values to each of the memory channels; when the experiment is complete, the sum in each channel

can be read out on an oscilloscope or a chart recorder, creating a nearly continuous graph of the averaged signal. Incidentally, the tens of thousands of electronic components necessary for such a computer are all housed in a package only half the size of the oscilloscope used for readout!

It should not be inferred from the above that the inherent signal-to-noise ratio must be of the order of one for the Enhancetron technique to become useful; rather, given enough scans, a good signal can be made from a signal originally much weaker than the noise. For example, 256 scans will allow a signal-to-noise ratio of 1/4 to be raised to four. Thus it was possible to detect absorptions in the 0.01% range through use of the Enhancetron.

The arrangement for sample cooling shown in Fig. 4.2 represents modification of an already existing photomultiplier housing. Thermal insulation was good enough to allow the coolant reservoir to hold a charge of liquid H_2 for about one hour, and thus sample temperatures of 20, 77 and 90 degrees Kelvin were possible with the use liquid H_2, N_2, or O_2. Higher temperatures were obtained simply by allowing the sample to warm up slowly after a charge of liquid N_2 had boiled away, until a thermocouple reading indicated that the desired temperature had been reached. The temperature was maintained within a few degrees of the desired value by periodically injecting small amounts of liquid N_2 into the reservoir.

Although effective for its intended purpose, the exact arrangement shown in Fig. 4.2 is not intended as a model for future construction, since at least one of its features could be improved upon. That is, it would be desirable to have photomultiplier cooling independent from sample cooling, for two reasons: First, a separate Dewar system for the sample would allow much better control of the sample temperature for values above $77^{\circ}K$, largely through the vast reduction in heat loss possible with such a system. For example, the sample could be almost completely surrounded by walls at $77^{\circ}K$ or $20^{\circ}K$, and the desired temperature achieved by balancing the radiative heat loss from the sample to the walls with a small electric heater whose power input would be controlled according to the output of a thermocouple or other suitable
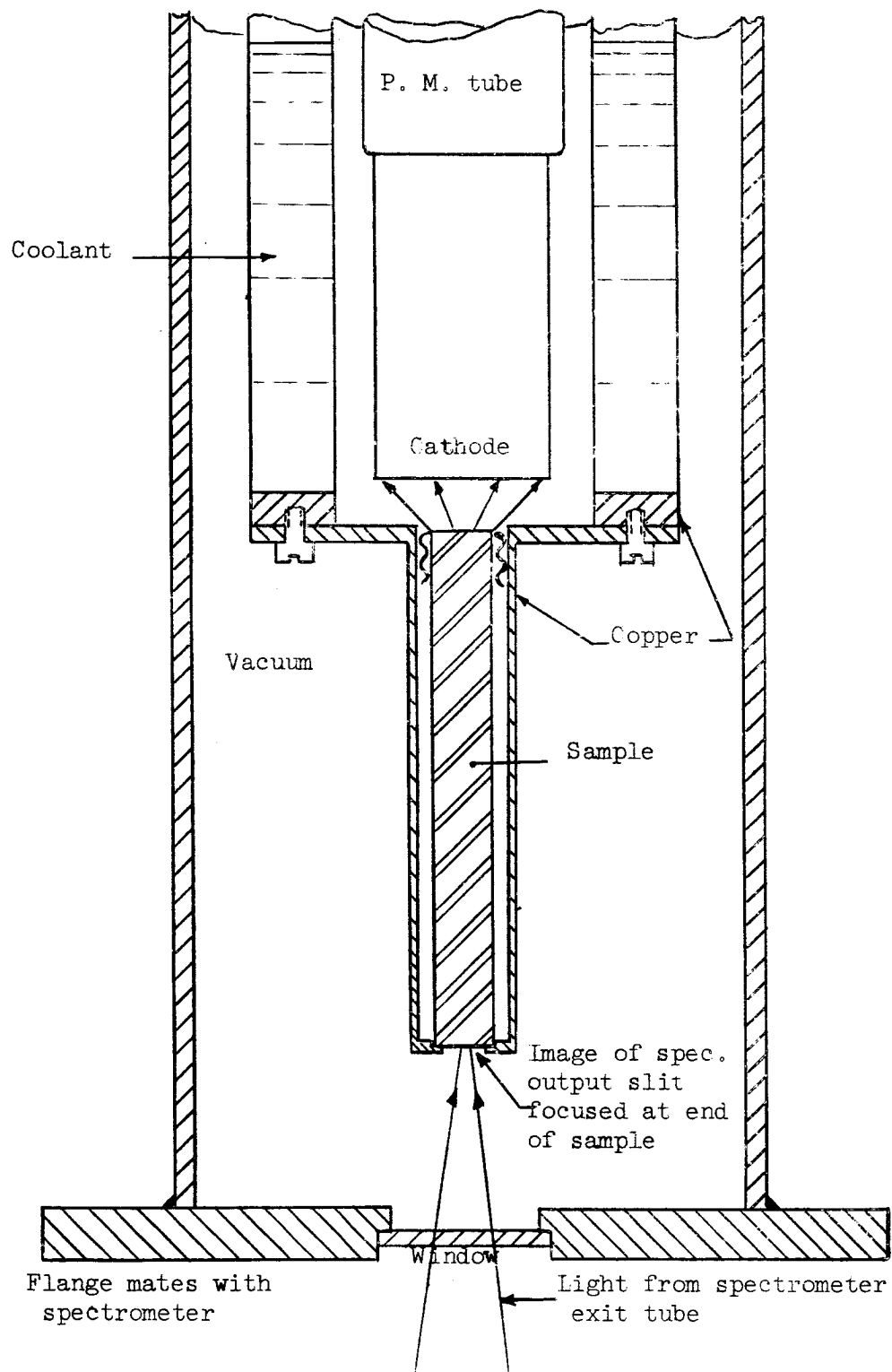
FIG. 4.2--Housing for sample and photomultiplier.

thermometer attached to the sample. And, of course, a separate Dewar system would be absolutely necessary if it were desired to use temperatures in the liquid He_4 range. In the second place, cooling of the photomultiplier is not at all necessary for an absorption experiment, where thermionic emission contributes only a small fraction to the total cathode current, and hence does not produce any measurable effect upon the signal-to-noise ratio. In fact, for the particular tube used, quantum efficiency in the region of the long wavelength tail of the cathode response curve was significantly reduced in lowering the temperature from room temperature to $77^{\circ}K$.

The features important to retain from the above are the use of the sample itself as a light pipe and the intimate relation of the cathode to the output end of the sample, which allows a large solid angle of light to be gathered. The arrangement in which the sample is placed between the lamp and the spectrometer (already rejected on other grounds) does not allow nearly as much light to be transmitted to the detector, since passage through the long sample destroys the lamp filament image, thereby reducing the intensity at the spectrometer entrance slit; furthermore, the large area of the photocathode is wasted when looking at a sharp image of the spectrometer exit slit.

4.3. DETERMINATION OF J FOR THE FIRST NEAREST NEIGHBORS

That part of the first nearest neighbor spectrum determined by means of the absorption and fluorescence studies to be described below contains a great many transitions, and a purely textual description would soon become laden with a bewildering array of numbers. Hence we give the final result first, in the form of an energy level diagram (Fig. 4.3); constant reference to that diagram will make the following description of the behavior of the various transitions much easier to follow. Unless otherwise indicated, all wavelength values listed will be those measured at $77^{\circ}K$; in the text, those values will often be given only to the nearest $\overset{\circ}{A}$ unit. Where appropriate, values precise to $\pm$ 0.2$\overset{\circ}{A}$ will be indicated in Fig. 4.3.
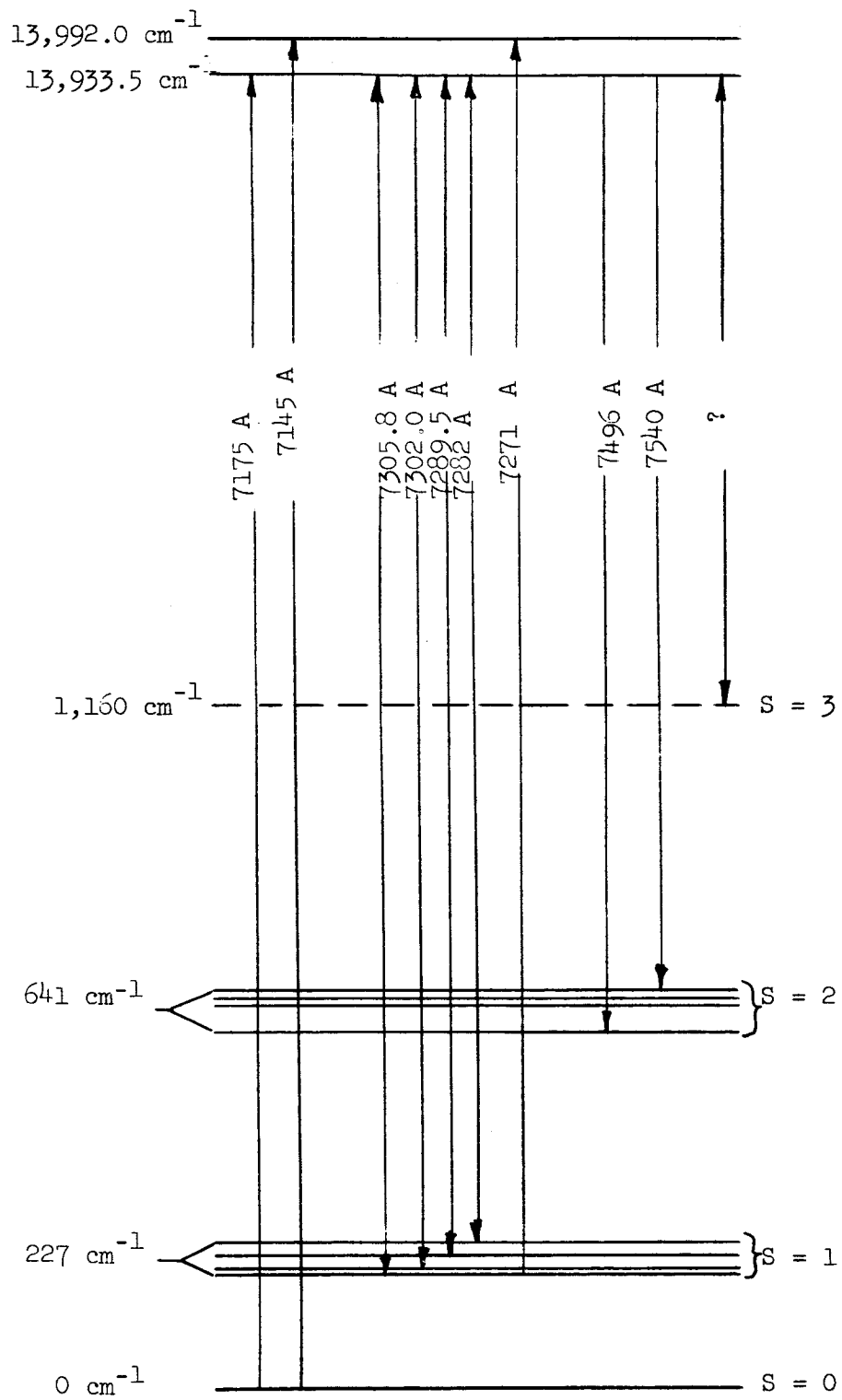
FIG. 4.3--First nearest neighbor energy level diagram. Arrowheads indicate
how a line has been observed (in emission, in absorption, or both ways)

In Chapter III it was established that the first nearest neighbor fluorescence line at 7302Å represents a transition from the lowest optically excited state to either the $S = 1$ or $S = 0$ level of the ground state exchange multiplet; hence a study of the strength of that line in absorption as a function of temperature was of primary importance. The absorption strength was measured at five different temperature values in the range $77^{\circ}K$ to $180^{\circ}K$; the relative strength is plotted versus T^{-1} in Fig. 4.4. The error intervals surrounding each data point indicate the difficulty involved in making accurate determination of the integrated line strengths in the presence of adjacent absorption lines, line braoden- ing with increasing temperature, and the rather severe noise problem encountered at the lower temperatures. Nevertheless, the data points clearly indicate that the absorption begins on a level whose separation from the true ground state is on the order of 220 cm^{-1} to 260 cm^{-1}. The line drawn through the data points represents the relative increase in population of a level 240 cm^{-1} above the ground state.

The transition from the true ground state ($S = 0$ level) of the first neighbor multiplet to the lowest optical level was thus indicated to occur almost certainly somewhere in the region between 7165Å and 7185Å. A search of the larger region 7200Å to 7135Å revealed more than a half dozen lines in absorption at $77^{\circ}K$, but all of these except two disappeared at $20^{\circ}K$. The two remaining lines, occurring at 7175Å ($13,933.5$ cm^{-1}) and 7145Å ($13,992.0$ cm^{-1}) (see Fig. 4.5) retained nearly constant absorption strength as the temperature was lowered from $77^{\circ}K$ to $20^{\circ}K$. Furthermore, the line at 7175Å is separated by 243 cm^{-1} from the first neighbor line at 7302Å, in excellent agreement with the observed temperature dependence of the 7302Å line. Hence, the absorp- tion line at 7175Å almost certainly represents the transition from the $S = 0$ level to the lowest optically excited state of the first nearest neighbors. Repetition of the 59 cm^{-1} separation between the 7145Å and 7175Å lines in absorptions from the $S = 1$ complex shows the line at 7145Å to be a transition from the $S = 0$ level to a higher optically excited state.
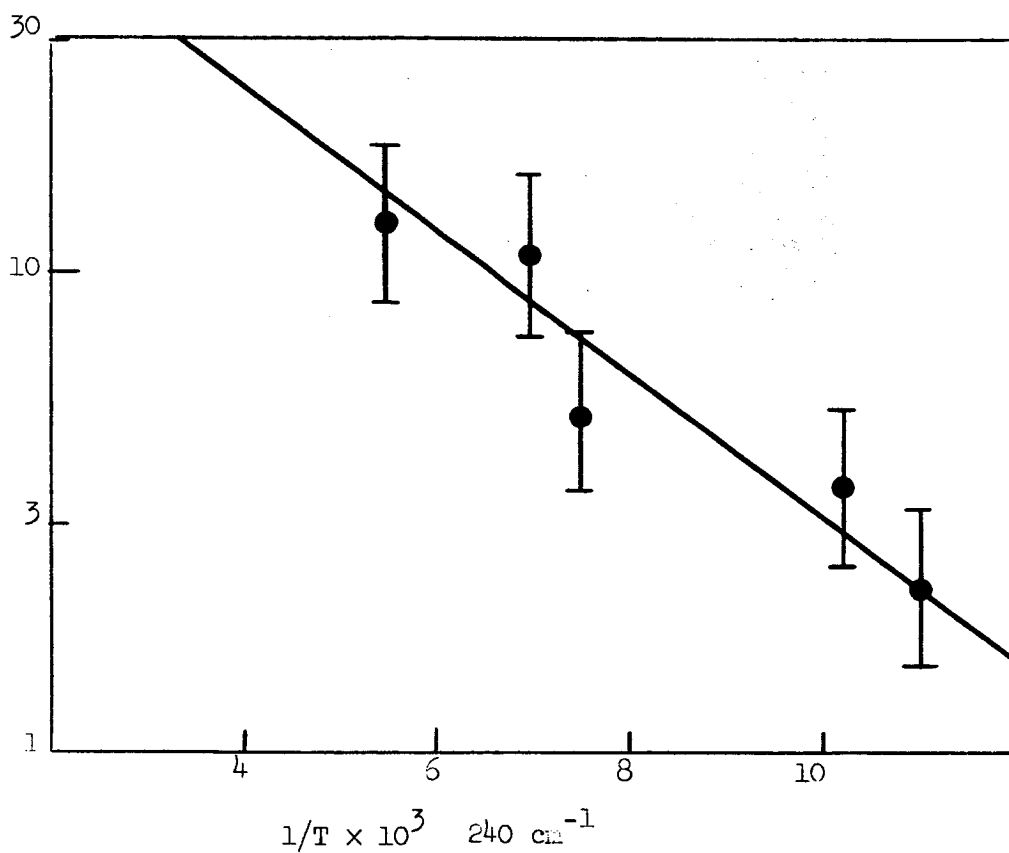
FIG. 4.4--Increase in absorption strength with temperature of the first
nearest neighbor line at 7302 Å . The line drawn through the
experimental points represents population of a level 240 cm^{-1}
above its ground state.
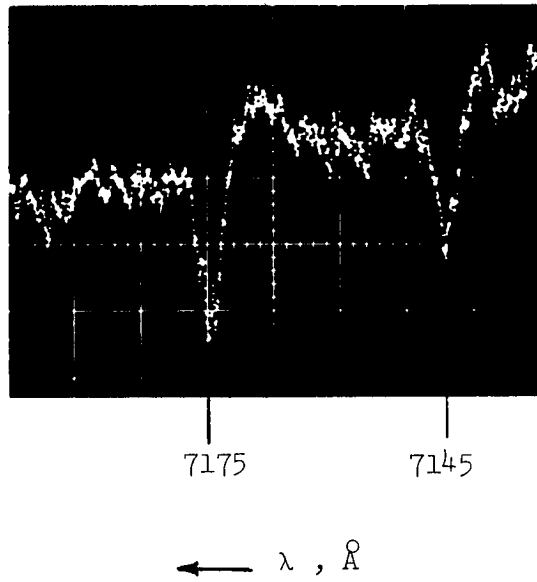
FIG. 4.5--Enhancetron output showing first neighbor absorption lines at
20° K . These lines correspond to transitions from the true
ground state, S = 0 .

We are now in a position to indentify the complex of absorption lines appearing in the immediate neighborhood of the line at 7302Å. It had already been suspected that the S = 1 state is broken into at least three levels by anisotropic exchange or other effects, since fluorescence of a very dark (Cr_2O_3 conc. ~ 2%) ruby sample at 77°K had revealed two other lines in the immediate vicinity of the 7302Å line, at approximately 7289.5Å and 7282Å. Fluorescence at 4.2°K of the sample used in the absorption studies revealed two members of the S = 1 triplet, the third still masked by a strong vibronic at that concentration (1.0% Cr_2O_3). Final proof of the multiple nature of the S = 1 state of the first neighbors rests with the fact that all three lines, 7302Å, 7289.5Å, and 7282Å, exhibit essentially the same increase in absorption strength with increasing temperature.

Figure 4.6 shows the complex of absorption lines originating on the S = 1 triplet as they appear at two different temperatures. In addition to the three lines mentioned above, another set displaying the same increase with temperature can be seen beginning at a frequency approximately 60 cm^{-1} to the blue of the line at 7302Å; it is therefore assumed that this second set represents transitions from the S = 1 triplet to the higher of the two optically excited levels mentioned previously, although the limited wavelength region scanned does not allow a complete check to be made on the existence of the highest frequency members of this set.

Figure 4.7 shows an additional splitting of the S = 1 state which is not resolved for temperatures above 77°K; the line at 7302Å, whose center appeared shifted to 7304Å at higher temperatures, is resolved at 77°K from a second component at 7305.8Å. The possibility that the two lines represent transitions from the same component of the S = 1 state to a split excited level seems to be ruled out by the clean singlet nature observed for the transition from S = 0 to the lowest optical state (see Fig. 4.5). Thus it would seem that the S = 1 state is split into at least four distinct levels, and hence a lifting of the three-fold degeneracy of the spin part of the wavefunction cannot explain all of the splittings observed in the S = 1 complex. Nevertheless, if the finer splitting of the line at 7302Å is ignored, the possibility
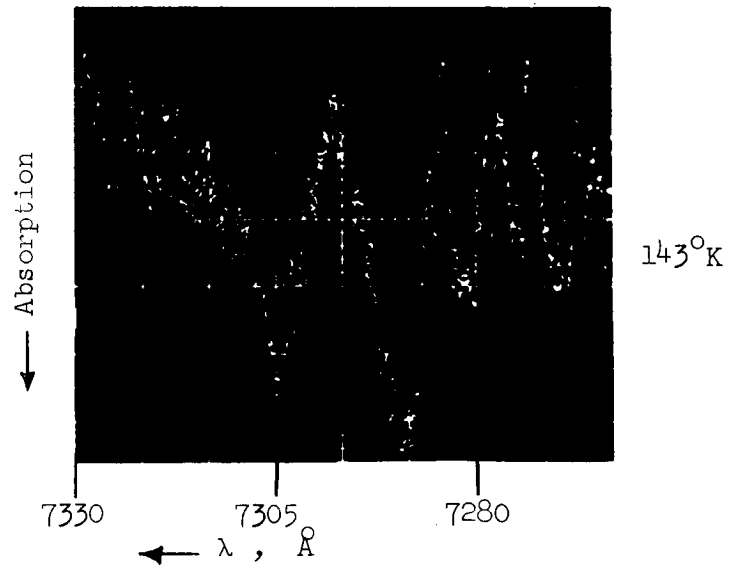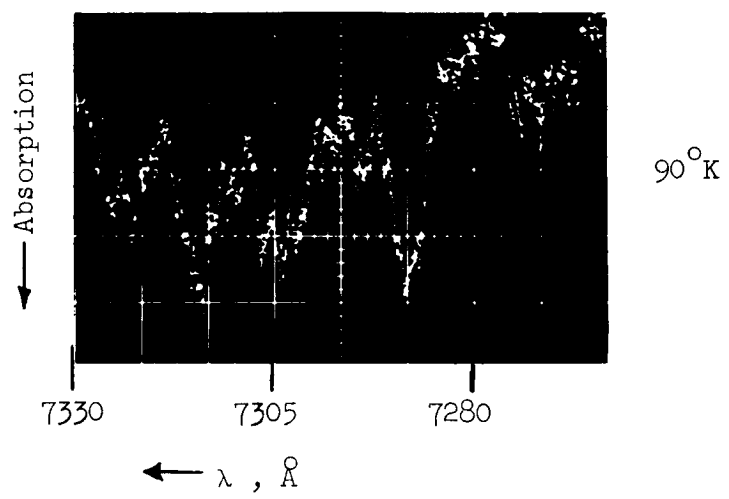
FIG. 4.6--Behavior of the cluster of lines near 7300 Å with temperature.
Intensity scales of the two photographs can be compared on a
one to one basis.
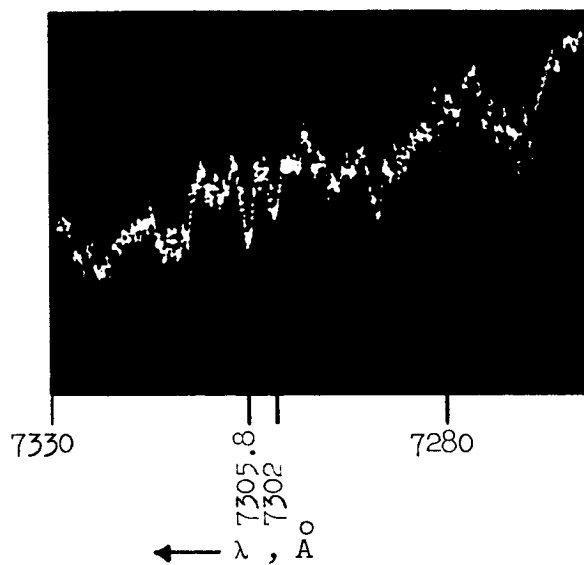
FIG. 4.7--Resolution of line at 7302 Å into two components when the temperature is lowered to 77°K. At higher temperatures the two components merge into an unresolved line centered at about 7304 Å .

that the hamiltonian contains anisotropic exchange terms may provide
the most plausible explanation for the gross three-fold splitting of
the S = 1 level, since the same term would then also predict the
single level observed for the S = 0 state. The finer splittings might
then be explained in terms of the existence of vibrational states for
the Cr ion pair, somewhat analogous to the vibrational levels of a free
diatomic molecule.

No attempt was made to see absorptions originating on the S = 2
level or complex of levels, since that complex was known to lie more
than 600 cm^{-1} above the true ground state, making population of the
S = 2 complex too small at temperatures for which the linewidths would
be sharp to allow detection of absorptions. Thus, the linking together
of transitions beginning or terminating on the S = 2 complex with
those involving the S = 1 complex must rest with the common piezo-
spectroscopic behavior observed for those lines, as related in Chapter III.

In view of the complex splitting observed for the S = 1 state, an
even greater number of components is expected from the S = 2 state.
In fact, several components can be inferred from the low temperature
(4.2°K) fluorescence spectrum of the good quality sample used in the
absorption studies. Figure 4.8 is a microphotometer trace of the
relevant region of that spectrum; the piezospectroscopic studies have
indicated that the well resolved line at 7496.1Å and the broad feature
at 7540Å belong to the first neighbors, while the same studies have
shown that the other features (indicated by a dashed outline) belong
to the third neighbor spectrum. The broad feature at 7540Å may contain
as many as three unresolved components.

From the above it can be seen that the S = 1 and S = 2 complexes
span rather large regions of approximately 45 cm^{-1} and 70 cm^{-1}, respec-
tively. Thus it is difficult to make accurate determination of a center
for each complex, such that all lines of each complex would lie at that
center if the various and unknown sources of splitting did not exist.
In the absence of a more appropriate formula, the average of the two
outermost members of each complex is taken here. On that basis, split-
ting between S = 0 and S = 1 becomes approximately 227 cm^{-1}, and
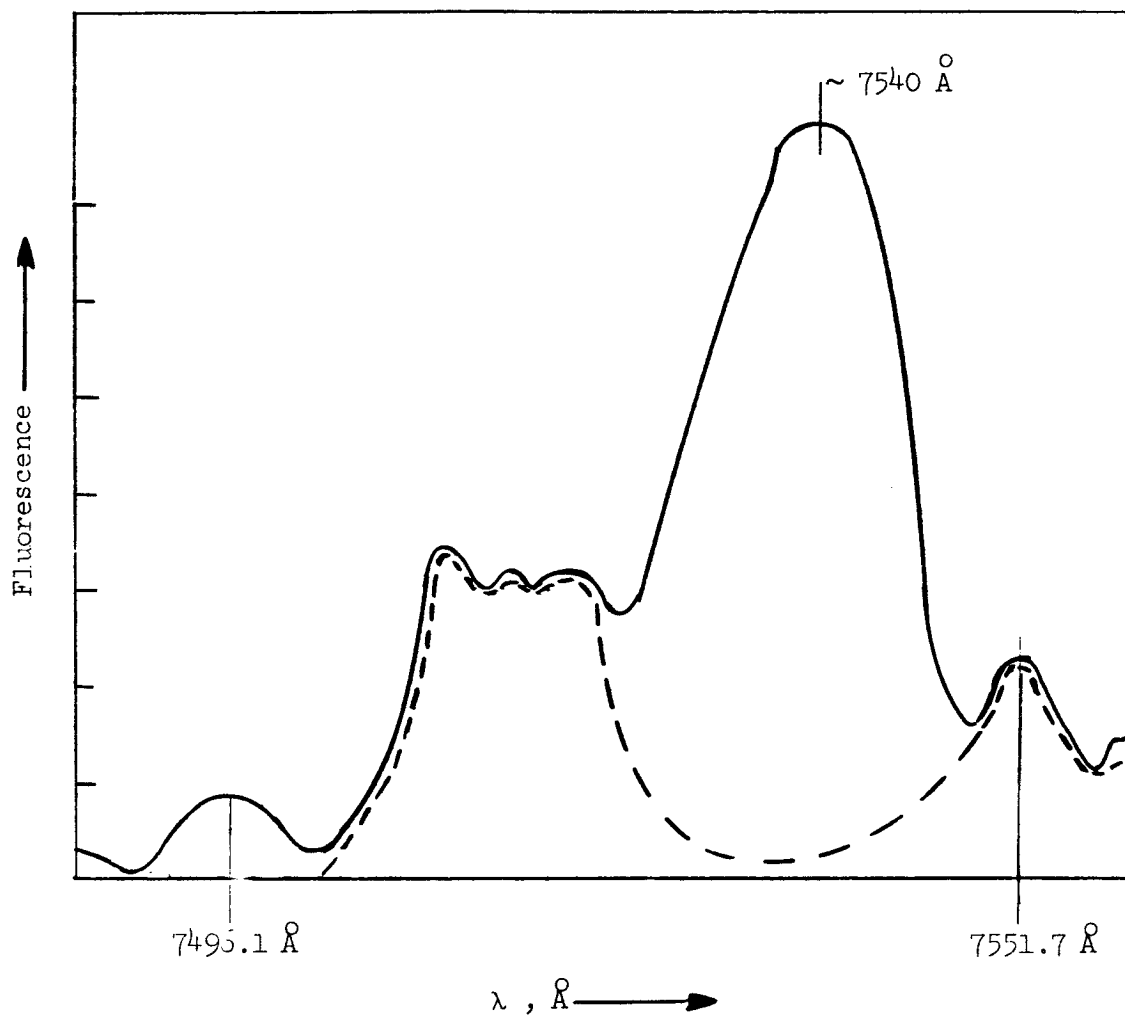
FIG. 4.8--Microphotometer trace of fluorescence plate of 1% Cr_2O_3 ruby
at 4.2° K. Third neighbor lines are shown dashed, first
neighbor lines are solid.

that between $S = 1$ and $S = 2$ becomes approximately 414 cm^{-1}. Although those two intervals do not fit the simple Lande interval rule, a fit can be made with only a small biquadratic correction, such as has already been found necessary for the second and fourth neighbor exchanges.

On the basis of the above mentioned intervals, the values to be inserted in the biquadratic expression (1.4) are $J = -184$ cm^{-1} and $J = -6.7$ cm^{-1}. The center of the $S = 3$ complex is then predicted to lie 1160 cm^{-1} above the $S = 0$ level, implying that transitions from the lowest optical state to the $S = 3$ complex should occur in the neighborhood of 7830Å. A rather diffuse feature can be seen just a little farther to the red, centered at roughly 7900Å, but that feature could equally well be a vibronic of the rather strong set of lines at 7540Å of the $S = 2$ complex. Furthermore, although calculation of transition strengths is generally considered impossible for the pair spectra, in view of the many parameters that simply have to be guessed in the process of making such a calculation, that calculation may yet prove tractable in the somewhat special case of the first nearest neighbors; it will be shown later that such a calculation, when based on the simplest set of assumptions, yields a vanishingly small strength for either electric or magnetic dipole transitions from the lowest optical state (essentially an $S = 1$ state) to the $S = 3$ state. Thus, observation of transitions to $S = 3$ may be forbidden in a very fundamental way.

It should be mentioned here that at least some of the first neighbor transitions (those clearly distinguishable from background in the fluorescence plates) appear to be strongly polarized with respect to the C_3 axis. For example, for observations made at right angles to C_3, the line at 7540Å is strong for E parallel to C_3 and completely eliminated for E perpendicular to C_3. The possible implications of such polarizations will be discussed later in conjunction with a calculation of transition probabilities.

It cannot be claimed that the above studies have given an absolutely certain answer to the questions originally asked of them, and in the meantime the finer details revealed in the course of those studies have

raised a whole host of new questions. Nevertheless, the ground state exchange multiplet can be considered rather well established in general outline, and the large J value appropriate to an understanding of the antiferromagnetic arrangement in Cr_2O_3 is now known to a good approximation, i.e., $J = -227 \pm 20$ cm^{-1} .

4.4. DETERMINATION OF THE THIRD NEAREST NEIGHBOR EXCHANGE MULTIPLET

Absorption strength of the third neighbor line at $7452\text{\AA}$ ("N_0") has been observed to increase rapidly with increasing temperature; the best measurement to date indicates an increase by a factor possibly as small as two times, but more likely on the order of three or four times between the temperatures $77^\circ K$ and $142^\circ K$. Thus the level from which the N_0 line originates was indicated to lie at least 100 cm^{-1} above the true ground state of the third neighbor exchange multiplet, and a search for the remaining members of that multiplet was begun.

Examination of piezospectroscopic plates again yielded most of the desired information; five features[1] were found having essentially the same piezospectroscopic behavior as that of the N_0 line. At a temperature of $20^\circ K$ or lower, a line at $7404\text{\AA}$ could be seen in the fluorescence spectrum of samples containing 1% Cr_2O_3, where previously (i.e., at lower concentrations or at higher temperatures) the line had been hidden by a strong vibronic, presumably of the R_2 line. The new line at $7404\text{\AA}$ had the same width as the N_0 line, and appeared to undergo the same splitting as that of the N_0 line for stress applied parallel to C_2 , the only sample orientation studied at the necessary combination of high concentration and low temperature.

Two of the features mentioned above were found at $7516\text{\AA}$ and at $7551.7\text{\AA}$, in the neighborhood of the $S = 2$ complex of the first neighbors; they would probably have remained undiscovered if it were not for the fact that the considerably stronger, adjacent first neighbor lines

---

[1]The word feature is used here to indicate fluorescent emission before distinction can be made between a vibronic and a true pair line.

are greatly attenuated in the polarization $E \perp C_3$. Thus, for study of
these two, the only useful orientation is that with stress parallel to
C_3; nevertheless, positive identification of these lines with the same
excited level which gives rise to the N_0 line can be made on the basis
of the unmistakable and unique piezospectroscopic behavior of third
neighbor lines. That is, under stress parallel to C_3, the lines at
7516Å and 7551.7Å move the same distance to the blue as does the N_0
line, whereas the first neighbor lines move to the red.

Although the line at 7551.7Å is a singlet having the same shape and
width as the N_0 line, the greater width and somewhat square topped
shape of the feature centered at 7516Å indicate that it contains two
unresolved components of nearly equal intensity, at approximately 7513Å
and 7519Å, each component having individually the same width as the N_0
line. Thus it is most probable that the above mentioned features are
indeed lines, and not vibronics of one of the other third neighbor lines,
although the latter possibility cannot be absolutely excluded. In the
following it will be assumed that true lines exist at 7513Å, 7519Å, and
7551.7Å.

By way of contrast, the two remaining features showing piezospec-
troscopic behavior the same as that of the N_0 line are each broad and
highly asymmetric in shape, with peaks occurring at about 7666Å and
7706Å. Position and shape of these two strongly indicate that they are
vibronics of the N_0 line.

Figure 4.9 shows an energy level scheme suggested by the above
mentioned data. Since all are present in fluorescence at $4.2^\circ K$, the
various known third neighbor lines have been assigned to transitions
from the lowest optically excited state to the $S = 3$, $S = 2$, and
$S = 1$ levels of an antiferromagnetic ground state exchange multiplet.
The $S = 3$ state is considered to be split into several components,
possibily by anisotropic exchange terms in the hamiltonian, yielding the
transitions at 7551.7Å, 7519Å, and 7513Å. The $S = 2$ and $S = 1$ levels
may also be split, but so far only one transition is known for each. If
the average position of the $S = 3$ complex is taken as the mean of the
two extreme frequencies, exchange splitting between the $S = 3$ and $S = 2$
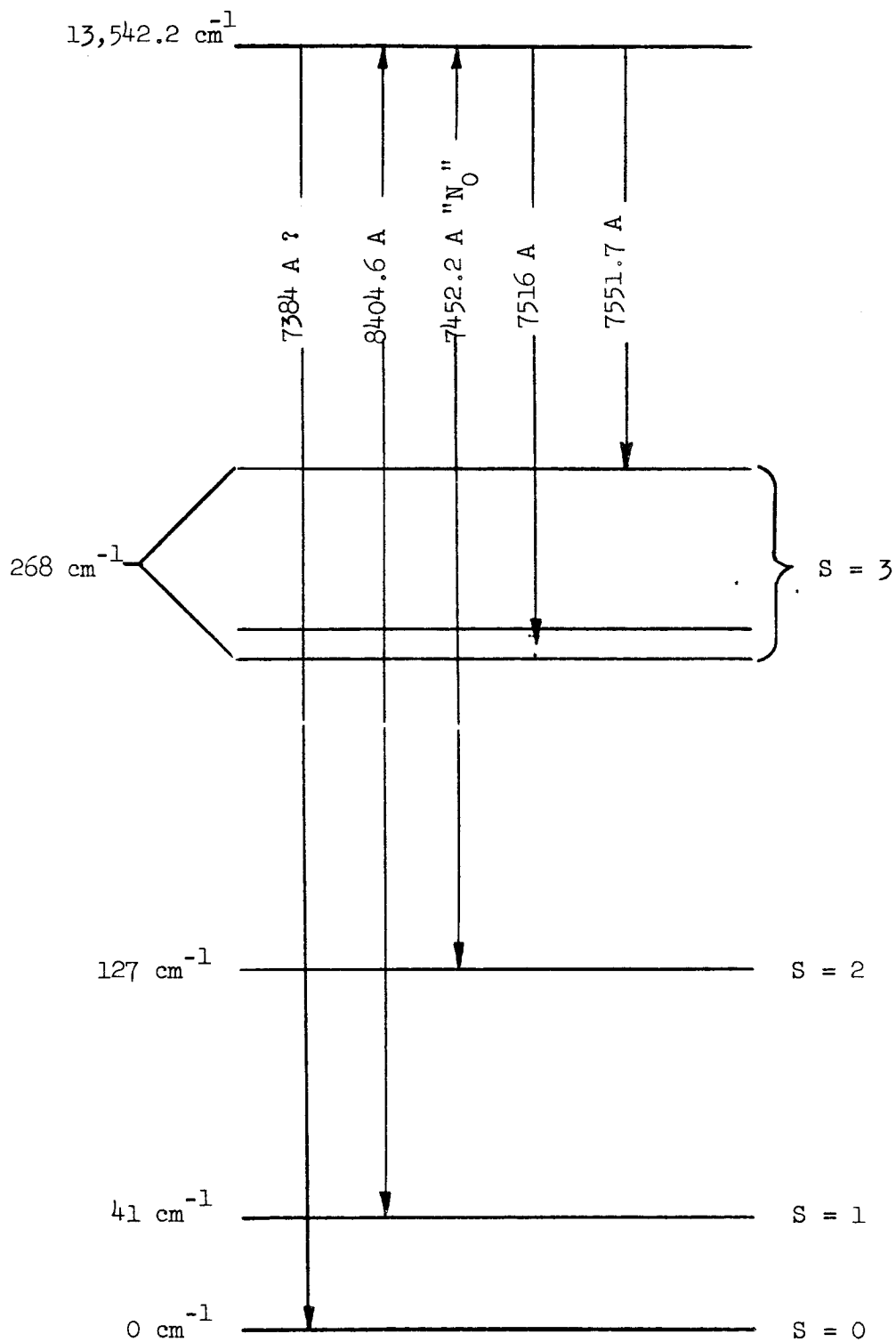
FIG. 4.9--Third neighbor energy level diagram. Arrowheads indicate how a line
has been observed (in emission, in absorption, or both ways). For
alternate possibilities, see Fig. 4.10.

levels is $\overline{140}$ cm^{-1}. When the above value is combined with the 86 cm^{-1} separation between $S = 2$ and $S = 1$, the values $J = -46$ cm^{-1} , and $j = 0.2$ cm^{-1} can be computed for insertion into the biquadratic expression (1.4).

The exchange hamiltonian thus determined implies an exchange splitting of approximately 41 cm^{-1} between the $S = 1$ and $S = 0$ states, and hence the transition from the lowest excited state to $S = 0$ is predicted to occurr at about 7382.5Å. In fact, a weak line can be seen at about 7384Å on a fluorescence plate corresponding to a sample temperature of 20°K; considering the somewhat arbitrary criterion used for determination of the average position of the components of the $S = 3$ complex, the appearance of a line 1.5Å from the predicted position for a transition to $S = 0$ can be considered to give an excellent fit. Furthermore, on another plate of fluorescence of the same sample at the same temperature, but with stress applied such that the N_0 line was split, the line at 7384Å disappeared into the emulsion grain noise, consistent with its also having undergone a splitting. Unfortunately, the line at 7384Å is not visible on any of the other plates of other dark samples at low temperatures, but the line is so weak that a rather lucky set of circumstances may be required to see it at all.

The energy level scheme of Fig. 4.9 is consistent with the somewhat meager absorption data obtained before the writing of this paper required a temporary suspension of those studies. A calculation of the population of the various levels as a function of temperature shows that the N_0 absorption should increase in strength by a factor of about two times between the temperatures 77°K and 142°K, in agreement with the lowest of the range of values indicated by the absorption measurements at those two temperatures. The same calculation indicates that absorption of the 7404Å line should increase by a factor of about four times as the temperature is raised from 20°K to 77°K, and remain nearly constant between 77°K and 142°K, consistent with the absorption data mentioned on page 101.

Thus far, the argument has been in favor of the energy level scheme of Fig. 4.9, but it should be made clear that the proposed scheme is

by no means firmly established at this point. In the first place, better and more complete data are needed, of the kind provided by the piezospectroscopic studies as well as that provided by absorption studies. In addition, the proposed scheme presents certain features which may be considered rather implausible from a theoretical standpoint, such as the large splitting of the $S = 3$ complex (the separation between outermost components is nearly 67 cm^{-1}), or such as the fact that the implied J value is vastly different from that known for the fourth nearest neighbors, despite the rather similar atomic arrangement for third and fourth nearest neighbors. However, for a theory which predicts just such a change in sign of J between the third and fourth neighbor pairs, see Section 5.2 of Chapter V.

In fact, at least one other possible energy level scheme involving a _ferromagnetic_ exchange is not entirely ruled out by the data known so far. If the lines at $7404Å$ and at $7384Å$ can be excluded from the third neighbor scheme, then the energy level diagram shown in Fig. 4.10a becomes highly plausible. In addition to the fact that it avoids the difficulties already mentioned above in connection with the scheme of Fig. 4.9, it allows for a more rapid rate of increase in absorption strength of the N_0 line with increasing temperature in the $77°K$ to $142°K$ range, providing better agreement with the absorption data on that line. The ferromagnetic scheme indicates a J value on the order of $J = 60$ cm^{-1} .

If, in addition to exclusion of the line at $7404Å$, the feature centered at $7516Å$ is considered to be a vibronic, another _antiferro-magnetic_ scheme is made possible, this time with a J value of approximately $J = -60$ cm^{-1} . The scheme is shown in Fig. 4.10b; here too, as in the scheme of Fig. 4.10a, the advantages are that it is no longer necessary to explain a large splitting within a given S state, and that better agreement is provided with the observed increase in absorption strength of the N_0 line with increasing temperature.

Despite the fact that no one of the above mentioned schemes is definitely excluded by the rather meager data obtained to date, at least the following is certain; in contrast to previous conclusions
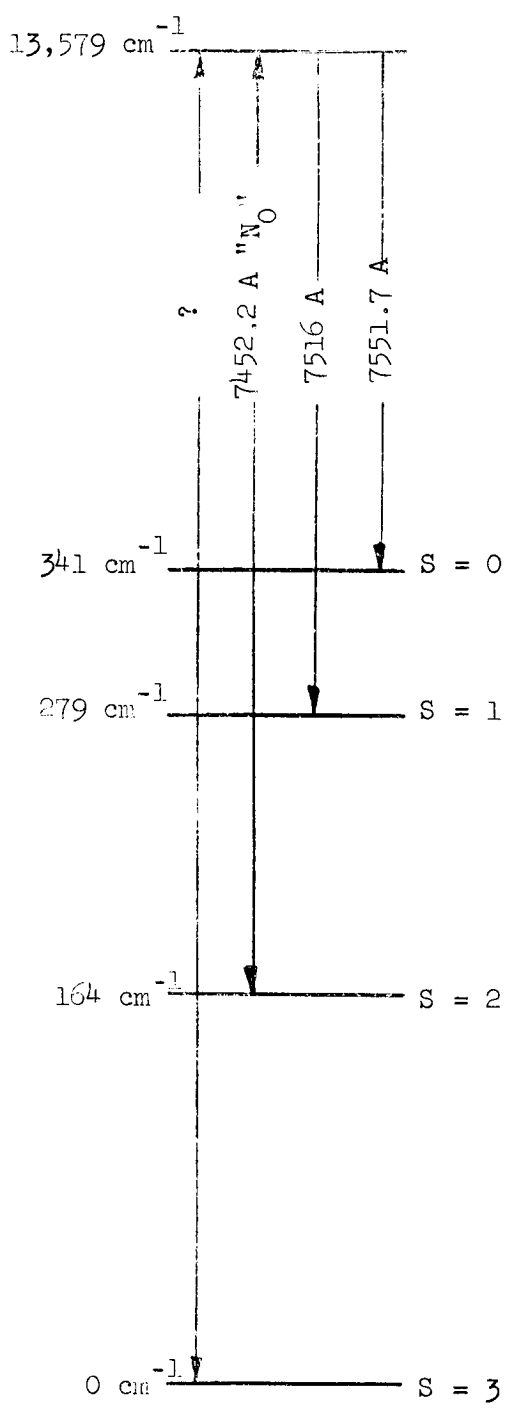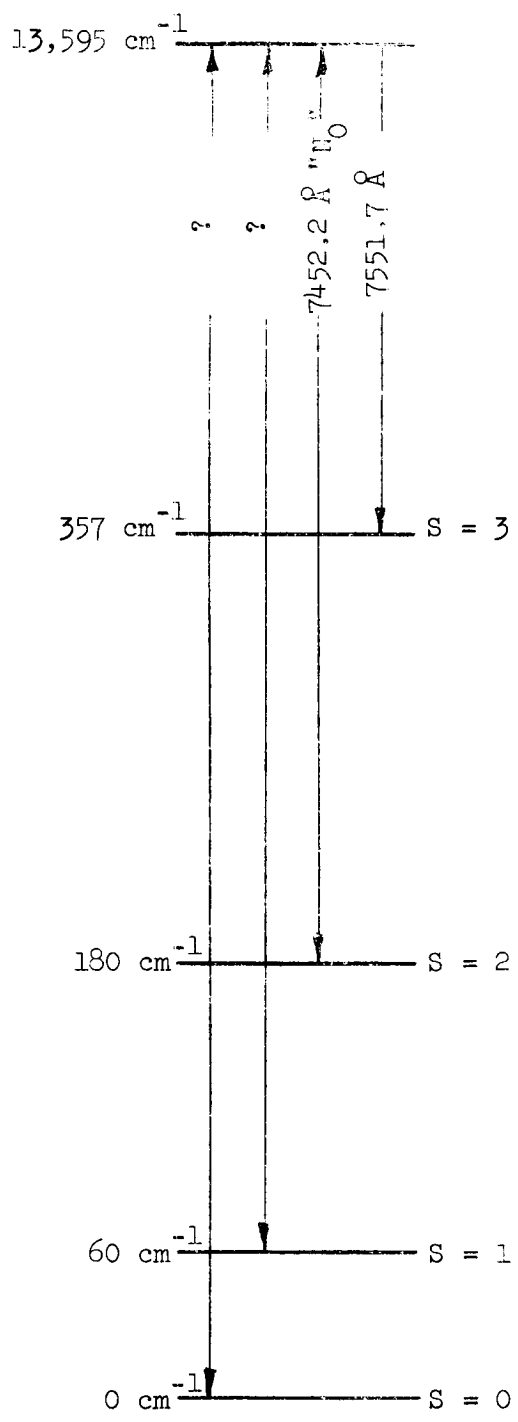
FIG. 4.10--Possible third neighbor energy level schemes not entirely ruled out by present data. For most favored scheme, see Fig. 4.9.

that $|J_3| < 1$ cm^{-1} (the J value for the ith nearest neighbor will be indicated by J_i), it is now known that $|J_3|$ is rather large, i.e., $|J_3| > 41$ cm^{-1}. In addition, considerations of antiferromagnetic ordering in Cr_2O_3 exclude the possibility of the large positive value (ferromagnetic coupling) suggested above for J_3, when the more certain experimentally determined values for J_1, J_2, and J_4 are taken into account. (For a discussion of the ordering, see Section 5.2 of Chapter V.) Thus, we can probably also say that it is now known that $J_3 < -41$ cm^{-1}. In addition, it has been demonstrated that the tools necessary to determine experimentally the true J value do indeed exist, and that a more thorough application of them should allow a definite choice to be made among the various possibilities.

V. CONCLUSIONS

5.1 SUMMARY OF EXCHANGE VALUES FOR NEAR NEIGHBOR PAIRS

The principal results of this paper are summarized in Table 5.1;
only the exchange integrals listed for the second and fourth nearest
neighbors were known previously. The other two exchange couplings and
all the identifications of the exchange couplings with particular near
neighbor types constitute the major new results of this work. The J
value listed for the third neighbors is to be considered tentative; for
details and reservations concerning this assignment, see Chapter IV,
Section 4.4.

TABLE 5.1

Neighbor Type	J, cm^{-1}	j, cm^{-1}	$E\ (S = 1) - E(S = 0)$, cm^{-1}
First	- 183.5	- 6.7	227
Second	- 11.56	+ 0.19	10.3
Third	- 46	+ 0.2	41
Fourth	+ 6.94	+ 0.14	- 7.9

The rather precise values of J and j listed for the first and third
neighbors should be qualified in the following way: fairly large aniso-
tropic splitting within the various S states makes assignment of an
average location of the various components of a given S state to be
somewhat uncertain; the values listed were based on the median position.
If it ever will be possible to take a more appropriate average, or if
other components are discovered, the values listed above for J may be
changed by a few percent, and those listed for j drastically altered.

5.2 CORRESPONDENCE BETWEEN THE MEASURED J VALUES IN RUBY AND THE THEORY OF ANTIFERROMAGNETISM IN Cr_2O_3

The theory of antiferromagnetism is concerned with three kinds of problems:

(1) the calculation of J values for the important near neighbor types; (2) the determination of an ordered spin arrangement at low temperatures by a given set of exchange forces; and (3) the generation of theories connecting the measured or calculated set of J values to the macroscopic magnetic constants T_N (Neel temperature), X_N (magnetic susceptibility at the Neel point), and Θ (the Curie-Weiss constant). Here T_N is the temperature below which antiferromagnetic ordering sets in; well above T_N the behavior is essentially paramagnetic, as described by the law

$$(T) = \frac{C}{T + \Theta} \quad . \tag{5.1}$$

The various aspects of the problem are sufficiently formidable that much of the present theory is capable of making only qualitative predictions, in spite of the great amount of effort that has been spent by a rather sizable number of theoreticians.

However, the purely theoretical difficulties are not entirely to blame for lack of well established models, since until now there has been a paucity of the kind of experimental data central to the problem; that is, a complete set of independently determined J values has never previously been known for such a complex structure. Thus the problem is usually bound up in a circle of ignorance: attempts to deduce a set of J values from knowledge of the quantities T_N, Θ, X_N are based upon models of uncertain validity; the models are in turn uncertain because they have never been tested against a known set of J values of even moderate accuracy. Furthermore, with respect to study of the more complex structures, such as corundum, there are too many non-negligible J values to be determined from the three macroscopic parameters mentioned above. In the following discussion it will be shown how the essentially complete set of important J values, as determined by the experimental results of

this study, will allow independent evaluation of theories of exchange and theories of ordering, at least for Cr_2O_3, and possibly for the closely related compound α-Fe_2O_3 as well.

The calculation of exchange couplings in metal oxides necessarily becomes involved with the very complicated problem of super exchange, since many of the metal ion separations are too great to allow for direct overlap of their wavefunctions. Instead, the exchange often must take place through one of the P orbitals of an intervening oxygen ion, one lobe of the P orbital interacting with one of the metal ions, the other, oppositely directed lobe interacting with the second metal ion. Thus, a linear array (metal-oxygen-metal bond angle = 180°) is expected to allow for the greatest super-exchange, while a 90° bond angle is expected to give essentially zero exchange. Hence, for bond angles in the neighborhood of 90°, if a coupling is nevertheless observed it is usually explained in terms of direct contact of the metal ion wavefunctions. The intermediate case, involving bond angles on the order of 135°, is often considered to be ambiguous, since that range of bond angle usually suggests several distinct possibilities for the super-exchange mechanism, as well as sometimes allowing for a competing direct exchange.

It has been suggested by J. B. Goodenough[69] that the direct exchange is possible in oxides of the corundum family, of which Cr_2O_3 and α-Fe_2O_3 are representatives. Goodenough classifies the exchange interactions according to the manner in which the two octahedra of oxygen ions surrounding the cations of a pair mate with each other; if they share a common face (first neighbors) or a common edge (second neighbors), direct cation-cation interactions are not only possible but made necessary as well by the fact that the bond angles in each instance are very nearly 90°. (The exact angles in Cr_2O_3 are 88° and 94° for the first and second neighbors, respectively.) However, if the two octahedra share only one corner (third and fourth neighbors), the bond angles are in the intermediate range (132° for third neighbors and 112° for fourth), and a super-exchange is indicated. Furthermore, Goodenough predicts that all four exchanges will be antiferromagnetic, with absolute values of J less than 350 cm^{-1} for the direct exchanges, and of the order of 100 cm^{-1} for the two super-exchanges.

The above prediction of direct exchange is well borne out by the J value of -183.5 cm^{-1} measured for the first neighbors. On the other hand, the prediction about the J values for the two super-exchanges does not fare nearly as well, since it runs counter to the fact that the exchange observed for the fourth neighbors is ferromagnetic. The contradiction most assuredly does exist, since of all the J values given in Table 5.1 that listed for the fourth neighbors is the most certain. Therefore, a better theory of the super-exchange must be found.

W. P. Osmund has suggested a rather ingenious scheme of super-exchange relating to the third and fourth neighbor pairs of both Cr_2O_3 and $\alpha\text{-}Fe_2O_3$;[70] the chief justification of that scheme can now be the fact that it correctly predicts the signs of the third and fourth neighbor exchanges in Cr_2O_3 as given by the direct experimental observations of this work. The theory is particularly noteworthy for its ability to account for the observed difference in sign of the two exchanges in question, in spite of the fact that the differences in atomic arrangement of the two corresponding pair types are rather subtle.

The Osmund theory was originally suggested by, and is intimately bound up with, the different antiferromagnetic spin arrangements of Cr_2O_3 and $\alpha\text{-}Fe_2O_3$ as known from neutron diffraction studies (see Fig. 5.1). Before recounting the theory itself, we digress momentarily in order to fill in the background relating to the problem of magnetic ordering. To facilitate reference to the various exchange integrals, the value for the ith nearest neighbor pair will be refered to as J_i in the following.

It will be noticed from Fig. 5.1 that the relative spin alignments of the second and fourth neighbors are different in the two compounds represented there. In addition to Osmund himself, a number of other writers have suggested that the sign of J_4 may be important in establishing the difference in the two spin arrangements; among the others are Y. Y. Li,[71] A. Iida,[72] and E. F. Bertaut.[73-75] Thus a question first alluded to in Chapter I is raised once more: how many exchange interactions are required to determine the complete antiferromagnetic spin arrangement?

$$J_1$$
$$J_2 \qquad J_0$$
$$J_4 \quad J_3$$

II Fe$_2$O$_3$- α III Cr$_2$O$_3$
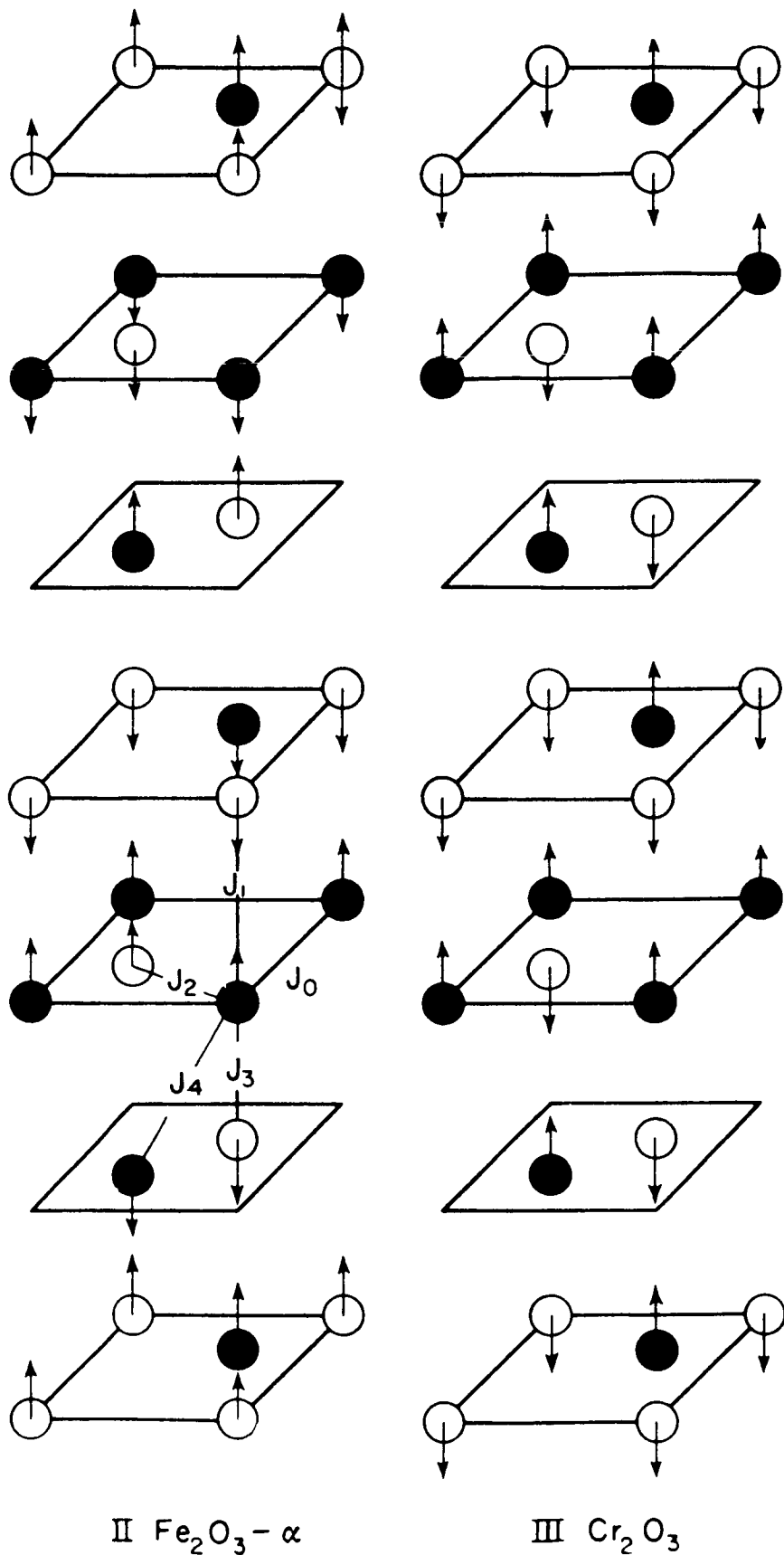
FIG. 5.1--Antiferromagnetic spin ordering for -Fe$_2$O$_3$ and Cr$_2$O$_3$. The coupling labeled J_0 should be called J_6 to suit the convention used here, (from Bertaut[74]).

Goodenough has suggested (on the basis of his assumption that all four J values are antiferromagnetic) that if J_1 and J_2 predominate, the arrangement found in Cr_2O_3 will occur; on the other hand, if J_3 and J_4 predominate, the Fe_2O_3 arrangement must occur.[76] Although correct as far as it goes, the above is misleading in that it does not consider all the possibilities. In fact, it can be shown that predominance of any two of the exchanges J_1, J_2, J_3 and J_4 will completely determine a spin arrangement, with one very important exception: when J_1 and J_3 predominate, a third exchange is required to completely determine the spin arrangement. Since this latter, exceptional case is just that indicated to occur in Cr_2O_3 by the J values listed in Table 5.1, it will be considered in greater detail.

That the combination J_1, J_3 is insufficient to completely determine a magnetic ordering can be seen from the following: the Cr_2O_3 lattice can be viewed as a collection of bipyramids of the Cr_2O_3 molecule, each bipyramid containing one first neighbor Cr pair. Each bipyramid is surrounded by a first shell of six other bipyramids; connection between the central bipyramid and the first shell is only by way of second and fourth neighbor types. As strange as it may seem (until one has looked at a three dimensional model of the Cr_2O_3 lattice), the third neighbors connect the central member to a second, outer shell. Thus, there are two interpenetrating "lattices" of bipyramids, such that J_1 and J_3 by themselves can provide no link between the two, but only interconnect the various members within each lattice.

Thus it would seem that the value (including sign) of J_4, or perhaps of some combination of J_2 and J_4, is important to the determination of the complete spin arrangements of Cr_2O_3 and $\alpha-Fe_2O_3$. In connection with this point it is interesting to note that Bertaut (reference 74) has hypothesized that the difference $J_2 - 2J_4$, which he considers to be positive in Fe_2O_3 and negative in Cr_2O_3, provides the determining factor. Indeed, the directly measured J values justify Bertaut's assumption concerning the sign of $J_2 - 2J_4$ for Cr_2O_3, i.e., from the values listed in Table 5.1, it can be seen that $J_2 - 2J_4 = -25.5$ cm^{-1}. One might go one step beyond Bertaut's contention to theorize that since

J_2 probably is antiferromagnetic in α-Fe_2O_3 as well, the difference in the two oxides will be brought about by a change in sign of J_4 .

We are now in a position to appreciate Osmund's theory, which can be summarized as follows: two of the three oxygen p orbitals will lie very nearly along the two almost perpendicular arms of the first neighbor metal-oxygen-metal bond angle, the third normal to the plane of the bond angle. Each cation has available to it three t_{2g} and two e_g orbitals. Since the configurations of Cr^{3+} and Fe^{3+} are d^3 and d^5 , respectively, both orbitals are half filled in Fe_2O_3, but in Cr_2O_3, t_{2g} is half filled and e_g is completely empty. Geometry of the corundum lattice and location of the t_{2g} and e_g orbitals are such that the situations shown schematically in Fig. 5.2 are obtained for the third and fourth neighbor exchanges.

For the third neighbors, the p orbital whose axis is normal to the first neighbor metal-oxygen-metal bond angle connects t_{2g} orbitals on both cations M_a and M_b of the pair; if the spin of M_a is called (+) , then its already half filled t_{2g} orbital can only accept a (-) spin from the oxygen, making the opposite end of the p orbital (+) ; in accepting a (+) spin from the oxygen, the t_{2g} of M_b must orient its own spins in the (-) direction, thereby making the exchange anti-ferromagnetic.

For the fourth neighbors, one of the other p orbitals is involved, and connects an e_g orbital on M_a with a t_{2g} orbital on M_b . This time the two oxides present two distinct situations: the half-full e_g orbital of α-Fe_2O_3 leads to an antiferromagnetic exchange, by the same mechanism listed for the third neighbors; but in Cr_2O_3 the empty e_g orbital of M_a accepts a spin of the <u>same</u> sign as that on M_a , in keeping with Hund's rule, and thereby leads to a ferromagnetic exchange. As for the geometry involved in making the oxygen and cation orbitals according to the above scheme, the reader is referred to Fig. 2 of reference 70. In connection with this, it is very helpful to have a three-dimensional model of the corundum lattice available for study.

Third neighbors
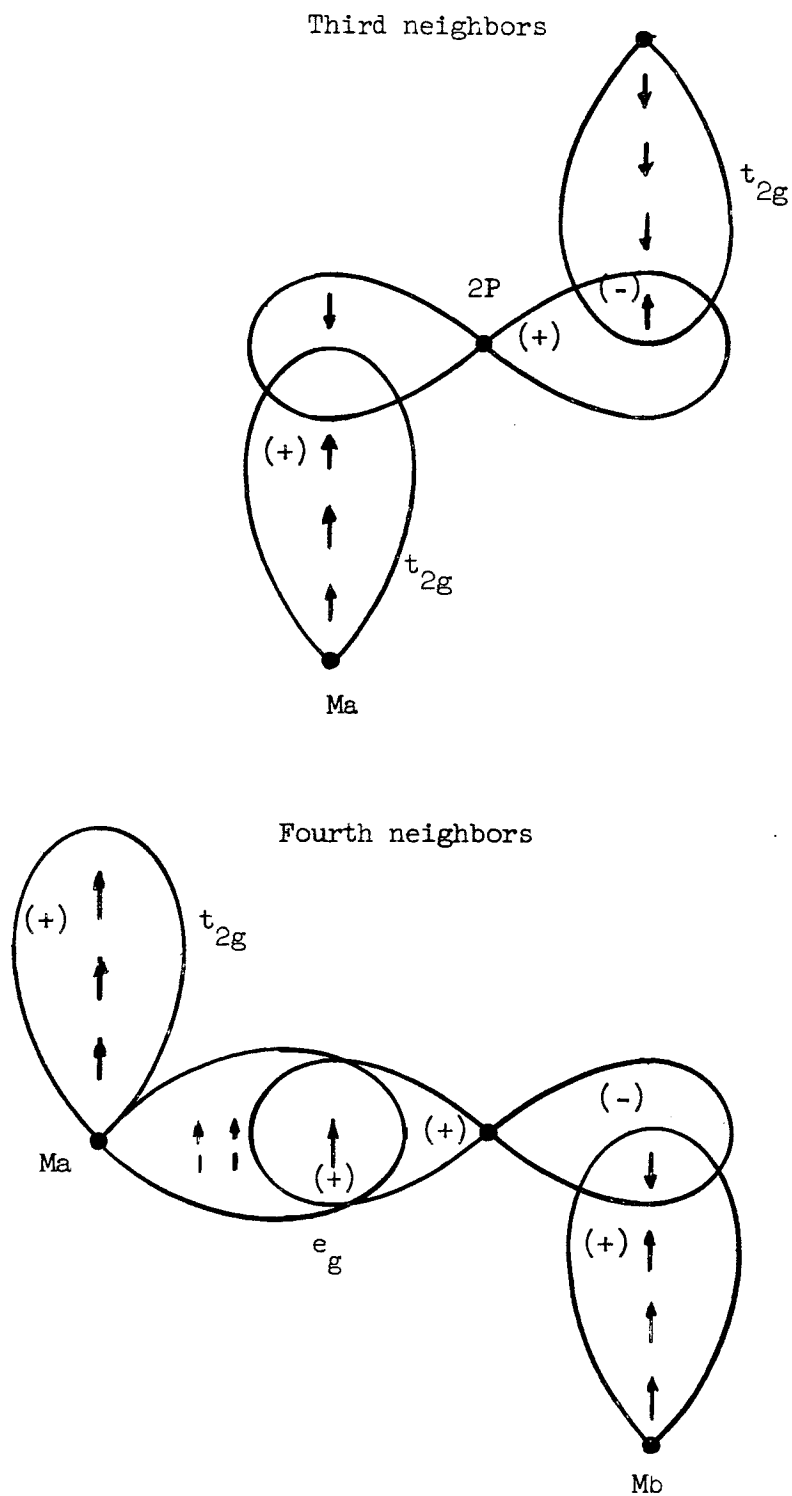
Fourth neighbors

FIG. 5.2--Schematic illustration of Osmund's theory of super-exchange
in the third and fourth neighbor pairs. The metal ion sites
are labeled Ma and Mb.

Now to summarize: Osmund's theory of super-exchange in the third and fourth neighbor ion pair fits very well with all that is known or can be deduced from the experimental studies of this work. In the first place, it correctly predicts the signs observed in Cr_2O_3 for J_3 and J_4 . Secondly, from the observed relative sizes of the four most important J values, it is known that J_1 and J_3 are the two predominating couplings. Yet in that special case, it can be shown that the sign of J_4 must be positive (ferromagnetic) in Cr_2O_3 and negative in $\alpha\text{-}Fe_2O_3$ in order to account for the difference in antiferromagnetic spin arrangement found in the two oxides; Osmund's theory predicts just that change of sign for J_4 .

The measured set of J values can be tested against a formula[1] for Θ given by J. S. Smart:[77]

$$\Theta = -\left(\frac{S(S+1)}{3k}\right) \sum_i z_i J_i \qquad , \qquad (5.2)$$

where S is the spin per atom ($S = 3/2$ for Cr^{3+}) and z_i is the number of ith nearest neighbors per atom (in corundum, $z_1 = 1$, $z_2 = z_3 = 3$, $z_4 = 6$). The test should be a good one, since expression (5.2) is thought to be exact. Inserting the J values of Table 5.1 and using the conversion factor $1 \text{ cm}^{-1} = kT$, where $T = 1.438^\circ K$, we obtain $\Theta = 565^\circ K$, in excellent agreement with the measured value of $\Theta = 550 \pm 20 \text{ cm}^{-1}$, as taken from the susceptibility measurements of Foëx and Graff.[78] The data of reference 78 are reproduced in Fig. 5.3; note that the measurements extend to nearly $1300^\circ K$, a temperature nearly four times as large as T_N , thereby allowing a correct determination of Θ .

---

[1] Expression (5.2) has been altered by a factor of two to conform with the definition of J used here.
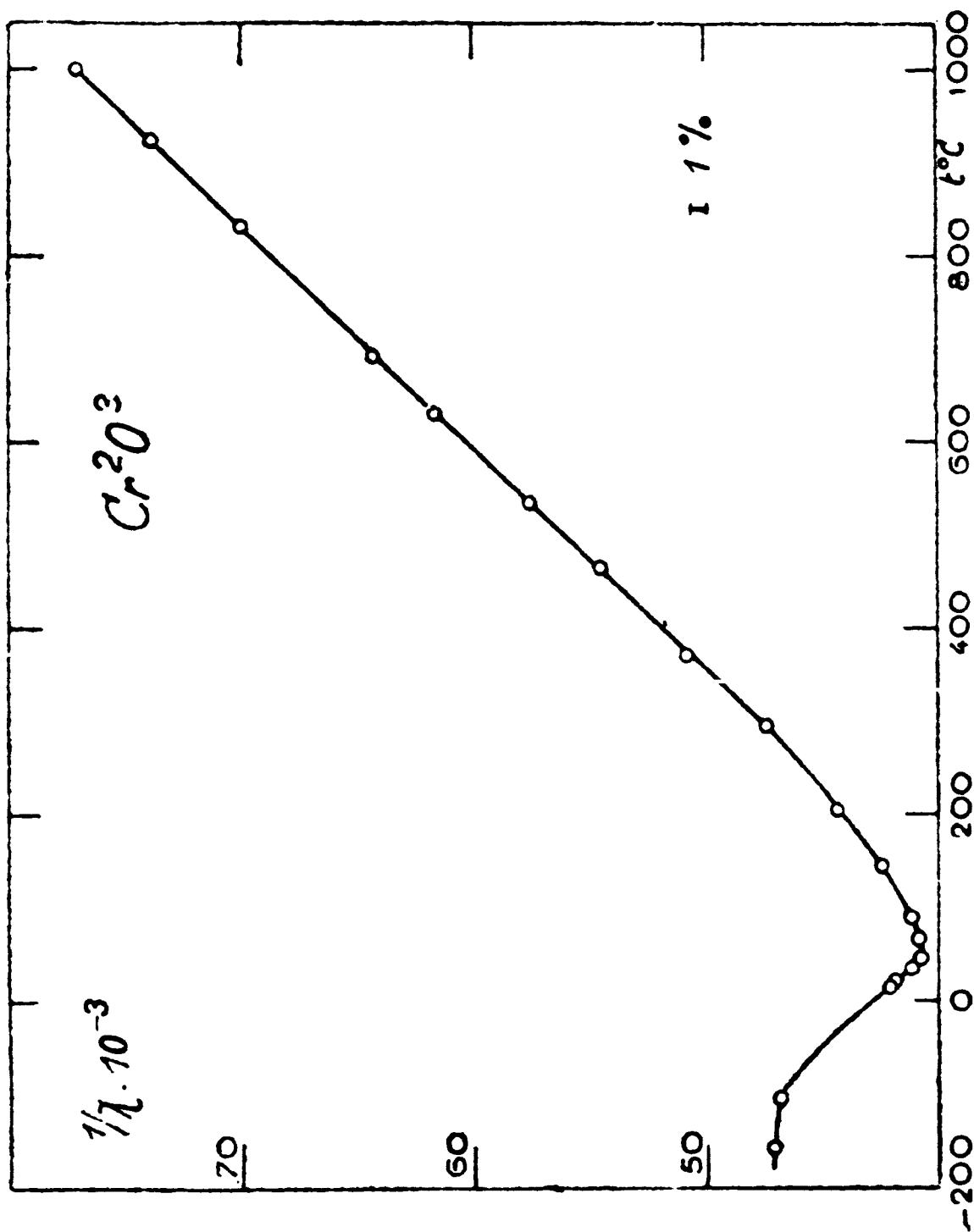
FIG. 5.3—Variation of I/X , (reference 78).

It should be noted here that an incorrect value of $\Theta = 1070^{\circ}K$ is often quoted in the literature; yet reference to the original measurements is hard to find. A review article by Nagamiya and Yosida[79] finally led us to two papers which give graphs of $1/X(T)$ in the range above T_N: the Foëx and Graff paper quoted above, and a more modern one by Trounson et al.[80] Although the authors themselves are not to blame, reference 80 proved to be the source of error, since the measurements of Θ given there only cover the temperature range below $\sim 2T_N$, and yet the often quoted Θ value had obviously been extracted from them. It should be realized that a correct value of Θ cannot be deduced from such measurements, as can easily be seen from the way that the curve of Fig. 5.3 deviates at temperatures below $\sim 2T_N$ from the true straight line paramagnetic behavior seen at higher temperatures.

To the best of our knowledge, there is no adequate theory to relate T_N to the measured set of J values; the only workable theories correspond to the much simpler situation in which one or at most two J values are important in the determination of even the long range ordering. (A good example of such a situation to which a successful theory has been applied is the study by Harris, Lines and Owen[81] of $K_2Ir\,Cl_6$ in solid solution with K_2PtCl_6.) Despite the lack of a valid quantative theory for Cr_2O_3, at least the following qualitative observation can be made: from the above discussion, it has been seen that a relatively small exchange coupling (J_4) is required to complete the long range ordering; the Neel point may then tend to occur closer to a temperature at which this smaller coupling will be broken by thermal effects, consistent with the fact that the observed ratio of T_N/Θ is much less than one. The problem in Cr_2O_3 may possibly be solved by a more complex version of the spin-wave theory applied in reference 81; the theory itself is described in a paper by Lines.[82] It is hoped that the set of J values determined by the experimental studies of this work will inspire the development of a valid theory of ordering in the corundum and other complicated structures.

Finally, it should be pointed out that the presence of anisotropic terms in the exchange hamiltonian, as suggested by the observed splitting

of S levels in the first and perhaps other neighbors, may have an influence on the antiferromagnetic ordering. In the first place, such terms are usually required to establish the axis along which the spins are observed to align themselves; for Cr_2O_3 and α-Fe_2O_3 , this axis is C_3 . The anisotropic terms are also supposed to enter in to the determination of the exact value of T_N ; for an example, see reference 81.

5.3. CORRESPONDENCE BETWEEN THE MEASURED J VALUES IN RUBY AND THE ABSORPTION SPECTRUM OF Cr_2O_3

The optical absorption spectrum of Cr_2O_3 as measured and interpreted by Wickersheim[83] is indicated by the energy level diagram of Fig. 5.4. Transitions originating on the ground state $m_s = -3/2$ level and terminating on the various exchange split components of the optically excited state were observed at $4.2°K$ and were found to be quite sharp. The one transition observed to originate from the $m_s = -1/2$ level could only be detected at temperatures above $100°K$, and was very diffuse.

Figure 5.4 implies an interpretation based on the molecular field model. That is, each transition is supposed to involve just one ion, where the energy levels of that ion have been split by an effective magnetic field created by all the neighbors exchange coupled to it. The concept of an effective magnetic field is the result of assuming that a time average of all the interacting spins can be taken; then the exchange hamiltonian becomes

$$H_{ex} = \left\langle -\sum_i z_i J_{ij}\, \vec{s}_i \right\rangle_{av} \cdot \vec{s}_j \qquad (5.3)$$

In (5.3) above, the levels of the jth ion are split by the field created by all the spins s_i . If the axis of magnetic ordering is called z , then the average taken in (5.3) assumes that $\bar{s}_{ix} = \bar{s}_{iy} = 0$, and that $\bar{s}_{iz} = \pm s_i$ at low temperatures.
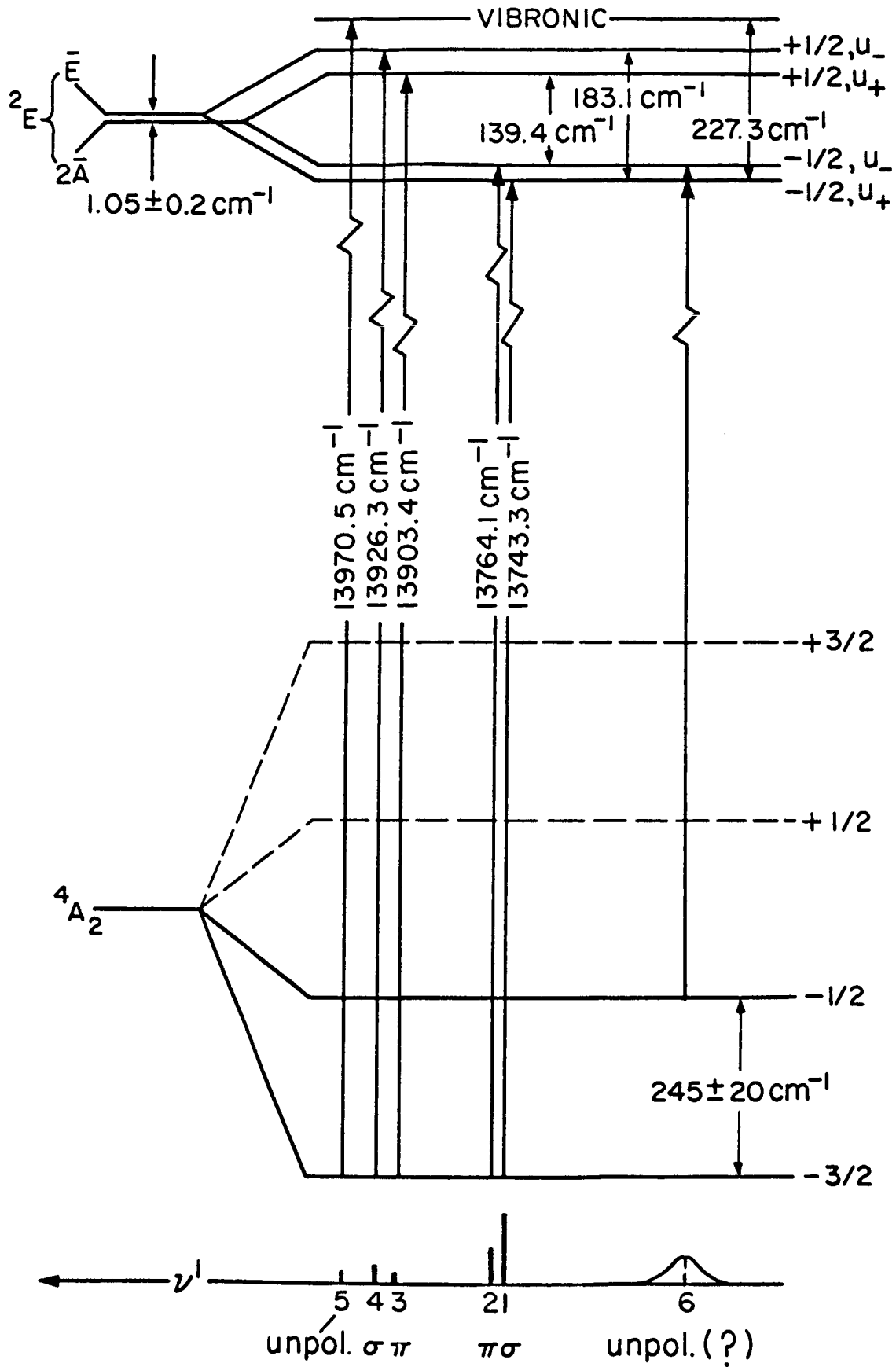
FIG. 5.4--Energy level diagram for Cr_2O_3, (from Wickersheim[83]).

Inserting the J values listed in the first column of Table 5.1 and the numbers $z_1 = 1$, $z_2 = z_3 = 3$, $z_4 = 6$, $s_1 = s_2 = s_3 = -s_4 = 3/2$ into (5.3) yields a predicted splitting of ~600 cm^{-1} between adjacent m_s levels. The fact that the predicted splitting is more than twice as great as that observed should not be at all surprising, since the approximations of the molecular field theory are gross, and no more than order of magnitude results are expected from them. In fact, the error here is very similar to that produced in a molecular field calculation of T_N; in both instances the calculated values are on the order of two or three times too large.[1]

Both R. L. White[84] and M. E. Lines[85] have suggested to us that a better approximation may be provided by a model which views the first nearest neighbor pair as the entity subject to transitions and calculates the effect of the molecular field created by all the other exchange coupled ions on the energy eigenvalues of that pair. The spin hamiltonian is then approximated by the form

$$H = -J_1 S_1 \cdot S_2 + \bar{S}\lambda(S_{1z} - S_{2z}) , \qquad (5.4)$$

where

$$\lambda = -3J_2 - 3J_3 + 6J_4 ,$$

and $\bar{S}$ is the magnitude of the average spin per site. Although it is not at all easy to calculate exact eigenvalues from expression (5.4),

_____

[1] Proponents of the molecular field theory may wonder if one of the less favored assignments for J_3 listed at the end of Chapter IV would allow better agreement with the observed splitting in Cr_2O_3. The answer is no, since the larger antiferromagnetic coupling would obviously give a worse result, and the ferromagnetic value of $J_3 = +60$ cm^{-1} leads to a predicted splitting which is much too small (120 cm^{-1}). Furthermore, as indicated previously, we strongly reject the possibility of a ferromagnetic coupling for J_3, since such a coupling, when combined with the three more certain J values, leads to the wrong spin arrangement and would predict the wrong value for Θ.

an approximate treatment seems to yield differences between the true ground state and the first excited state on the order of $3/2\,J_1$, which would allow much better agreement between the measured exchanges and the spectrum of Cr_2O_3. Incidentally, the exact eigenvalues for a hamiltonian similar in form to (5.4) have been worked out for Cr_2O_3 by Pratt and Bailey,[86] but unfortunately their calculation uses the J values according to Statz,[60] values which are inconsistent with those found by this study.

Still better treatments of the problem are known, such as the Green function method recommended to us by Lines,[85] but such a calculation is very difficult and is certainly beyond the scope of this work. However, the calculation should be made, and we hope that the unique opportunity to test the method against the empirical numbers of this work will inspire at least one ambitious theoretician.

Of course, it is possible that the J values measured for isolated Cr ion pairs in ruby are not identical to those of pure Cr_2O_3; but until a truly adequate theoretical treatment has been applied to the problem of the ground state splitting in Cr_2O_3, and no reasonable agreement found between the observed splitting and that predicted from the J values given here, we are free to continue to assume that measurements on the dilute solid solution are valid for pure Cr_2O_3. As evidence in favor of this very important assumption, we can site two facts mentioned previously: first, the fact that the J values measured in ruby fit all we know of the ordered spin arrangement in Cr_2O_3, and second, the close agreement between the predicted and measured values of the Curie-Weiss constant Θ .

5.4. THE PIEZOSPECTROSCOPIC SENSITIVITY OF THE RUBY PAIR LINES

Next to the measured J values themselves, the piezospectrocopic sensitivities of the pair lines should be of great theoretical interest. A good theory of the piezospectroscopic effect is highly desired for several reasons: (1) The identification of optical transitions with given pair types should eventually be put on a better foundation than the

self-consistency argument used here, especially if it is intended to extend the method to the study of other magnetic materials. (2) The piezospectroscopic effect will undoubtedly be important to the technology of tunable lasers some day; if the phenomenon is well understood, it may be possible to predict the existence of other tunable atomic frequencies useful as laser transitions. (3) The phenomenon should be understood for its own sake, and for the extra understanding of the optically excited state that would be created by a theoretical study of the pressure shifts.

In order to facilitate discussion of the piezospectroscopic effect, it will be necessary to make a few definitions. First, the piezospectroscopic sensitivity itself will be defined as the frequency shift of the most intense line of a multiplet obtained for the standard pressure of 100 Kg/mm^2 and for the angle of applied stress in the mirror plane which yields the maximum shift. The exchange multiplet of a given pair type will refer to the quartet of lines originating on the lowest of the optically excited states and terminating on the exchange split ground state. The center of gravity of an exchange multiplet will refer to the position of the single line that would be produced if the ground state exchange integral J were made zero, while the excited state exchange integral K retains its full strength. The term red shift will indicate the separation of the center of gravity of an exchange multiplet away from the R_1 line position.

On the assumption that the inter-ion exchange represents the sole perturbation of the optical transitions of a pair away from the energy levels of an isolated ion, and also assuming that $K \sim J$, then the red shift for a given pair type should be approximately $5/4\ J$ for antiferromagnetic coupling and $3/4\ J$ for ferromagnetic coupling. However, the observed red shift for a given multiplet is usually about one order of magnitude greater than that amount, and seems to be (roughly) in direct proportion to the piezospectroscopic sensitivity, as indicated in Table 5.2 below.

TABLE 5.2

Pair Type	4	2	3	1
Red shift, cm^{-1}	136	228	1,043	1,210
Piezo. sens., cm^{-1}	-6	-11	-34	-23
J , cm^{-1}	+7	-11	-46	-183

The J values have been included in Table 5.2 since they also correlate with the piezospectroscopic sensitivities if the sign of J_4 is ignored and if J_1 is excluded.

A good theory of the piezospectroscopic effect will undoubtedly make use of, and be able to explain, the correlations shown in Table 5.2, in addition to accounting for the following equally important facts:

(1) The observed pressure shifts are approximately proportional to the component of strain along the pair axis.

(2) The various members of a given exchange multiplet exhibit a common piezospectroscopic sensitivity, as discussed in Section 3.6 of Chapter III.

(3) The piezospectroscopic sensitivity of the R lines is approximately $- 3 \ cm^{-1}$, and the shift is nearly independent of the direction of applied stress.

The piezospectroscopic effect may involve modulation by the stress of one or more of the following:

(1) A large exchange in the excited state (i.e., $K \gg J$).

(2) A large crystal field directed along the pair axis.

(3) Terms in the hamiltonian expressing the effects of covalent bonding.

It should be understood that the distinction between (2) and (3) above is only in terms of the different mechanisms leading to a modified hamiltonian, since the formal appearance of the terms introduced may be identical.

The first possibility mentioned above is probably not of major importance, since the partially known excited state splittings indicate that, in general, K is of the same order of magnitude as J , or at least not more than a few times J . Possibility (2) seems to be ruled out by the lack of a good mechanism for the production of a strong axial field; for example, the idea that lattice distortions brought about by the extra size of the Cr^{3+} ion over that of the Al^{3+} could cause a large odd field term seems rather implausible.

The third suggestion can be supported in the following way: First, it is known that the Cr^{3+} ion is about 20% covalent bonded to the various near neighbor Al^{3+} sites (first through fourth nearest neighbors) from the ENDOR studies of Laurance, McIrvine, and J. Lambe.[87] The covalent bonding of a Cr ion to one of its neighboring Al ions may be drastically altered by substitution of a second Cr ion for the Al, on account of the different electronic configurations of the two ion types; thus the covalent bond between the two members of a Cr ion pair constitutes an odd member in the full set of bonds to all neighboring metal ion sites. From the above consideration one could then understand the relation of the pressure effect to the Cr ion pair axis, as well as the large red shifts. The covalency theory also suits the notion that covalency and super-exchange go hand in hand, as suggested by the fact that the values J_2 , J_3 , J_4 are in proportion to the piezospectroscopic sensitivities of their associated pair types (although J_2 may not represent a super-exchange).

It should be understood that the above is offered only as a suggestion, and that many other explanations are possible. At the time of this writing, it must be admitted that the fundamental origin of the effect found so useful here still remains a mystery.

5.5. APPLICATION OF THE PIEZOSPECTROSCOPIC EFFECT TO LASER TECHNOLOGY

No matter what the ultimate explanation of the piezospectroscopic effect may be, the large frequency shifts and splittings produced and observed in the course of this study constitute a body of empirical fact that may be of great value to laser technology. Now it is true that

many applications merely require the production of large peak powers, or the generation of a very pure and stable frequency, where there is no requirement as to the exact frequency used (except perhaps that it lie somewhere within a rather broad range to which a given detector type is sensitive). Yet many other potential applications, such as the use of lasers to replace filtered white light in spectroscopy, require that the laser frequency be tunable, usually over as large a range as possible. The need is particularly acute for a strong coherent source continuously tunable over the far infrared region of the spectrum, where conventional sources are pitifully weak, making impossible the sensitive, high resolution studies enjoyed in the visible and microwave regions.

Although laser action has already been obtained at various spot frequencies in the far infrared, it is hard to imagine any mechanism by which such transitions could be tuned over regions even several orders of magnitude smaller than say ± 50% of the unperturbed frequency. However, if the far infrared radiation is produced by beating together two lasers operating in the optical region, the laser frequencies need be tuned away from each other by just a few percent in order to cover an infrared region of several hundred wavenumbers. In the usual atomic transitions, even that smaller degree of tuning is considered impossible of achievement. But the Cr ion pair transitions can be tuned over just such a range, through the application of uniaxial stress.

Furthermore, the pair lines are in general eminently suited for laser action by virtue of their sharpness and the fact that most terminate on levels that can be rather easily depopulated by cooling of the laser rod. The N_1 and N_2 lines have already been made to undergo laser action[50] and, if only some way could be found to favor the installment of third neighbor pairs during the growth of a ruby crystal, it should be possible to make the highly pressure sensitive N_0 line display laser action.

Finally, it should be pointed out that use of the pair lines would allow production of the two desired laser frequencies within one and the same laser rod, thereby automatically guaranteeing the spatial coherence necessary to achieve efficient beating together of the two optical frequencies.

REFERENCES

1. Edmond Becquerel, _La Lumiere — Ses Causes et Ses Effets_, (Librairie de Firmin Didot Freres, Fils et Cie, Imprimeurs de L'Institut, Paris, 1867), Chapter IV.

2. Lecoq de Boisbaudran, Comptes Rendues 103, 1107 (1886).

3. E. Becquerel, Comptes Rendues 103, 1224 (1886).

4. Lecoq de Boisbaudran, Comptes Rendues 104, 330 (1887).

5. _Ibid._, p. 554.

6. _Ibid._, p. 824.

7. Lecoq de Boisbaudran, Comptes Rendues 107, 468 (1888).

8. _Ibid._, p. 490.

9. G. C. Schmidt, Annalen der Physik 13, 622 (1904).

10. H. du Bois and G. J. Elias, Annalen der Physik 27, 233 (1908).

11. J. Becquerel, Phys. Zeit. 8, 932 (1907).

12. A. Miethe, Deutch. Physik. Ges. Berichte 9, 715 (1907).

13. J. Becquerel, Comptes Rendues 151, 1344 (1910).

14. J. Becquerel, Comptes Rendues 152, 183 (1911).

15. H. du Bois and G. J. Elias, Annalen der Physik 35, 617 (1911).

16. C. E. Mendenhall and R. W. Wood, Phil. Mag. 30, 316 (1915).

17. H. Bethe, Annalen der Physik 3, 133 (1929).

18. O. Deutschbein, Annalen der Physik 14, 712 (1932).

19. _Ibid._, p. 729.

20. O. Deutchbein, Annalen der Physik 20, 828 (1934).

21. O. Deutchbein, Zeitschrift für Physik 77, 489 (1934).

22. O. Deutchbein, Physik. Zeitschrift 33, 874 (1932).

23. M. N. Saha, Nature 125, 163 (1930).

24. H. E. White, Phys. Rev. 33, 672 (1929).

25. Y. Tanabe and S. Sugano, J. Phys. Soc. Japan 9, 753 (1954).

26. _Ibid._, p. 766.

27. Y. Tanabe and S. Sugano, J. Phys. Soc. Japan 11, 864 (1956).

28. Y. Tanabe and H. Kamimura, J. Phys. Soc. Japan 13, 394 (1958).

29.   S. Sugano and Y. Tanabe, J. Phys. Soc. Japan $\underline{13}$, 880 (1958).

30.   S. Sugano and I. Tsujikawa, J. Phys. Soc. Japan $\underline{13}$, 899 (1958).

31.   A. L. Schawlow, J. Appl. Phys. $\underline{33}$, Supp. 1, 398 (1962).

32.   D. S. McClure, Electronic Spectra of Molecules and Ions in Crystals, (Solid State Reprints, Academic Press, New York, 1964).

33.   M. Hammermesh, Group Theory and Its Application to Physical Problems, (Addison-Wesley, Reading, Mass., 1962).

34.   S. Sugano, A. L. Schawlow, and F. Varsanyi, Phys. Rev. $\underline{120}$, 2045 (1960).

35.   A. L. Schawlow, A. H. Piksis, and S. Sugano, Phys. Rev. $\underline{122}$, 1469 (1961).

36.   G. F. Imbusch, Physics Department Dissertation and Microwave Laboratory Report No. 1190, Stanford University (1964).

37.   I. Wieder, Rev. Sci. Instr. $\underline{30}$, 995 (1959).

38.   T. Maiman, Phys. Rev. Letters $\underline{4}$, 564 (1960).

39.   S. F. Jacobs, thesis, Johns Hopkins University, Baltimore, 1957 (unpublished).

40.   A. L. Schawlow, D. L. Wood, and A. M. Clogston, Phys. Rev. Letters $\underline{3}$, Y502 (1959).

41.   N. A. Tolstoi and A. P. Abramov, Opt. i Spektroskopiya $\underline{14}$, 691 (1963) or (English translation) Opt. Spectry. $\underline{14}$, 365 (1963).

42.   L. R. Maxwell and T. R. McGuire, Rev. Mod. Phys. $\underline{25}$, 279 (1953).

43.   W. G. Wyckoff, Crystal Structures (Interscience Pub., New York, 1960), Chapter V, table p. 11.

44.   P. W. Anderson, "Exchange in Insulators," in Magnetism, G. Rado and H. Suhl, eds. (Academic Press, New York, 1963), Vol. 1, p. 26.

45.   K.W.H. Stevens, "Spin Hamiltonians," Ibid, p.20, ref. 44.

46.   J. Owen, J. Appl. Phys., Suppl., $\underline{32}$, 213S (1961).

47.   A. M. Clogston, "Emission Spectrum of Exchange Coupled Chromium Ions in Ruby," (unpublished).

48.   A. L. Schawlow, private communication.

49.   A. L. Schawlow, "Infrared and Optical Masers," in Quantum Electronics (Columbia University Press, New York, 1960).

50.   A. L. Schawlow and G. E. Devlin, Phys. Rev. Letters $\underline{6}$, 96 (1961).

51.   A. L. Schawlow, Sci. Am. $\underline{204}$, 6 (1961).

52.   R. T. Daly, Paper No. TB16, Opt. Soc. of Am. meeting at Los Angeles, October 1961.

53. P. Kisliuk, A. L. Schawlow, and M. D. Sturge in _Advances in Quantum Electronics_ (Columbia University Press, New York, 1964), p. 725.

54. P. Kisliuk and W. F. Krupke, "Exchange Interactions between Pairs of Cr Ions in Ruby," Internal Report, Aerospace Corp., El Segundo, Calif. (1964).

55. We are indebted to H. Statz for transmitting this table to us.

56. B. N. Brockhouse, J. Chem. Phys. $\underline{21}$, 961 (1953).

57. R. Nathan, T. Riste, G. Shirane, and C. G. Shull, Bull. Am. Phys. Soc. II, $\underline{2}$, paper FA4 (1957).

58. M. Tachiki and Takeo Nagamiya, J. Phys. Soc. Japan $\underline{13}$, 452 (1958).

59. L. Rimai, H. Statz, M. J. Weber, and G. A. deMars, Phys. Rev. Letters $\underline{4}$, 125 (1960).

60. H. Statz, L. Rimai, M. J. Weber, and G. A. deMars, J. Appl. Phys. $\underline{32}$, Suppl., 218S (1961).

61. J. Owen, J. Appl. Phys. $\underline{32}$, Suppl., 213S (1961).

62. A. A. Kaplyanskii and A. K. Przhevuskii, Doklady Akademii Nauk SSSR $\underline{142}$, 313 (1962) or (English translation) Soviet Physics-Doklady $\underline{7}$, 37 (1962).

63. H. D. Conway, _Mechanics of Materials_, (Prentice-Hall, New York, 1950), p. 30.

64. E. A. Wood, _Crystal Orientation Manual_, (Columbia University Press, New York, 1963), p. 30.

65. J. B. Wachtman, W. E. Tefft, D. G. Lam, and R. P. Stinchfield, J. Res. of National B. Standards, $\underline{64A}$, 213 (1960).

66. D. S. McClure, J. Chem. Phys. $\underline{36}$, 2757 (1962).

67. S. C. Moss and R. E. Newnham, Zeitschrift für Kristallographie $\underline{120}$, 359 (1964).

68. J. O. Artman and J. C. Murphy, Phys. Rev. $\underline{135}$, A1622 (1964).

69. J. B. Goodenough, Phys. Rev. $\underline{117}$, 1442 (1960).

70. W. P. Osmund, Proc. Phys. Soc. of London $\underline{79}$, 394 (1962).

71. Y. Y. Li, Phys. Rev. $\underline{102}$, 1015 (1956).

72. A. Iida, J. Phys. Soc. Japan $\underline{11}$, 1300 (1956).

73. E. F. Bertaut, Comptes Rendues $\underline{252}$, 252 (1961) and errata _Ibid_. $\underline{252}$, 2032 (1961).

74. E. F. Bertaut, Phys. and Chem. Solids $\underline{21}$, 256 (1961).

75. E. F. Bertaut, "Spin Configurations of Ionic Structures," in Magnetism, G. Rado and H. Suhl, eds., (Academic Press, New York, 1963), Vol. III.

76. J. B. Goodenough, "Magnetism and Crystal Structure in Nonmetals," Ibid, p. 16, ref. 75.

77. J. S. Smart, "Evaluation of Exchange Interactions from Experimental Data," Ibid, p. 66, ref. 75.

78. G. Foex and M. Graff, Comptes Rendues 209, 161 (1939).

79. T. Nagamiya and K. Yosida, Advances in Phys. 4, 17 (1955).

80. E. P. Trounson, D. F. Bleil, R. K. Wangness, and L. R. Maxwell, Phys. Rev. 79, 543 (1950).

81. E. A. Harris, M. E. Lines, and J. Owen, "Paramagnetic Resonance from Three Exchange Coupled Lines," in Paramagnetic Resonance, W. Low, ed., (Academic Press, New York, 1963), Vol. II, p. 553.

82. M. E. Lines, Proc. Royal Soc. London A271, 105 (1963).

83. K. A. Wickersheim, J. Appl. Phys. Suppl. 34, 1224 (1963).

84. R. L. White, private communication.

85. M. E. Lines, private communication.

86. G. W. Pratt and P. T. Bailey, Phys. Rev. 131, 1923 (1963).

87. N. Laurance, E. C. McIrvine, and J. Lambe, J. Phys. Chem. Solids 23, 515 (1962).